ABSTRACT

MAYS, ROBIN LYNN. Tuning Bulk and Surface Properties of Polymers for Micro- and Nanofabrication. (Under the direction of Dr. Jan Genzer and Dr. Michael D. Dickey).

This work describes the modification of bulk and surface properties of polymers used in micro- and nanofabrication. Techniques used for the fabrication of small-scale features require precise tuning of surface chemistry and wettability as well as mechanical strength and elasticity. Silicone elastomeric networks such as poly(dimethylsiloxane) (PDMS) are the foundation for the field of soft lithography, but PDMS is difficult to modify chemically and mechanically. We therefore explore the modification of mechanical and surface properties of alternate polymeric materials to improve functionality in micro- and nanodevices.

We use photochemistry as a tool to modify the mechanical properties of silicone elastomers and to crosslink thiol-ene formulations. Curing siloxane networks over a mold produces replicas which can be used to make microchannels or other microfluidic components. Although PDMS is commonly used to build microchannels, by using poly(vinylmethylsiloxane) or PVMS as a more reactive microchannel matrix, we can locally modify the properties of the network to tune a microchannel for solvent compatibility. Increasing the crosslink density of a PVMS network through local crosslinking of the vinyl side groups by photoinitiated free radical chemistry results in a rigid polymeric network. Microchannels made from UV-treated PVMS resist swelling in organic solvents. Although the modulus of the UV-treated PVMS networks is orders of magnitude higher than untreated PVMS, the surface is chemically similar to the original network. Additionally, we investigate the use of nanoparticles as mechanical reinforcing agents in PVMS networks. By incorporating appropriate amounts of silica nanoparticles into elastomeric networks, the

polymer films demonstrate improved elongation and toughness, making them suitable for microfluidic applications.

For increased functionality of PVMS surfaces in microfluidic devices, we investigate the attachment of biological molecules to vinyl functional groups. We deposit stimuli responsive materials, specifically elastin-like polypeptides or ELPs, onto vinyl functional silicon surfaces. ELPs collapse in warm aqueous solutions, and therefore we deposit heated, collapsed ELPs onto surfaces to increase the grafting density of the polypeptides. The morphology and thickness of the deposited ELP brush layers are characterized. Using several chemically similar ELPs with varying amino acid sequence and distribution, we correlate the bulk solution collapse behavior with the morphology of surfaces in AFM. Heated deposition experiments reveal that a high grafting density of the ELP brush results in a loss of stimuli-responsive behaviors. These conclusions impact future modification of PVMS surfaces or other substrates with densely packed polypeptides.

A further area of investigation is the preparation of mechanically tunable thermoset polymers using photochemistry. We assess the impact of modulus and surface chemistry on the adhesion of a rigid polymer resin to a metallic surface such as gold. Nanowires used in microfluidic electronic devices are manufactured through a process called nanoskiving, in which a gold layer is embedded in a polymer resin and then sliced thinly into wires. Because nanoskiving originated from biological microtomy, the original resins developed for this technique are poorly suited chemically for metal encapsulation and room temperature microtomy. We therefore evaluate the performance of several thiol-ene based photocurable resins, which cure rapidly, exhibit low shrinkage, and are mechanically tunable. We

demonstrate the use of several epoxies and thiol-enes as gold wire embedding resins and compare the mechanical and adhesion properties of the resins.

Tuning Bulk and Surface Properties of Polymers for Micro- and Nanofabrication

by
Robin Lynn Mays

A dissertation submitted to the Graduate Faculty of
North Carolina State University
in partial fulfillment of the
requirements for the degree of
Doctor of Philosophy

Chemical Engineering

Raleigh, North Carolina

2015

APPROVED BY:

_____	_____
Jan Genzer Committee Co-Chair	Michael D. Dickey Committee Co-Chair
_____	_____
Orlin D. Velev	Julie Willoughby

DEDICATION

For Maxine and Bejo.

BIOGRAPHY

Robin was born and raised in Greensboro, North Carolina. Discovering an early love of science through frequent visits to science museums and plenty of time outside (spent catching bugs and playing in mud), Robin applied for admission to the North Carolina School of Science and Mathematics in Durham. She attended junior and senior years of high school at NCSSM, discovering the wacky world of polymer science, and vowed to pursue this interest in college. Robin next attended Virginia Tech and majored in Chemical Engineering, continuing to learn about polymers through chemistry courses and a polymer processing course. After graduating, she moved on to work for Eastman Chemical Company in the polymers division as a development engineer. Though the work was interesting, Robin decided to return to graduate school to research polymer chemistry and material properties as a part of the Chemical and Biomolecular Engineering Department at North Carolina State University.

ACKNOWLEDGMENTS

Despite differences in research field or project topic, all Ph.D. students learn that a successful experience in graduate school is the result of the cooperation of a rather large group of people.

First of all, I would like to thank my advisors, Jan "Honza" Genzer and Michael Dickey, for their guidance and patience. Michael first reached out to me as a potential NCSU student and encouraged me to join the department here in Raleigh, and I'm very grateful that he did. Michael has demonstrated how to guide a large research group with respect and compassion, all while fostering curiosity and passion for our work. Jan has taught me thoroughness and precision in my research, encouraging me to explore any research hypothesis to the fullest detail in pursuit of new scientific understanding, after which we can all grab a good beer. I also thank my committee members, Orlin Velev and Julie Willoughby, whose insightful questions and helpful remarks guided my research.

I would also like to thank my research groups for their support and collaboration. Although I am grateful to every member of both of my research groups, I would like to thank in particular Ying Liu for her warmth, thoughtfulness and help getting me started in the lab, Sharvil Desai for his encouragement at the start of my project, Dhana Savithri and Ju-Hee So for getting the Dickey lab going in the right direction, Kirill Efimenko for his boundless siloxane polymer knowledge, Julie Albert for her support and vast wisdom gained through experience, and Matt Melillo for being a synthesis buddy. I would also like to thank my amazing undergraduate helpers: Jackson Menius, who first taught me how to crosslink a

PVMS network, Katie Nagley, who is most responsible for my nanoparticle work, Kate Sintavanon, genuinely kind and unfailingly productive, and Annabelle Davey, who worked tirelessly on the ELP project and who is at times frighteningly sharp.

I owe a great debt to my collaborators as well: Tosh Chilkoti and Sarah MacEwan for synthesizing ELPs and answering all my questions, Stefan Zauscher for use of his AFM and Zehra Parlak for being so helpful in showing me how to use it, Ryan Chiechi and Parisa Pourhossein for their work on the nanoskiving project, and the Gorman lab, for giving me dry ice, dry solvents, and helping me with solvent distillation over the years.

The Chemical and Biomolecular Engineering Department at NCSU has been a tremendously supportive environment, for which I am very grateful as I have never been short of help or equipment. Thank you to all the faculty members and graduate students who worked with me and helped me; hopefully I was able to help a few people on their projects as well. The CBE office staff are an amazing group of people who are genuinely concerned with helping the graduate students along their path, which has been wonderful and greatly appreciated.

And last, but certainly not least, the three fellas who got me through the most difficult months: Aaron Hawkins, Vikram Seshadri, and Berç Kalanyan. Thank you for all the movie nights, homework sessions, kind words, support, and friendship. I could not have done it without you.

TABLE OF CONTENTS

LIST OF TABLES

LIST OF FIGURES

CHAPTER 1. Introduction

1.1. Micro- and Nanofabrication Background

The expansive research and engineering field of microfabrication has roots in the electronics industry, where consumer demand drives the development of smaller and faster electronic devices.[1] Integrated circuits, the backbone of electronic devices, are fabricated largely through photolithography, which is limited in resolution by the optical diffraction of light through the photomask.[2] Even with the use of deep UV radiation (λ<250 nm), the resolution of features fabricated through photolithography is limited to ~50-200 nm.[3] Prior to the 1990s, microfabrication primarily involved the construction of various electronic components on rigid substrates, such as silicon and glass.[4] For targeted commercial applications such as diagnostics, bioanalysis, and environmental analysis which require rapid, inexpensive manufacturing techniques, polymer substrates are preferred due to their low cost and advantageous physical properties, such as oxygen permeability and optical transparency.[5]

The formation and replication of nanostructures by polymeric materials extends to numerous applications, including optics, data storage, and biological devices.[3] Microelectromechanical systems (MEMS), which were originally constructed only from rigid materials such as glass or silicon but are increasingly incorporating polymeric components, make use of the high throughput production processes developed by the semiconductor industry for biochemical applications, requiring pumps, sensors, and actuators all within one chip.[6] This idea of encompassing an entire analytical lab or biological assay on one device is often referred to as "lab on a chip",[7] and has been demonstrated for various systems including DNA analysis.[8] Because of the small volumes used in these systems, the time scales over

which heat and mass transfer take place shrink, enabling fine control over chemical reactions, biological separations, and drug discovery.[7]

Numerous strategies for creating micro- and nanopatterned polymeric components exist in the literature.[1,2,9] As seen in Figure 1.1, several techniques are available for fabricating micron scale polymeric features.[5] For thermosets such as those used in photolithography, modification after curing is difficult, often requiring plasma etching or other relatively harsh physical treatment methods. Using thermoplastics offers simpler processing, but often at the cost of fine detail in microfabrication, as molded thermoplastics do not completely fill in corners or edges of a mold. Softer elastomers, which can be either physically or chemically crosslinked, are often utilized for their easy manipulation and flexibility.

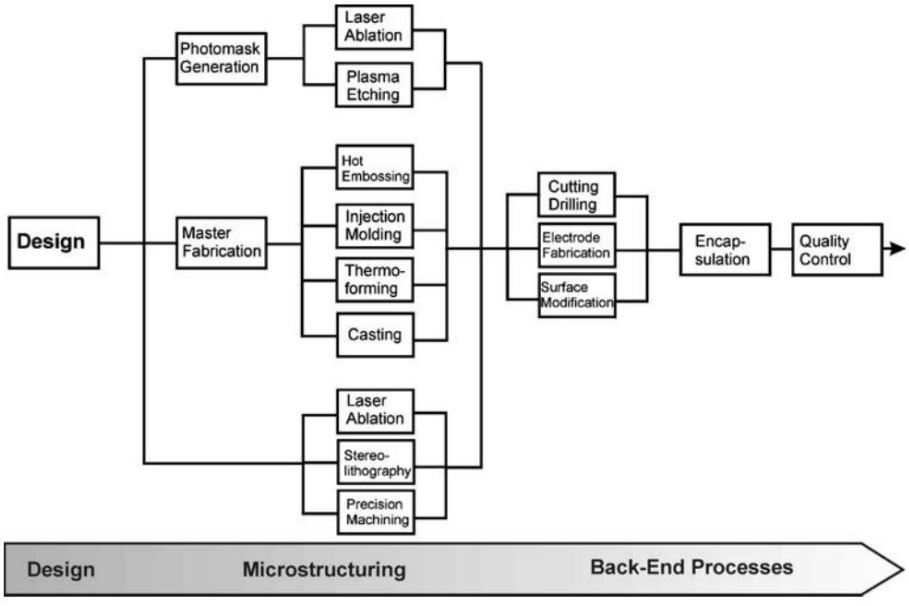

Figure 1.1: Techniques for microfabrication of devices from polymeric materials.[5]

1.1.1. Lithographic Techniques

Photolithography uses light to transfer a pattern to a photo-sensitive resist, as depicted in Figure 1.2, followed by an etching step to remove the uncured photoresist. The result is a highly accurate, mechanically and chemically durable pattern, which can be used as a part of an integrated circuit or as a master mold for patterning a polymer. Although photolithography is limited by both the optical diffraction of light through the mold as well as the depth of focus of the light system,[9] it is still used for generating a master mold for other replication procedures, such as soft lithography.

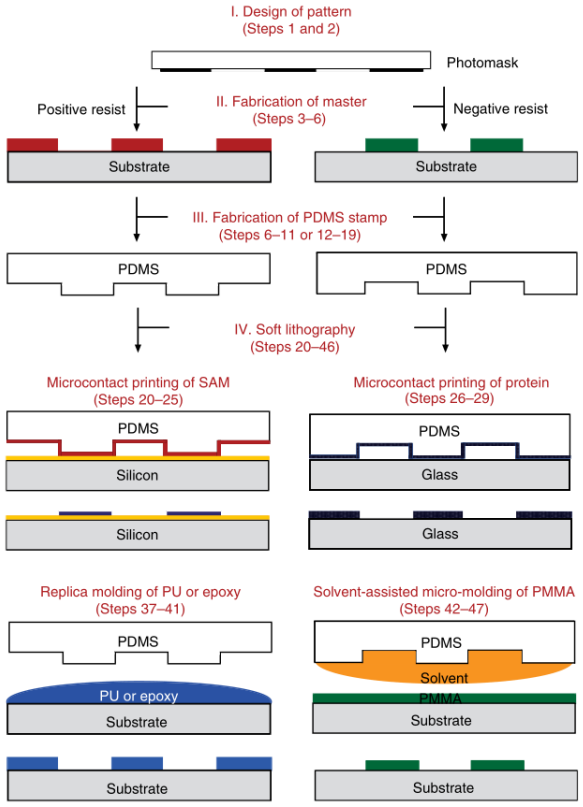

Figure 1.2: Common soft lithography techniques.[10]

Soft lithography includes a variety of procedures all of which use soft elastomeric components, made typically of poly(dimethyl siloxane) (PDMS), for the creation of microscale surface features.[2] Initially developed by the Whitesides research group at Harvard University, soft lithographic techniques became immensely popular due to the low cost, lack of specialized equipment needed, and control over surface chemistry patterning that these methods offer.[10] PDMS is ca. 50 times cheaper than silicon on a volumetric basis.[11] Additionally, elastomeric materials form tight seals with rigid substrates, such as glass and silicon.[11] Some commonly used soft lithography techniques include replica molding, microcontact printing, and solvent assisted micromolding,[2] all shown in Figure 1.2. Replica molding in particular has been widely used for creating microfluidic channels as well as other microdevices.

Replica molding involves the casting of an elastomeric material onto a rigid master mold, generating an elastomeric replica. The fidelity of the replica depends on the interaction of the master with the replica material, including wetting properties and van der Waals forces between the two materials.[2] PDMS is commonly used as a replica material for microfluidics and nanofluidics[12] as well as a master for microcontact printing. Because of the elastomeric nature of the PDMS network, it is easily released from the master even when replicating complex features.[1] The properties of siloxane polymers, including PDMS, will be discussed further below.

The master mold for replica molding can be manufactured by photolithography or other patterning techniques. For example, diblock copolymers self-assemble into complex topographies with features on the order of a few to a hundred nanometers, depending on the

molecular weights of the blocks and processing conditions.[13,14] Colloidal assembly also generates highly ordered, hexagonal patterns which can be replicated by PDMS.[15,16] Micro- and nanomachining through focused ion beam milling or scanning probe machining, while comparatively slow, have high spatial resolution.[17] Natural materials, such as leaves or insect wings, have also been used as master molds.[18–20]

In microcontact printing, an elastomeric mold is coated with "ink" (*vide infra*), which is then transferred to a target substrate (see Figure 1.2). This process is not limited by optical diffraction and is usually inexpensive, depending on the materials used.[21] The inked areas can be used to selectively protect a gold layer from etching[22] or to initiate polymer growth from the substrate, but also the ink can consist of a polymeric material that can covalently or physically attach to the substrate.[23]

Nanoimprint lithography (NIL), in contrast to soft lithography, uses rigid molds to imprint a polymer melt or a pre-polymer resist (as depicted in Figure 1.3). The mold is brought into contact with a thermoplastic melt or a resist to deform it. The resist during imprinting must have a lower Young's modulus than that of the mold as well as a relatively low viscosity[24] in order to be successfully molded. Once the resist is cured (or the melt is cooled), the mold is removed. The final step involves the removal of the residual layer of resist with etching. Nanoimprint lithography requires simple equipment at low costs while offering sub-100 nm resolution features, which makes it attractive both for industrial manufacturing and academic research.

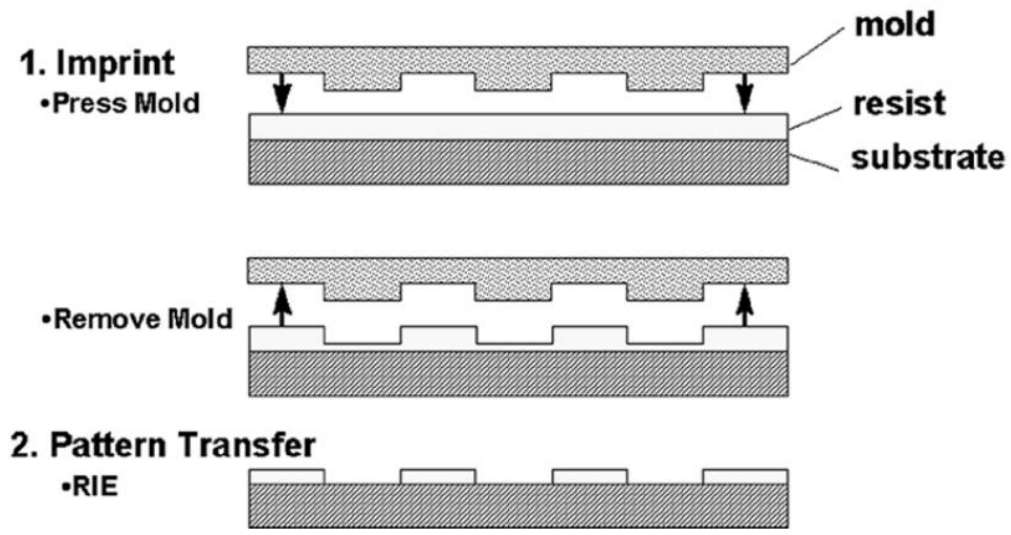

Figure 1.3: Nanoimprint lithography process. In step 1), the mold is pressed onto the polymer melt or pre-polymer resin. Once the resist is cooled or cured until solid, the mold is removed. In step 2), the residual layer is removed through etching (such as reactive ion etching or RIE).[24]

1.1.2. Material Issues and Limitations

The various soft lithography methods require the polymer being used to possess specialized mechanical and chemical properties. For example, microcontact printing requires that the material used has specific mechanical properties to prevent feature collapse or distortion.[21] The modes of failure, like those seen in Figure 1.4, include lateral collapse (neighboring features touch and adhere), buckling, roof collapse, and surface tension induced feature rounding. Exchange of soft materials with a higher modulus material eliminates these problems, but can lead to issues of cracking or lack of conformal contact with the surface being patterned.[21,25] In addition, many organic solvents swell PDMS stamps, which alter the

dimensions of the stamp,[22] while hydrophilic inks will not wet the hydrophobic surface of PDMS.[23]

Similar restrictions apply to replicating nanostructures with replica molding techniques. If the tensile modulus of the material used to replicate the master mold is less than 2 MPa, then the features on the replica may be distorted through lateral or vertical collapse.[3] A modulus less than 2 MPa of the replica limits the feature sizes to greater than 300 nm and the aspect ratio (height/width) to a minimum of 0.4.[3] By molding with polymers of higher strength (with Young's modulus between 4 and 10 MPa), minimum feature size decreases to ~30 nm wide and 2 nm high. Some estimate that features below 50 nm require a tensile modulus of 100 MPa or more.[26] Ideally, the replica material would possess enough toughness to avoid tearing or breaking of the molded polymer and the rigidity to avoid feature collapse.

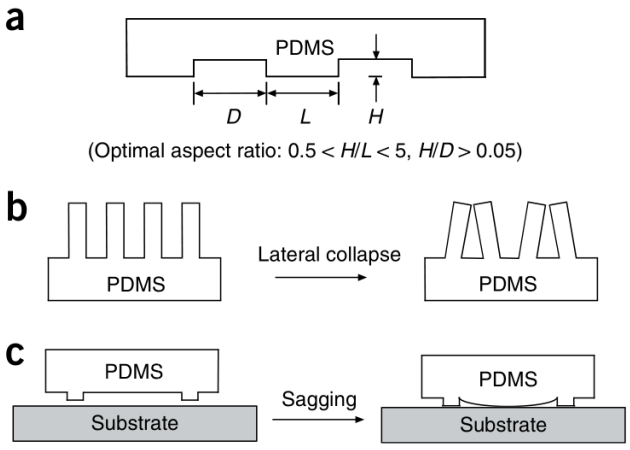

Figure 1.4: Potential problems with soft molds. (A) The initial PDMS mold; (b) lateral collapse for aspect ratios H/L > 5; and (c) roof collapse with aspect ratios H/L < 0.5.[10]

Nanoimprinting relies on the mechanical molding of the polymer resist, which requires vastly different mechanical properties of the mold and the resist than soft lithography. The mold itself must be rigid with a high mechanical strength and must not deform even at elevated temperatures, while still being flexible enough to conform to a large substrate.[24] Additionally, if the resin being patterned is photocurable, the mold must also be transparent. A mold material with a tunable modulus is advantageous for NIL, as the rigidity of the mold can be adjusted for the viscosity and shear modulus of the resist being used.[27] The surface chemistry of the mold and the resist also impact the quality of the replica. Surface energy alone is not necessarily a strong predictor of good mold release.[28]

Several materials have been suggested as alternatives to PDMS networks to achieve high aspect ratio replicas including photocurable PDMS,[29,30] perfluoropolyethers,[31] and organic-inorganic hybrids.[32] A highly crosslinked network of siloxane rings, with a modulus of over 1 GPa, produces a successful NIL mold material.[33] While many of these materials are useful for the fabrication of master molds, PDMS remains one of the simplest materials to use for constructing microfluidic devices. We will therefore discuss the specific requirements of microfluidic materials and surfaces.

1.2. Microfluidics

Microfluidics includes bioassays, purification and separation on a microliter scale, nanoparticle preparation,[34,35] flexible electronics,[36] and even soft robotics.[37] Complex fluid flow phenomena occur in the confined geometries of microfluidic channels, allowing the study of non-linear behavior of polymer solutions, rheological properties of wormlike

micelles, and plug flow of colloidal solutions.[38] Additionally, even smaller scale devices, nanofluidic devices, can manipulate DNA strands, perform electrokinetic experiments, and analyze increasingly dilute solutions.[39] Researchers favor microfluidic systems for many reasons: only a small amount of reagent is necessary, multiple devices can be run in parallel, and prototyping a new device is not very time-consuming.[40,41]

Chemical engineers and physicists were particularly motivated to expand this research area due to the interesting phenomena which take place and can be observed on a microliter scale. Fluid flow in small devices is laminar, mass transport is dominated by viscous dissipation, and heat transfer occurs rapidly.[40] As the dimensions of a microchannel shrink, the impact of surface forces, such as surface tension or substrate-fluid interactions, dominate any volumetric forces.[42] The literature on microfluidic devices and device fabrication is far too expansive to exhaustively detail it here. Rather, we highlight a few important applications and considerations of microfluidics, as well as mechanical or chemical property requirements, to frame the importance of tuning both bulk and surface properties in microfluidic systems.

Microfluidic devices offer advances in synthetic chemistry by carefully controlling reaction time and component mixing to generate uniform polymers or nanoparticles as compared to traditional batch synthesis.[43] For example, performing a living anionic polymerization in a microfluidic reactor with a relatively high concentration of monomer (42 vol%) results in a final product with a high molecular weight and a narrow PDI.[44] Nanoparticle synthesis can also be more finely controlled in microfluidic devices, producing a more uniform population of particles than in batch synthesis.[45] In order to perform organic

syntheses on a microfluidic chip, the device must resist common organic solvents, including tetrahydrofuran (THF), toluene, benzene, dioxane, and alcohols.

Bio-microfluidics involves the use of biopolymers or biomimetic materials to manipulate fluids on the nano- or microscale.[46] Microfluidic devices have already been used to perform chromatography,[47] bioanalysis,[48,49] DNA amplification,[50] and cellular manipulation.[51] In addition, the study of the growth and manipulation of tissues, known as tissue engineering, benefits from highly controlled cellular microenvironments, which microfluidics can provide.[52] Point-of-care biomedical applications utilize the small size and ease of use of microfluidics for devices like glucose testing in diabetics and home pregnancy tests;[53] these devices often use commodity thermoplastics, paper, or textiles due to low cost.[54] Materials that were traditionally used for electronic components do not necessary lend themselves naturally to the manipulation of biological compounds; therefore much research is devoted to the chemical alteration of polymers,[55] glass/silicon,[56,57] or metals, to function properly in aqueous systems. Any material used for commercial biomedical devices must be evaluated for toxicity or leaching.[58] The limitations of PDMS for use in cell cultures were explored in detail by the Beebe research group, as indicated in Figure 1.5.[59] Unreacted oligomers can leach out of the siloxane network into the cell culture media, potentially influencing protein movements across cell membranes or other signaling processes.[60]

The fabrication of micro- or nanofluidic devices relies on a vast toolbox of techniques for producing accurate, precise dimensions of channels.[61] Functioning devices require components such as membranes, mixers, filters, and switches.[62] The operations of a lab-on-

a-chip system can be broken into a few categories: sample preparation, separations, sensing and detection, and fluid manipulation.[53]

Problem	Cause	Applications Affected	Solution
Deformation 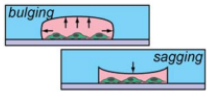	- High compliance (low stiffness) - Low aspect ratio	- Endothelial cell response to shear	- Modify curing parameters - Avoid low aspect ratios - Avoid high pressure flows
Evaporation 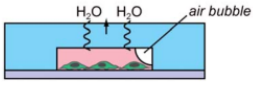	- Permeability to water vapor	- Static no-flow experiments - Osmolarity-sensitive experiments - Cell death from bubble propagation	- Coat with Parylene - Ensure environments humidified - Incorporate media baths or sacrificial liquid reservoirs
Absorption 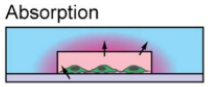	- High permeability of material	- Soluble factor signaling studies involving small hydrophobic molecules	- Coat with Parylene - Coat with paraffin wax
Leaching 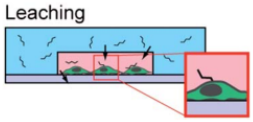	- Uncrosslinked oligomers	- Protein trafficking across membrane - Signaling through membrane-bound receptor proteins	- Coat with Parylene - Soxhlet extraction
Hydrophobic Recovery 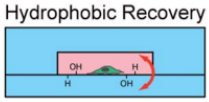	- Surface diffusion of low molecular weight chains	- Unstable surface treatment or functionalization	- Use surface-treated device as soon as possible after treatment - Use hybrid devices with non-PDMS culture surface

Figure 1.5: Issues integrating PDMS systems with cell biology.[59]

Sample preparation includes filtration, extraction of desired analytes, and purification. Separation steps involve chromatography, electrophoresis, or fractionation. Sensors encompass a wide range of methods, depending on the sample type and device. Optical sensors can be carried out with fluorescently labeled compounds and excitation by laser sources. Monitoring can also be realized through electrochemical detection, mass

spectrometry, or surface plasmon resonance. Fluid manipulation relies on traditional chemical engineering processes, with components such as pumps and valves.

All of these component categories depend on the physical and chemical properties of the materials used for device construction. Because membranes need to maintain their shape to be functional, they are often constructed out of more rigid materials, which are then integrated in a PDMS device.[63] Elastomeric valves, sometimes referred to as "Quake" valves (after the initial designer Stephen Quake from Stanford University), take up little space and require small forces to actuate because of their flexibility.[11] Optofluidic devices, which are optical devices constructed with microfluidic technology, are made of fluids, dyes, and elastomers, with the tunability of the device dependent on both the refractive indices and the possible deformation of the elastomer.[64]

Although there is ongoing debate in the research community as to whether PDMS is a suitable material for commercial production of microfluidic devices,[58,59] it remains the popular material of choice for microfluidics researchers. It is important, therefore, to discuss the unique chemical and physical properties of PDMS networks and siloxane polymers.

1.2.1. Siloxane Networks

Because of its low surface energy, flexibility, chemical inertness, and ease of use,[65] PDMS has become a ubiquitous tool of research. Several properties of the Si-O backbone are unique in the polymer world. The bond length of Si-O (1.64 Å) is longer than the C-C bond length (1.53 Å).[66] The angle of the Si-O-Si bond is 143° (and can extend up to 180°), much larger as compared to the polyethylene C-C-C bond angle of 112° (or the general

carbon tetrahedral bond of 109.5°).[67,68] Whereas for polyethylene the energy barrier for rotation is 14 kJ/mol, the rotational energy barrier for the siloxane backbone is nearly zero.[68] Because the backbone of a siloxane chain is inherently flexible regardless of the side groups, most siloxane networks exhibit remarkable surface reorientation in response to new environments.[68,69]

The thermal and chemical properties are also unique as compared to traditional organic polymers. The siloxane bond energy of 450-570 kJ/mol is much higher than either the carbon-carbon bond (346 kJ/mol) or the carbon-oxygen bond (358 kJ/mol).[67,68] Additionally, the nature of the Si-O bond is surprisingly ionic in character, considering the difference in electronegativities in the silicon and oxygen atoms.[70] The glass transition temperature (T_g) of PDMS, which is related to the backbone flexibility, is approximately –125°C.[66] Because the thermal conductivity of PDMS is 0.2 W/mK,[71] silicones are frequently used as insulating materials.

Despite the general utility of this material, researchers often struggle to overcome problems with the hydrophobic nature of PDMS which influences surface wettability and solvent resistance. Several approaches to alter the wettability and solvent resistance of PDMS have been developed,[72,73] which we will discuss further below. One approach to this problem is to use small molecules to react with and coat the interior of the channel with organic or inorganic groups to alter solvent resistance.[32] Another solution is to physisorb polymers onto selective sites on the microfluidic channel to alter the wettability of the channel.[74] Using UV light and small molecules or monomers, the methyl side groups will

participate in free radical reactions and the small molecules will graft onto PDMS,[75] tailoring the surface properties.

Particularly in the area of microfluidics, the limitations of PDMS prevent wide-scale commercialization of lab-on-a-chip diagnostic systems and other devices. As well as the problems mentioned above, production of PDMS devices involves slow curing steps, which would not be feasible in a manufacturing setting.[76] There are several variations which make use of siloxane chemistry but are faster curing networks that can be used as alternatives.[29,33] Additionally, alternate crosslinking mechanisms can produce rigid PDMS, referred to as hard-PDMS or h-PDMS.[25] This h-PDMS formulation makes use of the rapid hydrosilylation reaction by incorporating vinyl functionalized siloxane polymers and oligosiloxane molecules, decreasing the molecular weight between crosslink points in the network. Rather than modifying PDMS networks physically or chemically, there are alternative polymers which suit the requirements for micro- and nanofabrication. Research groups have reported using thiol-enes,[77] epoxies,[78] fluoroelastomers,[31,79,80] or thermoplastics[81] as replacements for PDMS.

Poly(vinylmethylsiloxane) or PVMS combines the flexibility of PDMS but with the added benefit of reactive vinyl functionality. The vinyl group can be modified through several chemical reactions including thiol-ene addition,[82] hydrosilylation,[83] hydrophosphination,[84] epoxidation,[85] and more.[86–88] PVMS can be used to anchor proteins, enzymes, or other biologically-active molecules to enhance compatibility for cell growth.[89] Photochromic compounds can be embedded in PVMS and alterations of the vinyl groups can affect the network's optical properties.[90] Amphiphilic elastomer networks can be created by

attaching various side groups to the vinyl group, which creates a stimuli responsive surface.[69,91] Because of these advantages, we investigated the use of PVMS for microfluidic devices in this dissertation. We were interested in modifying both the surface and bulk properties of an elastomeric network for micro- and nanofabrication applications. There are several tools available for polymer property surface and bulk modification, which we will discuss below.

1.2.2. Surface Modifications

For components in a microfluidic system to function, material properties such as modulus[92] and surface chemistry[93] must be carefully tuned. Properties such as wettability and adhesion influence both fabrication processes as well as the final microfluidic device, which is in contact with a particular fluid. For example, in microcontact printing, the stamp should have sufficient wettability to pick up the "ink", but also needs to maintain its shape rather than swelling in the solvent.[22] Polymers are generally not compatible with organic solvents as polymers will tend to solubilize and deform in the presence of organic solvents.[94] In order to use polymers with organic solvents, microchannels must be coated with an organic solvent repellant layer or with a silica-like layer,[31,32,94–96] which will be discussed further below. In addition, polymers are frequently hydrophobic, which makes their utilization in biological systems difficult.

When evaluating surface modifications, it is important to clarify the types of modifications and functionalizations that can be implemented. The deposition and covalent attachment of small molecules which spontaneously assemble at a surface, forming self-

assembled monolayers (SAMs), is a starting point for many surface modification techniques. These SAMs can be used to graft ligands, grow surface-anchored polymer assemblies, or simply to protect a surface from undesirable adsorption.[97] Alternatively, noncovalent interactions between a surface and an adsorbing molecule can be used to modify a substrate via physisorption. Electrostatic interactions may be strong enough to immobilize proteins, enzymes, or ligands on a surface.[97] Oxygen plasma, UV/ozone, or UV light modify polymer interfaces and can be referred to as physicochemical modification.[97]

Because PDMS is so frequently used in microfluidics, there is a wealth of literature regarding the modification of PDMS surface properties.[73,98–102] Several modification methods have been used on PDMS devices: gas phase processing including plasma, UV/ozone, or chemical vapor deposition; liquid chemical treatments such as layer-by-layer deposition, sol-gel coatings, or silanizations; and physisorption of polymers or proteins.[73,99] PDMS lacks chemically functional groups. Researchers thus employ intense, often harsh, techniques to "activate" these surfaces for covalent bonding. Blasting the inert PDMS surface with oxygen plasma or UV/ozone degrades the material to the point that silanol groups form. Similarly, strong acids and bases can be used to activate the PDMS surface, also generating silanol and other hydrophilic groups.[101] The alternative is to rely on physisorption of surfactants, amphiphilic copolymers, or peptides, presumably with strong enough interactions with the PDMS surface that the physisorbed layer will not wash away over time.[99] Physisorbed coatings suffer from thermal and mechanical instabilities and therefore are not as robust as covalent modifications.

Surface modifications can bestow static or dynamic properties on the polymeric surface, depending on whether the surface modifications are reactive or stimuli-responsive. Static surface modifications often rely on the chemical attachment of small molecules such as silanes to alter wettability or ionic characteristics.[103] Additionally, patterning a microchannel with regions of differing wettability will "pin" organic or aqueous phases in place in a channel, creating stable liquid/liquid interfaces.[104] We will discuss surfaces with dynamic properties, specifically stimuli responsive surfaces, in greater depth below.

Stimuli Responsive Materials

Stimuli-responsive materials change their properties in response to various environmental stimuli such as pH, temperature, light, magnetic fields, or chemical agents.[105–107] Integrating stimuli-responsive materials on the surface of microfluidic devices enables fine control over fluid flow[56] as well as the sensing or manipulation of biological or chemical compounds.[97] For example, stimuli-responsive hydrogels are employed as actuators,[108] directing flow by changing in volume as a response to an environmental trigger. Polymers which move in response to a stimulus are useful for drug delivery, actuators and sensors, robotics, textiles, coatings, and other applications. Block copolymers or polymers with multiple moieties can potentially increase responsiveness if both blocks of the copolymer respond to different stimuli.[105,109] While the literature on stimuli responsive materials is far too extensive to exhaustively cover here, we will briefly discuss the usage of these materials on surfaces, which can be applied in microfluidics for bioassays or other uses.

By integrating stimuli-responsive materials into microchannels, as shown in Figure 1.6, both active and passive fluid control through external stimuli is possible.[56] The response

time of these materials varies from microseconds to minutes, and response time is critical for performance in a device. Stimuli-responsive hydrogels are capable of transducing a response from an external stimulus into mechanical action for fluid control.[110] These and other stimuli-responsive materials can significantly improve the use of microfluidics for biological systems because of the need for effective manipulation and monitoring of biological compounds.[111] Substrates coated with stimuli-responsive materials can prevent undesirable adsorption while encouraging intended cellular attachment by controlling cellular or biomolecular interactions on surfaces or interfaces.[112]

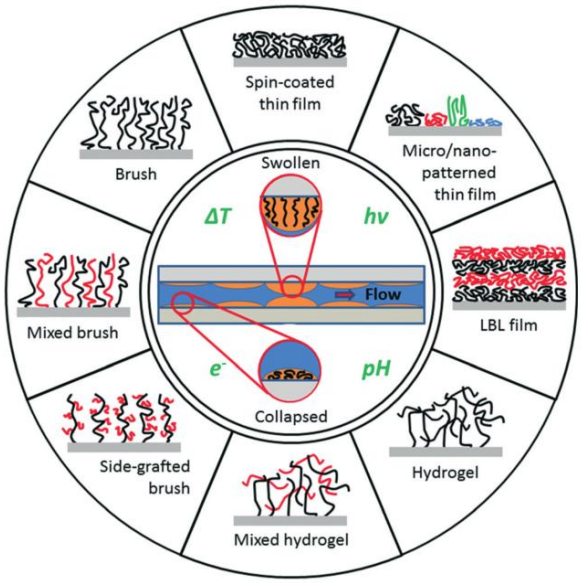

Figure 1.6: Stimuli responsive coatings integrated into a microchannel.[56]

One of the most studied and applied responsive polymers is poly(N-isopropylacrylamide) (PNIPAM), which collapses in aqueous solutions as the temperature of the solution is increased above ~32°C. This unusual property is a lower critical solution

temperature (LCST), and is contrary to most polymer solution behaviors which demonstrate increased solubility at higher temperatures. Because the LCST of PNIPAM occurs close to physiological temperatures, it shows great promise for biomedical applications. PNIPAM surfaces have been used for chromatographic separation,[113] cell attachment and release,[114] and membrane modification.[115] At low grafting densities, PNIPAM brushes exhibit behavior similar to behavior in the bulk, but at high grafting densities, the chains are conformationally constrained and can no longer rearrange in response to stimuli.[116]

We chose to use elastin-like polypeptides (ELPs) for the research in this dissertation because of their highly controlled amino acid composition, length, and transition temperature, which we will discuss further in Chapter 4.

1.2.3. Bulk Modifications

Polymers are useful materials for MEMs and microfluidics for several reasons: polymers allow mechanical flexibility, can be processed at low cost, and provide a wide catalog of chemical, mechanical, and biological functionalities.[6] In regards to the last point, polymers can be modified significantly to match the mechanical requirements of a system or system component. Especially with thermoset polymer networks, tuning the amount of crosslinking in the network can alter the modulus by orders of magnitude.[117] Increasing crosslink density by decreasing the molecular weight between crosslinks (M_c) has also been shown to tune effectively the mechanical properties of hydrogels.[118] Using this technique in a microfluidic setup, cell researchers can investigate the interactions of cells with substrates with varying stiffnesses.[119]

Additionally, choosing a stiff chain backbone will generate a more rigid network, whereas a flexible chain, such as a siloxane polymer, will create a softer, more elastic network. A polyurethane with a high molecular weight but a rigid, cyclic aliphatic group in the backbone forms a stiff network and can replicate nanofeatures by replica molding[27]. Swapping out one crosslinking agent for a more flexible molecule will take the tensile modulus of the polyurethane network from 320 MPa down to 20 MPa.[120]

Polymers make excellent structural materials for microfluidic systems because it is possible to choose a material with a specifically tailored modulus for each application.[117] Combining different layers and component pieces will provide additional functionality due to differing mechanical performances of each material. Microfluidic membranes must deform appropriately or resist deformation based on the pressure or flowrate within the device.[121] If the membrane is made of PDMS, for example, making the surrounding channel out of a more rigid material, such as poly(methylmethacrylate) (PMMA), ensures that only the PDMS layer will deform with pressure.[122] Microfluidic pumps rely on the careful tailoring of the flexibility of the diaphragm in the pumping chamber(s) with the application of pressure.[123]

Materials with micro- or nanostructures display complex mechanical properties, including mechanical metamaterials which may possess a negative dynamic modulus.[124] There is a growing interest in "dynamic" functional groups; these are molecular structures which chemically rearrange in response to external stimuli, including transitioning from a soft polymeric matrix to a harder matrix.[125] Dynamic covalent bonds in polymeric systems can rearrange in response to stress, breaking bonds and forming new bonds, even after polymerization.[126] For example, polyacylhydrazones form either hard or soft films through

monomer functional group tuning, and the softer films can be converted later into more rigid films with the dynamic inclusion of alternative monomers.[127]

Tuning of polymeric mechanical properties enables the construction of specialized components of microfluidic devices, as well as enabling dynamic behavior in response to the conditions within the microchannels. One important consideration when applying any polymeric material to a chemical or biochemical device is the resistance of that polymer matrix to swelling in the presence of aqueous or organic solvents.

1.2.4. Solvent Resistance

PDMS swells in the presence of many organic solvents and oils.[93] PDMS networks can both absorb small molecules when used in microfluidic applications[128] and leach out unreacted oligomers into solution.[93] Coating PDMS with protective layers such as glass-like layers[129] or fluoropolymers[130] prevents swelling. Although these coatings allow researchers to use familiar techniques and equipment to fabricate the initial PDMS channels, successfully generating solvent resistance requires several additional fabrication steps. For the fluoropolymer, for example, a precursor is first flowed through the channel, followed by baking in the oven, an additional flow step, and a final bake.[130] The generation of glass-like coatings by sol-gel techniques is time sensitive, which would undoubtedly lead to variations in coating quality and thickness based on the attentiveness of the researcher preparing these coatings.[129]

A common approach to deal with solvent resistance issues is to use alternative crosslinked polymers instead of PDMS. Commercially available perfluroropolyethers, once

crosslinked, resist swelling in common solvents.[79] These materials must be crosslinked stoichiometrically "off-ratio" in order to seal two layers of the perfluoropolyether to make a channel, and cannot be strongly adhered to glass.[79] Thiol-ene resins, also cured off-stoichiometric ratio, resist swelling when made using small molecules, as this leads to a highly crosslinked material. Because thiol-enes do not shrink significantly when curing, they replicate microchannel master molds with high fidelity, but these channels require a complicated procedure to seal.[76]

1.3. Polymer Modifications through Photochemistry

At the most basic level, photochemistry is the process through which a molecule absorbs a photon of energy causing the molecule's electronic state to transition from the ground state to an excited state, followed by a chemical reaction of some type.[131] Because light delivers more energy over a shorter timescale than thermal processes, photochemical pathways are convenient as well as efficient.[132] Additionally, light can be delivered locally for short periods of time, giving spatial and temporal control over the modification area. When light interacts with molecules, three reaction types are possible: isomerization reactions (cis to trans or vice versa), bond formation, or bond cleavage.[132] In order for any of these reactions to occur, however, the target molecule must absorb the wavelength of light being used, and the photon must have enough energy to transition an electron from a lower orbital to a higher orbital.[131,132]

In polymer science, light can be used to synthesize polymer chains,[133] to crosslink chains into networks,[134] or even to provide energy for motion in polymer sheets.[135] High

energy photons can also degrade polymeric materials, which can be a problem if long exposures are required to activate a crosslinking or polymerization reaction. In PDMS, light can attack methyl side groups, removing the entire group or abstracting a hydrogen, which leads to further free radical reactions.[136] Additionally, in the presence of both oxygen and UV light, silanol groups and silylhydroperoxide groups can form from a silyl radical, creating a more hydrophilic network.[137] Using either UV/Ozone or oxygen plasma will create surface silanol groups and increase hydrophilicity, though the effects are usually temporary.[138] We will primarily be discussing the use of photochemical reactions for the modification of surface and bulk properties of polymers in this dissertation. We will now discuss photoinitiated reactions used in this dissertation, namely free radical reactions and thiol-ene reactions.

1.3.1. Free Radical Reactions

Although there are thermally induced and photo-induced free radical reactions, we will discuss only photoinitiated reactions in this section. In the case of photoinitiated free radical polymerizations, an initiator species first generates a radical which can then attack a monomer. Generally, only the initiation step relies on light; the propagation and termination steps usually take place in either light or dark.[139] There are several families of photoinitiators depending on the mechanism by which they generate a free radical. The most effective is the photoscission of a photoinitiator generating a pair of free radicals.[140] Other types of initiators generate radicals through hydrogen abstraction or through a photoinduced electron transfer.[140]

Photopolymerization can refer to both the creation of polymer chains through photoinitiator and monomer system or to the crosslinking of existing polymer chains, which can react through side groups upon exposure to light, into a network. For both of these processes, the increase in viscosity during the free radical reaction influences the ultimate conversion of reactive groups as well as the overall reaction kinetics.[141] Free radicals have a short life span and are susceptible to quenching by oxygen. Therefore if the radicals are unable to find an unreacted functional group nearby, the radical is essentially wasted. In crosslinked systems, as the crosslinking density increases, radicals become more mobile through propagation reactions than by diffusion, called reaction diffusion-controlled termination.[142] This high concentration of free radicals (despite the dwindling number of available double bonds for reaction), which are now diffusion controlled results in an increase in the radical reaction rate, referred to as autoacceleration or the Trommsdorff effect.[142]

As discussed in further in Chapter 2 and Chapter 5, photoinitiated crosslinking represents an effective tool for controlling mechanical properties of polymer networks. When crosslinking polymer films, it is important to note that for thick films, light may not penetrate the entire film, depending on the thickness and the absorption of the polymer.[139] Benzoyl groups are frequently used as the photoinitiators for free radical reactions as the aromatic carbonyl readily forms radicals through hydrogen abstraction or homolytic cleavage, as shown in Figure 1.7.[134] Acrylates and vinyl groups both participate in free radical mechanisms.

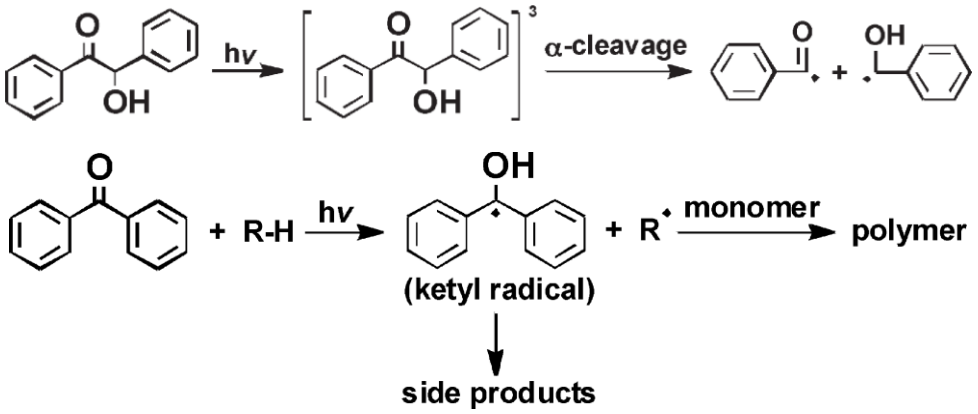

Figure 1.7: A) Homolytic cleavage of a benzoyl photoinitiator. B) Hydrogen abstraction of a benzoyl photoinitiator.[133]

1.3.2. Thiol-ene Chemistry

The history of reacting sulfur containing groups with carbon-carbon double bonds is long and extensive, dating back more than 80 years.[143] More recently, the popularity of thiol-ene reactions expanded largely due to the inherent advantages of this system, including quantitative yields, insensitivity to oxygen, low shrinkage, and easy adaptability to a wide range of thiol or ene containing molecules.[144] Photoinitiated thiol-ene reactions, depicted in Figure 1.8, represent a subset of free radical reactions: the mechanism involves step growth addition, but the propagation takes place through a free radical chain transfer process.[140] The initiation step of thiol-ene reactions generates a thiyl radical, where hydrogen is abstracted from the thiol group. This thiyl radical then attacks a carbon-carbon double bond, forming a carbon radical which can then attack another thiol, propagating the reaction.[145]

For thiol-ene systems to successfully crosslink, the rate of hydrogen transfer from the sulfur must be competitive with the rate of alkene polymerization or reaction.[139] In other

words, the vinyl group should not prefer to homopolymerize, but rather should participate in the alternating thiol/ene propagation mechanism.[145] While the thiol-ene reaction is remarkably tolerant of oxygen, it is necessary for the concentration of thiols to exceed the concentration of oxygen in the crosslinking system.[146]

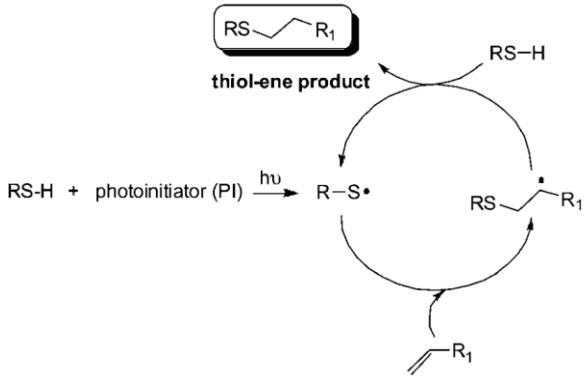

Figure 1.8: The basic photointiated thiol-ene reaction scheme.[146]

Thiol-ene reactions can also take place in the absence of photoinitiators.[147] This is quite advantageous for polymers designed to be used outdoors: polymer systems with photoinitiators will degrade and age poorly with exposure to sunlight. Thiol-ene polymerizations proceed rapidly when the reaction components are illuminated by 254 nm wavelength light.[147] This is due to the absorption characteristics of thiols, which tend to absorb strongly at wavelengths below 300 nm. It is possible, however, to crosslink a thiol-ene system with 365 nm light, although the mechanism of this reaction is still unclear.[148] The reaction kinetics of any thiol-ene system depend heavily on the types of thiol and alkene being used, as each system has a different reaction rate.[148] For example, the stability of the

carbon radical and the electron density of the vinyl group both impact the reaction reactions of a particular thiol-ene system, with a low electron density increasing the overall reaction rate and a stable radical decreasing the rate of chain transfer reactions.[149]

1.3.3. Photocurable Siloxanes

Photocurable silicones are used in medical products,[150] as coatings,[151] and for optical devices.[152] Thiol-ene, acrylate, and vinyl-based photocurable siloxane systems have all been reported in the literature. Polysiloxanes which can photocure contain either carbon-carbon double bonds or acrylate pendant groups. Thiol-ene formulations contain vinyl functional chains, as in the Sylgard-184® commercial kit (Dow Corning corporation), and another part mercaptosilicones.[140,153–155] These thiol-ene reactions may be used for either crosslinking of siloxane networks[156] or for side group modification.[157,158] Interestingly, thiol-ene cured siloxane networks do not necessarily exhibit autoacceleration during crosslinking,[159] possibly due to the high degree of flexibility of the siloxane backbone which would enable greater free radical mobility.

Silicone elastomer networks derived from thiol-enes are useful as rapidly curing, low modulus networks for applications such as ophthalmic devices, gaskets, and optical fiber coatings.[160] Much of the work done using vinyl functional siloxanes in thiol-ene curing systems has been reported in patent literature.[153–155] More recently, thiol-ene crosslinked silicone elastomers were impregnated with lanthanide compounds, giving the networks photoluminescence under UV light.[161] Photocurable thiol-ene siloxanes made from oligosiloxanes rather than polysiloxanes exhibit transparency and good thermal stability.[162]

The photoinduced crosslinking of siloxanes with acrylate pendant groups demonstrates the favorable material properties of silicones and the rapid crosslinking of polyacrylic esters.[141,151,163] One advantage of siloxane acrylates over traditional epoxies or non-siloxane based acrylates is optical transparency in the near-UV range.[164] However, because siloxanes are permeable to oxygen, the dissolved oxygen present in the siloxane polymer will inhibit the initiation of the reaction, delaying crosslinking of the acrylate until all oxygen is consumed.[141] Adjustments to the light intensity and the type of photoinitiator used in a siloxane-acrylate photocrosslinking system will increase the overall conversion rate.[165,166]

While there is not much research carried out on specifically using free radical reactions to crosslink PVMS, vinyl-pendant siloxane free radical reactions have been explored in the literature.[82,167,168] Vinylsiloxanes can be induced to participate in free radical reactions through the decomposition of peroxides into peroxide radicals when heated or exposed to light.[160] The silicon-vinyl bond will not undergo photoscission when irradiated by wavelengths of light in the visible range (λ>300 nm),[167] so photoinitiators must be used for visible light photocuring. Monomers containing vinyl groups are used for photopolymerizations, both for crosslinked network formation,[142] as depicted in Figure 1.9, and for polymeric chain synthesis. Vinyl functional siloxanes also undergo crosslinking under high energy gamma irradiation with no photoinitiator present.[169]

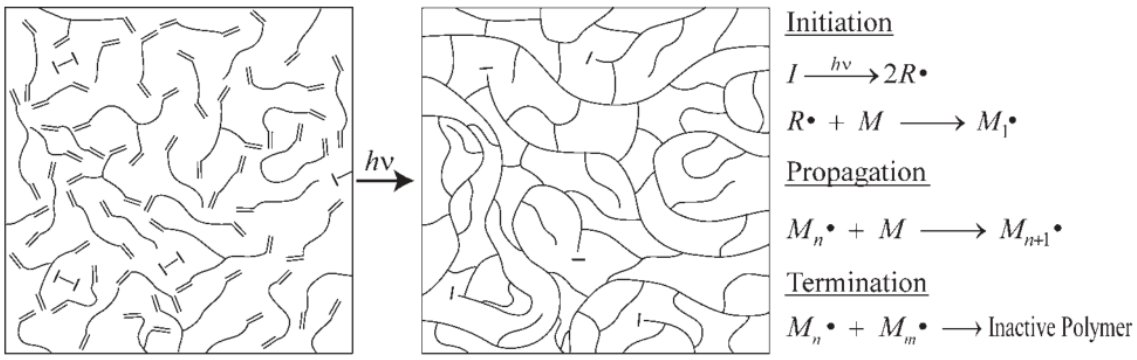

Figure 1.9: The photopolymerization process and steps.[142]

Photosensitive PDMS has been investigated and tested in the literature.[170–172] Benzophenone, a dicyclic benzoyl type compound, is most frequently used in photo-sensitive PDMS materials.[171–176] Although numerous free radical reactions have been proposed for PDMS,[177] benzophenone is known to be able to abstract hydrogen atoms from almost all polymers,[178] and is most likely attacking only the methyl groups of PDMS (*cf.* Figure 1.10). If C=C bonds are present as side groups in a poly(dimethyl-co-vinylmethyl siloxane) chain, the free radical reaction initiated by benzophenone or other photoinitiator is assumed to be taking place primarily through the vinyl groups.[173]

In microfabrication, UV-sensitive PDMS has been used both as a photoresist[171,175,179] and as a preparatory step for microchannel modification.[174] Siloxane photoresists usually show poor resolution (minimum resolution 60-100 μm), with sloping sidewalls and a lack of fidelity to the original features.[171,172,175] Photo-PDMS demonstrates some flexibility, elongating to approximately 50%, and a tensile modulus similar to that of Sylgard 184®.[171] For microfluidic modification, benzophenone dissolved in acetone and flowed through a

PDMS microchannel diffuses into the matrix around the channel, enabling UV grafting on the channel side walls.[174] In Chapter 2 of this dissertation, we use a similar method of photoinitiator delivery to a poly(vinylmethylsiloxane) microchannel, but with significantly different results after UV treatment.

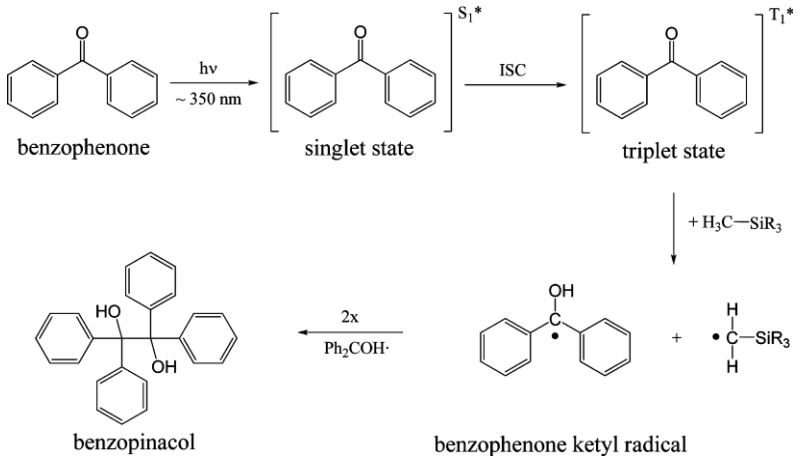

Figure 1.10: Mechanism of action of benzophenone when exposed to UV light in the presence of PDMS. Once in the triplet excited state, benzophenone relaxes by hydrogen abstraction from a methyl group.[174]

1.4. Outline of the Work in this Dissertation

Ideally, a material used for soft lithography, nanoimprint lithography, or microfluidics, should be tunable based on the specific requirements of the final device. Being able to tune both the surface chemistry and the mechanical properties of a polymer would enable its use in a wide range of applications. In this dissertation, we explore both surface modifications and mechanical adjustments for various micro- and nanodevices. We use photochemistry and the covalent attachment of stimuli-responsive peptides to modify elastomeric materials for micro- and nanofabrication.

First, we discuss the use of poly(vinylmethylsiloxane) (PVMS) for solvent resistant microchannels in Chapter 2. Through local crosslinking of the vinyl side groups, we are able to locally harden the material and avoid swelling in organic solvents. We demonstrate that although the modulus of the UV-treated PVMS network is orders of magnitude higher than untreated PVMS, the surface is chemically similar to the original network. PVMS has the potential to be used as a drop-in replacement for PDMS, with the added functionality that the vinyl groups offer.

Next, in Chapter 3, we investigate the use of nanoparticles as reinforcement agents in PVMS elastomeric networks. In contrast to the UV-treated PVMS microchannels, we target an elastic behavior in the PVMS networks, but with improved elongation and toughness. Using both fumed silica and *in situ* generated silica particles, we see improvements in the elongation and modulus of our reinforced PVMS networks.

We then turn to the modification of microfluidic surfaces with stimuli-responsive materials in Chapter 4. Our goal in this case is to generate an elastin-like polypeptide (ELP) brush on the surface of PVMS networks for thermally responsive behaviors. We first investigated a heated deposition technique to increase the grafting density of peptides on a control silicon surface. By depositing collapsed peptides in a heated solution, we found that temperature responsiveness was lost because the deposited aggregates exhibited high stability, due both to ELP concentration and to non-specific interactions with the substrate. We also performed initial investigations of the modification of PVMS with polypeptides by a simple grafting method.

Finally, in Chapter 5 we investigate the impact of modulus and surface chemistry on the nanofabrication method referred to as nanoskiving. Because nanoskiving originated from biological microtomy, the original resins used in this technique were poorly suited for metal encapsulation. We therefore investigate thiol-ene based photocurable resins, which cure rapidly, exhibit low shrinkage, and are mechanically adjustable. These resins are used to generate high quality sections of gold nanowires through ultramicrotomy. We demonstrate the performance of several epoxies and thiol-enes and compare the mechanical and adhesion properties of the materials. Using the thiol-ene resins, we evaluate the electrical performance of a nanoskived metal nanowires.

1.5. References

[1] Del Campo, A. & Arzt, E. Fabrication Approaches for Generating Complex Micro- and Nanopatterns on Polymeric Surfaces. Chem Rev 108, 911–945 (2008).

[2] Xia, Y. & Whitesides, G. M. Soft Lithography. Angew. Chem. Int. Ed. 37, 550–575 (1998).

[3] Wolfe, D. B., Love, J. C. & Whitesides, G. M. in Dekker Encyclopedia of Nanoscience and Nanotechnology 2657–2666 (2004).

[4] Becker, H. & Manz, A. Microsystem technology in chemistry and life science. (Springer, 1998).

[5] Becker, H. & Gärtner, C. Polymer microfabrication technologies for microfluidic systems. Anal. Bioanal. Chem. 390, 89–111 (2008).

[6] Liu, C. Recent Developments in Polymer MEMS. Adv. Mater. 19, 3783–3790 (2007).

[7] Dittrich, P. S. & Manz, A. Lab-on-a-chip: microfluidics in drug discovery. Nat. Rev. Drug Discov. 5, 210–218 (2006).

[8] Burns, M. A. et al. An Integrated Nanoliter DNA Analysis Device. Science 282, 484–487 (1998).

[9] Xia, Y., Rogers, J. A., Paul, K. E. & Whitesides, G. M. Unconventional Methods for Fabricating and Patterning Nanostructures. Chem. Rev. 99, 1823–1848 (1999).

[10] Qin, D., Xia, Y. & Whitesides, G. M. Soft lithography for micro- and nanoscale patterning. Nat. Protoc. 5, 491–502 (2010).

[11] Quake, S. R. From Micro- to Nanofabrication with Soft Materials. Science 290, 1536–1540 (2000).

[12] Huh, D. et al. Tuneable elastomeric nanochannels for nanofluidic manipulation. Nat. Mater. 6, 424–428 (2007).

[13] Bates, C. M., Maher, M. J., Janes, D. W., Ellison, C. J. & Willson, C. G. Block Copolymer Lithography. Macromolecules (2013). doi:10.1021/ma401762n

[14] Hamley, I. Nanostructure fabrication using block copolymers. Nanotechnology 14, R39 (2003).

[15] Choi, H. K., Kim, M. H., Im, S. H. & Park, O. O. Fabrication of Ordered Nanostructured Arrays Using Poly(dimethylsiloxane) Replica Molds Based on Three-Dimensional Colloidal Crystals. Adv. Funct. Mater. 19, 1594–1600 (2009).

[16] Hassanin, H., Mohammadkhani, A. & Jiang, K. Fabrication of hybrid nanostructured arrays using a PDMS/PDMS replication process. Lab. Chip 12, 4160 (2012).

[17] Arzt, E. & del Campo, A. Generating Micro- and Nanopatterns on Polymeric Materials.

[18] Zhang, G., Zhang, J., Xie, G., Liu, Z. & Shao, H. Cicada Wings: A Stamp from Nature for Nanoimprint Lithography. Small 2, 1440–1443 (2006).

[19] Chang, K.-C. et al. Nanocasting Technique to Prepare Lotus-leaf-like Superhydrophobic Electroactive Polyimide as Advanced Anticorrosive Coatings. ACS Appl. Mater. Interfaces 5, 1460–1467 (2013).

[20] Sun, M. et al. Artificial Lotus Leaf by Nanocasting. Langmuir 21, 8978–8981 (2005).

[21] Hui, C. Y., Jagota, A., Lin, Y. Y. & Kramer, E. J. Constraints on Microcontact Printing Imposed by Stamp Deformation. Langmuir 18, 1394–1407 (2002).

[22] Perl, A., Reinhoudt, D. N. & Huskens, J. Microcontact Printing: Limitations and Achievements. Adv. Mater. 21, 2257–2268 (2009).

[23] Kaufmann, T. & Ravoo, B. J. Stamps, inks and substrates: polymers in microcontact printing. Polym. Chem. 1, 371–387 (2010).

[24] Guo, L. J. Nanoimprint Lithography: Methods and Material Requirements. Adv. Mater. 19, 495–513 (2007).

[25] Schmid, H. & Michel, B. Siloxane Polymers for High-Resolution, High-Accuracy Soft Lithography. Macromolecules 33, 3042–3049 (2000).

[26] Lee, B. K. et al. Photocurable Silsesquioxane-Based Formulations as Versatile Resins for Nanoimprint Lithography. Langmuir 26, 14915–14922 (2010).

[27] Yoo, P. J. et al. Unconventional Patterning with A Modulus-Tunable Mold: From Imprinting to Microcontact Printing. Chem. Mater. 16, 5000–5005 (2004).

[28] Hagberg, E. C., Malkoch, M., Ling, Y., Hawker, C. J. & Carter, K. R. Effects of Modulus and Surface Chemistry of Thiol-Ene Photopolymers in Nanoimprinting. Nano Lett 7, 233–237 (2007).

[29] Choi, K. M. & Rogers, J. A. A Photocurable Poly(dimethylsiloxane) Chemistry Designed for Soft Lithographic Molding and Printing in the Nanometer Regime. J. Am. Chem. Soc. 125, 4060–4061 (2003).

[30] Choi, K. M. Photopatternable Silicon Elastomers with Enhanced Mechanical Properties for High-Fidelity Nanoresolution Soft Lithography. J Phys Chem B 109, 21525–21531 (2005).

[31] Rolland, J. P., Van Dam, R. M., Schorzman, D. A., Quake, S. R. & DeSimone, J. M. Solvent-Resistant Photocurable 'Liquid Teflon' for Microfluidic Device Fabrication. J. Am. Chem. Soc. 126, 2322–2323 (2004).

[32] Kim, B.-Y., Hong, L.-Y., Chung, Y.-M., Kim, D.-P. & Lee, C.-S. Solvent-Resistant PDMS Microfluidic Devices with Hybrid Inorganic/Organic Polymer Coatings. Adv. Funct. Mater. 19, 3796–3803 (2009).

[33] Zheng, P. & McCarthy, T. J. D4H/D4V Silicone: A Replica Material with Several Advantages for Nanoimprint Lithography and Capillary Force Lithography. Langmuir 27, 7976–7979 (2011).

[34] Ji, X.-H. et al. On-demand preparation of quantum dot-encoded microparticles using a droplet microfluidic system. Lab. Chip 11, 2561 (2011).

[35] Thiele, J. et al. Early development drug formulation on a chip: Fabrication of nanoparticles using a microfluidic spray dryer. Lab. Chip 11, 2362 (2011).

[36] So, J.-H. et al. Reversibly Deformable and Mechanically Tunable Fluidic Antennas. Adv. Funct. Mater. 19, 3632–3637 (2009).

[37] Ilievski, F., Mazzeo, A. D., Shepherd, R. F., Chen, X. & Whitesides, G. M. Soft Robotics for Chemists. Angew. Chem. Int. Ed. 50, 1890–1895 (2011).

[38] Nghe, P. et al. Microfluidics and complex fluids. Lab. Chip 11, 788 (2011).

[39] Abgrall, P. & Nguyen, N. T. Nanofluidic Devices and Their Applications. Anal. Chem. 80, 2326–2341 (2008).

[40] Squires, T. M. & Quake, S. R. Microfluidics: Fluid physics at the nanoliter scale. Rev. Mod. Phys. 77, 977–1026 (2005).

[41] Duffy, D. C., McDonald, J. C., Schueller, O. J. A. & Whitesides, G. M. Rapid Prototyping of Microfluidic Systems in Poly(dimethylsiloxane). Anal. Chem. 70, 4974–4984 (1998).

[42] Stone, H. A., Stroock, A. D. & Ajdari, A. Engineering Flows in Small Devices. Annu. Rev. Fluid Mech. 36, 381–411 (2004).

[43] Park, J. I., Saffari, A., Kumar, S., Günther, A. & Kumacheva, E. Microfluidic Synthesis of Polymer and Inorganic Particulate Materials. Annu. Rev. Mater. Res. 40, 415–443 (2010).

[44] Iida, K. et al. Living anionic polymerization using a microfluidic reactor. Lab. Chip 9, 339–345 (2009).

[45] Chan, E. M., Alivisatos, A. P. & Mathies, R. A. High-Temperature Microfluidic Synthesis of CdSe Nanocrystals in Nanoliter Droplets. J. Am. Chem. Soc. 127, 13854–13861 (2005).

[46] Domachuk, P., Tsioris, K., Omenetto, F. G. & Kaplan, D. L. Bio-microfluidics: Biomaterials and Biomimetic Designs. Adv. Mater. 22, 249–260 (2010).

[47] Malmstadt, N., Yager, P., Hoffman, A. S. & Stayton, P. S. A Smart Microfluidic Affinity Chromatography Matrix Composed of Poly(N-isopropylacrylamide)-Coated Beads. Anal. Chem. 75, 2943–2949 (2003).

[48] Khandurina, J. & Guttman, A. Bioanalysis in microfluidic devices. J. Chromatogr. A 943, 159–183 (2002).

[49] Bange, A., Halsall, H. B. & Heineman, W. R. Microfluidic immunosensor systems. Biosens. Bioelectron. 20, 2488–2503 (2005).

[50] Zhang, C., Xu, J., Ma, W. & Zheng, W. PCR microfluidic devices for DNA amplification. Biotechnol. Adv. 24, 243–284 (2006).

[51] Andersson, H. & van den Berg, A. Microfluidic devices for cellomics: a review. Sens. Actuators B Chem. 92, 315–325 (2003).

[52] Khademhosseini, A., Langer, R., Borenstein, J. & Vacanti, J. P. Microscale technologies for tissue engineering and biology. Proc. Natl. Acad. Sci. U. S. A. 103, 2480–2487 (2006).

[53] Nge, P. N., Rogers, C. I. & Woolley, A. T. Advances in Microfluidic Materials, Functions, Integration, and Applications. Chem. Rev. 113, 2550–2583 (2013).

[54] Sackmann, E. K., Fulton, A. L. & Beebe, D. J. The present and future role of microfluidics in biomedical research. Nature 507, 181–189 (2014).

[55] Goddard, J. M. & Hotchkiss, J. H. Polymer surface modification for the attachment of bioactive compounds. Prog. Polym. Sci. 32, 698–725 (2007).

[56] Kieviet, B. D., Schön, P. M. & Vancso, G. J. Stimulus-responsive polymers and other functional polymer surfaces as components in glass microfluidic channels. Lab. Chip 14, 4159–4170 (2014).

[57] Ren, K., Zhou, J. & Wu, H. Materials for Microfluidic Chip Fabrication. Acc. Chem. Res. 46, 2396–2406 (2013).

[58] Kuo, J. S. & Chiu, D. T. Disposable microfluidic substrates: Transitioning from the research laboratory into the clinic. Lab. Chip 11, 2656–2665 (2011).

[59] Berthier, E., Young, E. W. K. & Beebe, D. Engineers are from PDMS-land, Biologists are from Polystyrenia. Lab. Chip 12, 1224–1237 (2012).

[60] Regehr, K. J. et al. Biological implications of polydimethylsiloxane-based microfluidic cell culture. Lab. Chip 9, 2132 (2009).

[61] Chantiwas, R. et al. Flexible fabrication and applications of polymer nanochannels and nanoslits. Chem. Soc. Rev. 40, 3677–3702 (2011).

[62] Ng, J. M. K., Gitlin, I., Stroock, A. D. & Whitesides, G. M. Components for integrated poly(dimethylsiloxane) microfluidic systems. ELECTROPHORESIS 23, 3461–3473 (2002).

[63] Zheng, Y., Dai, W., Ryan, D. & Wu, H. Fabrication of freestanding, microperforated membranes and their applications in microfluidics. Biomicrofluidics 4, 036504 (2010).

[64] Song, W., Vasdekis, A. E. & Psaltis, D. Elastomer based tunable optofluidic devices. Lab. Chip 12, 3590–3597 (2012).

[65] Wilbur, J. L. et al. Elastomeric Optics. Chem. Mater. 8, 1380–1385 (1996).

[66] Mark, J. E. Some interesting things about polysiloxanes. Acc. Chem. Res. 37, 946–953 (2004).

[67] Inorganic polymers. (Nova Science Publishers, 2007).

[68] Clarson, S. J. Siloxane polymers. (Prentice Hall, 1993).

[69] Crowe-Willoughby, J. A. & Genzer, J. Formation and Properties of Responsive Siloxane-Based Polymeric Surfaces with Tunable Surface Reconstruction Kinetics. Adv. Funct. Mater. 19, 460–469 (2009).

[70] Oberhammer, H. & Boggs, J. E. Importance of (p-d).pi. bonding in the siloxane bond. J. Am. Chem. Soc. 102, 7241–7244 (1980).

[71] Kong, S. M., Mariatti, M. & Busfield, J. J. C. Effects of types of fillers and filler loading on the properties of silicone rubber composites. J. Reinf. Plast. Compos. 30, 1087–1096 (2011).

[72] Abbasi, F., Mirzadeh, H. & Katbab, A.-A. Modification of polysiloxane polymers for biomedical applications: a review. Polym. Int. 50, 1279–1287 (2001).

[73] Zhou, J., Ellis, A. V. & Voelcker, N. H. Recent developments in PDMS surface modification for microfluidic devices. ELECTROPHORESIS 31, 2–16 (2010).

[74] Logtenberg, H., Lopez-Martinez, M. J., Feringa, B. L., Browne, W. R. & Verpoorte, E. Multiple flow profiles for two-phase flow in single microfluidic channels through site-selective channel coating. Lab. Chip 11, 2030 (2011).

[75] Hu, S. et al. Tailoring the surface properties of poly (dimethylsiloxane) microfluidic devices. Langmuir 20, 5569–5574 (2004).

[76] Carlborg, C. F., Haraldsson, T., Öberg, K., Malkoch, M. & van der Wijngaart, W. Beyond PDMS: off-stoichiometry thiol–ene (OSTE) based soft lithography for rapid prototyping of microfluidic devices. Lab. Chip 11, 3136 (2011).

[77] Good, B. T., Reddy, S., Davis, R. H. & Bowman, C. N. Tailorable low modulus, reversibly deformable elastomeric thiol–ene materials for microfluidic applications. Sens. Actuators B Chem. 120, 473–480 (2007).

[78] Jung, K. H. & Bae, B.-S. Synthesis and characterization of photopatternable epoxy hybrid materials for the fabrication of thick and thermally stable microstructures with a high aspect ratio. J. Appl. Polym. Sci. 108, 3169–3176 (2008).

[79] Devaraju, N. S. G. K. & Unger, M. A. Multilayer soft lithography of perfluoropolyether based elastomer for microfluidic device fabrication. Lab. Chip 11, 1962 (2011).

[80] Williams, S. S. et al. High-resolution PFPE-based molding techniques for nanofabrication of high-pattern density, sub-20 nm features: a fundamental materials approach. Nano Lett. 10, 1421–1428 (2010).

[81] Rohr, T., Ogletree, D. F., Svec, F. & Fréchet, J. M. J. Surface functionalization of thermoplastic polymers for the fabrication of microfluidic devices by photoinitiated grafting. Adv. Funct. Mater. 13, 264–270 (2003).

[82] Herczynska, L., Lestel, L., Boileau, S., Chojnowski, J. & Polowinski, S. Modification of polysiloxanes by free-radical addition of pyridylthiols to the vinyl groups of the polymer. Eur. Polym. J. 35, 1115–1122 (1999).

[83] Chojnowski, J., Cypryk, M., Fortuniak, W., Ścibiorek, M. & Rózga-Wijas, K. Synthesis of Branched Polysiloxanes with Controlled Branching and Functionalization by Anionic Ring-Opening Polymerization. Macromolecules 36, 3890–3897 (2003).

[84] Silicon-Containing Polymers - The Science and Technology of Their Synthesis and Applications. (Kluwer Academic Publishers, 2000). at <http://www.springer.com/chemistry/inorganic+chemistry/book/978-0-412-83110-2>

[85] Bauer, J., Hüsing, N. & Kickelbick, G. Preparation of functionalized block copolymers based on a polysiloxane backbone by anionic ring-opening polymerization. J. Polym. Sci. Part Polym. Chem. 40, 1539–1551 (2002).

[86] Chojnowski, J., Cypryk, M., Fortuniak, W., Rózga-Wijas, K. & Ścibiorek, M. Controlled synthesis of vinylmethylsiloxane–dimethylsiloxane gradient, block and alternate copolymers by anionic ROP of cyclotrisiloxanes. Polymer 43, 1993–2001 (2002).

[87] Cai, G. & Weber, W. P. Synthesis and chemical modification of poly(divinylsiloxane). Polymer 43, 1753–1759 (2002).

[88] Gupta, S. K. & Weber, W. P. Ruthenium-Catalyzed Chemical Modification of Poly(vinylmethylsiloxane) with 9-Acetylphenanthrene. Macromolecules 35, 3369–3373 (2002).

[89] Ahmed, S. et al. Poly(vinylmethylsiloxane) Elastomer Networks as Functional Materials for Cell Adhesion and Migration Studies. Biomacromolecules 12, 1265–1271 (2011).

[90] Yang, H.-K., Evren Özçam, A., Efimenko, K. & Genzer, J. Photochromic materials with tunable color and mechanical flexibility. Soft Matter 7, 3766 (2011).

[91] Crowe-Willoughby, J. A., Stevens, D. R., Genzer, J. & Clarke, L. I. Investigating the Molecular Origins of Responsiveness in Functional Silicone Elastomer Networks. Macromolecules 43, 5043–5051 (2010).

[92] Schneider, F., Fellner, T., Wilde, J. & Wallrabe, U. Mechanical properties of silicones for MEMS. J. Micromechanics Microengineering 18, 065008 (2008).

[93] Lee, J. N., Park, C. & Whitesides, G. M. Solvent Compatibility of Poly(dimethylsiloxane)-Based Microfluidic Devices. Anal. Chem. 75, 6544–6554 (2003).

[94] Kitsara, M. & Ducrée, J. Integration of functional materials and surface modification for polymeric microfluidic systems. J. Micromechanics Microengineering 23, 033001 (2013).

[95] Renckens, T. J. A. et al. Micromolding of solvent resistant microfluidic devices. Lab. Chip 11, 2035 (2011).

[96] Vitale, A. et al. Unconventional Photolithography of Perfluoropolyethers for Solvent-resistant Microfluidics. Langmuir (2013). doi:10.1021/la402755q

[97] Surface design: applications in bioscience and nanotechnology. (Wiley-VCH, 2009).

[98] Almutairi, Z., Ren, C. L. & Simon, L. Evaluation of polydimethylsiloxane (PDMS) surface modification approaches for microfluidic applications. Colloids Surf. Physicochem. Eng. Asp. 415, 406–412 (2012).

[99] Wong, I. & Ho, C.-M. Surface molecular property modifications for poly(dimethylsiloxane) (PDMS) based microfluidic devices. Microfluid. Nanofluidics 7, 291–306 (2009).

[100] Zhou, J., Khodakov, D. A., Ellis, A. V. & Voelcker, N. H. Surface modification for PDMS-based microfluidic devices. ELECTROPHORESIS 33, 89–104 (2012).

[101] Makamba, H., Kim, J. H., Lim, K., Park, N. & Hahn, J. H. Surface modification of poly(dimethylsiloxane) microchannels. ELECTROPHORESIS 24, 3607–3619 (2003).

[102] Tu, Q. et al. Surface modification of poly(dimethylsiloxane) and its applications in microfluidics-based biological analysis. Rev. Anal. Chem. 31, (2012).

[103] Belder, D. & Ludwig, M. Surface modification in microchip electrophoresis. ELECTROPHORESIS 24, 3595–3606 (2003).

[104] Atencia, J. & Beebe, D. J. Controlled microfluidic interfaces. Nature 437, 648–655 (2005).

[105] Schattling, P., Jochum, F. D. & Theato, P. Multi-stimuli responsive polymers – the all-in-one talents. Polym. Chem. 5, 25–36 (2013).

[106] Meng, H. & Jinlian Hu. A Brief Review of Stimulus-active Polymers Responsive to Thermal, Light, Magnetic, Electric, and Water/Solvent Stimuli. J. Intell. Mater. Syst. Struct. 21, 859–885 (2010).

[107] Stuart, M. A. C. et al. Emerging applications of stimuli-responsive polymer materials. Nat. Mater. 9, 101–113 (2010).

[108] Kumar, A., Srivastava, A., Galaev, I. Y. & Mattiasson, B. Smart polymers: Physical forms and bioengineering applications. Prog. Polym. Sci. 32, 1205–1237 (2007).

[109] Kelley, E. G., Albert, J. N. L., Sullivan, M. O. & Thomas H. Epps, I. I. I. Stimuli-responsive copolymer solution and surface assemblies for biomedical applications. Chem. Soc. Rev. 42, 7057–7071 (2013).

[110] Dong, L. & Jiang, H. Autonomous microfluidics with stimuli-responsive hydrogels. Soft Matter 3, 1223–1230 (2007).

[111] Gulati, S. et al. Opportunities for microfluidic technologies in synthetic biology. J. R. Soc. Interface 6, S493–S506 (2009).

[112] Cole, M. A., Voelcker, N. H., Thissen, H. & Griesser, H. J. Stimuli-responsive interfaces and systems for the control of protein–surface and cell–surface interactions. Biomaterials 30, 1827–1850 (2009).

[113] Ebara, M., Hoffman, J. M., Hoffman, A. S. & Stayton, P. S. Switchable surface traps for injectable bead-based chromatography in PDMS microfluidic channels. Lab. Chip 6, 843–848 (2006).

[114] Mano, J. F. Stimuli-Responsive Polymeric Systems for Biomedical Applications. Adv. Eng. Mater. 10, 515–527 (2008).

[115] Schild, H. G. Poly(N-isopropylacrylamide): experiment, theory and application. Prog. Polym. Sci. 17, 163–249 (1992).

[116] Minko, S. Responsive Polymer Brushes. J. Macromol. Sci. Part C Polym. Rev. 46, 397–420 (2006).

[117] Wilson, S. A. et al. New materials for micro-scale sensors and actuators: An engineering review. Mater. Sci. Eng. R Rep. 56, 1–129 (2007).

[118] Fang, J. & Li, H. A Facile Way to Tune Mechanical Properties of Artificial Elastomeric Proteins-Based Hydrogels. Langmuir 28, 8260–8265 (2012).

[119] Cheung, Y. K. et al. Microscale Control of Stiffness in a Cell-Adhesive Substrate Using Microfluidics-Based Lithography. Angew. Chem. Int. Ed. 48, 7188–7192 (2009).

[120] Choi, S.-J., Kim, H. N., Bae, W. G. & Suh, K.-Y. Modulus- and surface energy-tunable ultraviolet-curable polyurethane acrylate: properties and applications. J. Mater. Chem. 21, 14325 (2011).

[121] Abate, A. R. & Weitz, D. A. Single-layer membrane valves for elastomeric microfluidic devices. Appl. Phys. Lett. 92, 243509 (2008).

[122] Zhang, W. et al. PMMA/PDMS valves and pumps for disposable microfluidics. Lab. Chip 9, 3088–3094 (2009).

[123] Iverson, B. D. & Garimella, S. V. Recent advances in microscale pumping technologies: a review and evaluation. Microfluid. Nanofluidics 5, 145–174 (2008).

[124] Lee, J.-H., Singer, J. P. & Thomas, E. L. Micro-/Nanostructured Mechanical Metamaterials. Adv. Mater. 24, 4782–4810 (2012).

[125] Ono, T., Fujii, S., Nobori, T. & Lehn, J.-M. Soft-to-hard transformation of the mechanical properties of dynamic covalent polymers through component incorporation. Chem. Commun. 46 (2007). doi:10.1039/b612035k

[126] Otsuka, H., Aotani, K., Higaki, Y. & Takahara, A. Polymer Scrambling: Macromolecular Radical Crossover Reaction between the Main Chains of Alkoxyamine-Based Dynamic Covalent Polymers. J. Am. Chem. Soc. 125, 4064–4065 (2003).

[127] Lehn, J.-M. Dynamers: dynamic molecular and supramolecular polymers. Prog. Polym. Sci. 30, 814–831 (2005).

[128] Toepke, M. W. & Beebe, D. J. PDMS absorption of small molecules and consequences in microfluidic applications. Lab. Chip 6, 1484 (2006).

[129] Abate, A. R., Lee, D., Do, T., Holtze, C. & Weitz, D. A. Glass coating for PDMS microfluidic channels by sol–gel methods. Lab. Chip 8, 516 (2008).

[130] Arima, V. et al. Fluoropolymers coatings on polydimethylsiloxane for retarding swelling in toluene. Thin Solid Films 520, 2293–2300 (2012).

[131] Balzani, V., Ceroni, P. & Juris, A. Photochemistry and photophysics: concepts, research, applications. (2014).

[132] Chatani, S., Kloxin, C. J. & Bowman, C. N. The power of light in polymer science: photochemical processes to manipulate polymer formation, structure, and properties. Polym. Chem. (2013). doi:10.1039/C3PY01334K

[133] Yagci, Y., Jockusch, S. & Turro, N. J. Photoinitiated Polymerization: Advances, Challenges, and Opportunities. Macromolecules 43, 6245–6260 (2010).

[134] Decker, C. Photoinitiated crosslinking polymerisation. Prog. Polym. Sci. 21, 593–650 (1996).

[135] Liu, Y., Boyles, J. K., Genzer, J. & Dickey, M. D. Self-folding of polymer sheets using local light absorption. Soft Matter 8, 1764–1769 (2012).

[136] Delman, A. D., Landy, M. & Simms, B. B. Photodecomposition of polymethylsiloxane. J. Polym. Sci. [A1] 7, 3375–3386 (1969).

[137] Rabek, J. F. Polymer photodegradation: mechanisms and experimental methods. (Chapman & Hall, 1995).

[138] Fritz, J. L. & Owen, M. J. Hydrophobic Recovery of Plasma-Treated Polydimethylsiloxane. J. Adhes. 54, 33–45 (1995).

[139] Schnabel, W. Polymers and light: fundamentals and technical applications. (Wiley-VCH, 2007).

[140] Fouassier, J.-P. & Rabek, J. F. Radiation Curing in Polymer Science and Technology. Vol. III, (Springer Science & Business Media, 1993).

[141] Müller, U., Jockusch, S. & Timpe, H.-J. Photocrosslinking of silicones. VI. Photocrosslinking kinetics of silicone acrylates and methacrylates. J. Polym. Sci. Part Polym. Chem. 30, 2755–2764 (1992).

[142] Bowman, C. N. & Kloxin, C. J. Toward an enhanced understanding and implementation of photopolymerization reactions. AIChE J. 54, 2775–2795 (2008).

[143] Hoyle, C. E., Lee, T. Y. & Roper, T. Thiol-enes: Chemistry of the past with promise for the future. J. Polym. Sci. Part Polym. Chem. 42, 5301–5338 (2004).

[144] Hoyle, C. E. & Bowman, C. N. Thiol-Ene Click Chemistry. Angew. Chem. Int. Ed. 49, 1540–1573 (2010).

[145] Xi, W., Scott, T. F., Kloxin, C. J. & Bowman, C. N. Click Chemistry in Materials Science. Adv. Funct. Mater. 24, 2572–2590 (2014).

[146] Lowe, A. B. Thiol-ene ‘click’ reactions and recent applications in polymer and materials synthesis. Polym. Chem. 1, 17 (2010).

[147] Cramer, N. B., Scott, J. P. & Bowman, C. N. Photopolymerizations of Thiol−Ene Polymers without Photoinitiators. Macromolecules 35, 5361–5365 (2002).

[148] Cramer, N. B., Reddy, S. K., Cole, M., Hoyle, C. & Bowman, C. N. Initiation and kinetics of thiol–ene photopolymerizations without photoinitiators. J. Polym. Sci. Part Polym. Chem. 42, 5817–5826 (2004).

[149] Cramer, N. B., Reddy, S. K., O’Brien, A. K. & Bowman, C. N. Thiol−Ene Photopolymerization Mechanism and Rate Limiting Step Changes for Various Vinyl Functional Group Chemistries. Macromolecules 36, 7964–7969 (2003).

[150] Wang, J. Z. Y. & Bogner, R. H. Solvent-free film coating using a novel photocurable polymer. Int. J. Pharm. 119, 81–89 (1995).

[151] Abdellah, L., Boutevin, B. & Youssef, B. Synthesis and applications of photocrosslinkable poly(siloxanes). Prog. Org. Coat. 23, 201–236 (1994).

[152] Colomines, G. L., Andre, S., Andrieu, X., Rousseau, A. & Boutevin, B. Synthesis and characterization of ultraviolet-curable fluorinated polydimethylsiloxanes as ultraviolet-transparent coatings for optical fiber gratings. J. Appl. Polym. Sci. 90, 2021–2026 (2003).

[153] Gordon, D. J. & Ziemelis, M. J. United States Patent: 4107390 - Radiation-curable organopolysiloxane coating composition comprising mercaptoalkyl and silacyclopentenyl radicals, method of coating and article therefrom. (1978).

[154] Lee, C. & Lutz, M. A. United States Patent: 4780486 - Fast ultraviolet radiation curing silicone composition. (1988).

[155] Viventi, R. V. United States Patent: 3816282 - RADIATION INDUCED POLYMERIZATION OF POLYSILOXANES. (1974).

[156] Müller, U., Kunze, A., Herzig, C. & Weis, J. Photocrosslinking of Silicones. Part 13. Photoinduced Thiol-Ene Crosslinking of Modified Silicones. J. Macromol. Sci. Part A 33, 439–457 (1996).

[157] Lunn, D. J. et al. Controlled Thiol-Ene Functionalization of Polyferrocenylsilane-block-Polyvinylsiloxane Copolymers. Macromol. Chem. Phys. 214, 2813–2820 (2013).

[158] Yang, H. et al. Polysiloxane-Based Liquid Crystalline Polymers and Elastomers Prepared by Thiol–Ene Chemistry. Macromolecules 46, 3406–3416 (2013).

[159] Cole, M. A. & Bowman, C. N. Evaluation of thiol-ene click chemistry in functionalized polysiloxanes. J. Polym. Sci. Part Polym. Chem. 51, 1749–1757 (2013).

[160] Jacobine, A. F. & Nakos, S. T. in Radiation Curing (ed. Pappas, S. P.) 181–240 (Springer US, 1992).

[161] Zuo, Y. et al. Preparation and characterization of luminescent silicone elastomer by thiol–ene 'click' chemistry. J. Mater. Chem. C 2, 2724–2734 (2014).

[162] Kim, J.-S., Yang, S., Park, H. & Bae, B.-S. Photo-curable siloxane hybrid material fabricated by a thiol–ene reaction of sol–gel synthesized oligosiloxanes. Chem. Commun. 47, 6051 (2011).

[163] Müller, U., Timpe, H.-J. & Neuenfeld, J. Photocrosslinking of silicones—5. Photo-induced polymerization of silicone with pendant acrylate groups in the presence of oxygen. Eur. Polym. J. 27, 621–625 (1991).

[164] Masson, F., Decker, C., Andre, S. & Andrieu, X. UV-curable formulations for UV-transparent optical fiber coatings: I. Acrylic resins. Prog. Org. Coat. 49, 1–12 (2004).

[165] Iojoiu, C., Harabagiu, V., Pinteala, M., Abadie, M. J. M. & Simionescu, B. C. Synthesis and photocrosslinking of benzyl (meth) acrylate substituted polydimethylsiloxanes: Influence of photoinitiator nature. J. Macromol. Sci. Part A 39, 467–488 (2002).

[166] Iojoiu, C., Abadie, M. J. M., Harabagiu, V., Pinteala, M. & Simionescu, B. C. Synthesis and photocrosslinking of benzyl acrylate substituted polydimethylsiloxanes. Eur. Polym. J. 36, 2115–2123 (2000).

[167] Israëli, Y., Cavezzan, J. & Lacoste, J. Photo-oxidation of polydimethylsiloxane oils: II—Effect of vinyl groups. Polym. Degrad. Stab. 37, 201–208 (1992).

[168] Konobeyevskii, K. S., Gusel'nikov, L. Y., Nametkin, N. S., Polak, L. S. & Chernysheva, T. I. Radiation polymerization of polyfunctional vinyl siloxanes. Polym. Sci. USSR 8, 604–607 (1966).

[169] Satti, A. J. et al. Synthesis, characterization, and gamma radiation effects over well-defined poly(vinylsiloxanes) copolymers. J. Appl. Polym. Sci. 124, 832–839 (2012).

[170] Tsougeni, K., Tserepi, A. & Gogolides, E. Photosensitive poly(dimethylsiloxane) materials for microfluidic applications. Microelectron. Eng. 84, 1104–1108 (2007).

[171] Cong, H. & Pan, T. Photopatternable Conductive PDMS Materials for Microfabrication. Adv. Funct. Mater. 18, 1912–1921 (2008).

[172] Jothimuthu, P. et al. Photodefinable PDMS thin films for microfabrication applications. J. Micromechanics Microengineering 19, 045024 (2009).

[173] Mabry, J. M. & Weber, W. P. Synthesis and thermal crosslinking of benzophenone-modified poly(dimethylsiloxane)s. J. Polym. Sci. Part Polym. Chem. 42, 5514–5522 (2004).

[174] Schneider, M. H., Tran, Y. & Tabeling, P. Benzophenone Absorption and Diffusion in Poly(dimethylsiloxane) and Its Role in Graft Photo-polymerization for Surface Modification. Langmuir 27, 1232–1240 (2011).

[175] Bhagat, A. A. S., Jothimuthu, P. & Papautsky, I. Photodefinable polydimethylsiloxane (PDMS) for rapid lab-on-a-chip prototyping. Lab. Chip 7, 1192 (2007).

[176] De Smet, N., Rymarczyk-Machal, M. & Schacht, E. Modification of Polydimethylsiloxane Surfaces Using Benzophenone. J. Biomater. Sci. -- Polym. Ed. 20, 2039–2053 (2009).

[177] Hillborg, H. & Gedde, U. W. Hydrophobicity changes in silicone rubbers. Dielectr. Electr. Insul. IEEE Trans. On 6, 703–717 (1999).

[178] Deng, J., Wang, L., Liu, L. & Yang, W. Developments and new applications of UV-induced surface graft polymerizations. Prog. Polym. Sci. 34, 156–193 (2009).

[179] Martínez Rivas, A. et al. Simplified and direct microchannels fabrication at wafer scale with negative and positive photopolymerizable polydimethylsiloxanes. Microfluid. Nanofluidics 9, 439–446 (2009).

CHAPTER 2. Solvent Resistant PVMS Microchannels*

* This chapter is partially based on: R. L. Mays, M. D. Dickey, J. Genzer, ***Lab Chip***, 2013, **13**, 4317-4320

2.1. Introduction

Microfluidics involves the manipulation of small volumes of fluid typically accomplished with micro-scale channels. Microfluidic channels are commonly fabricated in poly(dimethylsiloxane) (PDMS) because of numerous favorable properties, including optical transparency, ease of sealing, and chemical inertness.[1] However, PDMS can contaminate microfluidic solutions with unreacted oligomers,[2] absorb organic molecules from solution,[3] and swell upon exposure to most organic solvents.[4] Alternative polymeric materials, such as perfluoropolyethers[5,6] and thiol-enes,[7] have also been explored as replacements for PDMS. While some of these materials overcome the organic solvent swelling drawback of PDMS, sealing these devices can be problematic or cumbersome.[8]

Another drawback of PDMS is that the methyl side groups are notoriously difficult to modify chemically.[1,9,10] In contrast, a PVMS surface is easy to modify due to the presence of reactive vinyl bonds. It is often desirable to chemically tune the interface of microfluidic channels to achieve a specific wettability, or to pattern the local wettability in a channel.[11–13] In many biological applications, sensing and screening depends on the attachment of enzymes, ligands, or proteins to desired regions of the channel.[9,14] Extensive research exists on altering the surface properties of PDMS chemically, physically, or through grafting of polymers.[9,10,15]

Here, we demonstrate the utilization of PVMS, a material which can be chemically and mechanically modified, as a suitable drop-in replacement for PDMS. Previous applications of PVMS have included cell studies,[16] chemically responsive surfaces,[17] optically responsive materials,[18] and mechanically tunable networks.[19] The vinyl groups on

PVMS provide opportunities for applying thiol-ene click chemistry, cross metathesis, as well as free radical reactions to endow the base materials with useful new chemical functionalities. Like PDMS, PVMS can be end-group cross-linked to form elastomeric networks that behave similarly to PDMS networks, exhibiting low surface energy, low modulus, mechanical flexibility, optical transparency, and hydrophobicity. PVMS can be replica-molded into microchannels and sealed using methods identical to those employed in fabricating microchannels composed of PDMS.

By UV treating microchannels constructed from PVMS networks, we demonstrate siloxane-based microchannels that resist swelling in toluene. Although other research groups implement photo-sensitive PDMS in coatings or adhesive applications[20] or as photo-resists,[21–23] little work has been done on modifying photo-sensitive PDMS microchannels in situ.[13,24] PVMS homopolymers have not, to our knowledge, been used to construct microchannels. In our system, reactive hydroxyl end-groups on the synthesized polymers create a siloxane network, while the vinyl side groups remain available for further reactions in a later step. This method enables the localization of modifications by selectively delivering photoinitiator to specific regions of the polymer (in this case, the walls of the channel) for subsequent treatment with UV light. These reactions can change the local interfacial energy and chemical composition, mechanical properties, and permeability.

2.2. Experimental Methods

We synthesized hydroxyl-terminated PVMS by two methods, both of which have been previously reported in the literature.[25,26] Step-growth polymerization[25] involves the

reaction of short chain siloxanes with hydroxyl end groups (Dow Corning PJ Fluid) with lithium hydroxide (Sigma-Aldrich) dissolved in water. The reaction vessel was heated above 100°C to evaporate water, which is formed as a by-product. Typically, the reaction vessel maintained a temperature of 115°C ±5°C with 500 mL of short-chain siloxanes and 30 ppm LiOH for 4 or more hours under constant nitrogen flux and vigorous stirring, until the mixture became viscous. The viscosity increase over time indicated the approximate molecular weight of the polymer, with a targeted molecular weight of roughly ≈35 kDa. The addition of dry ice terminated the reaction, resulting in PVMS with hydroxyl end groups. This material was then purified by passing the material through a Celite® filter cake, followed by two extractions in methanol.

Alternatively, one-pot anionic ring opening polymerization (ROP)[25,26] produced hydroxyl terminated PVMS. First, catalyst synthesis involved the procedure for making dilithium diphenylsilanolate reported elsewhere[27] using diphenyl silane diol (Sigma-Aldrich) and n-butyl lithium (Sigma-Aldrich) as starting materials. Distilled cyclic vinyl methyl siloxane (Dow Corning) was added to dry THF in a reaction vessel and kept under argon while reacting with the dilithium initiator. A typical reaction would consist of 30 mmol vinyl methyl siloxane cycles, 0.3 mmol initiator, and 10 mL of dry THF. The reactions proceeded quickly, reaching full molecular weight in less than an hour. The reaction terminated with the addition of acetic acid, resulting in hydroxyl end groups on the polymers. The resulting polymer was purified twice in methanol before using. GPC determined the molecular weight of the materials, all of which were between 20 and 45 kDa.

A tin catalyst (tin(II) 2-ethylhexanoate, Sigma Aldrich) diluted in tetrahydrofuran (THF) (ratio of 1:9 v/v of tin to THF) and a short chain crosslinker of poly(vinylmethoxysiloxane) (PVMES; Gelest VMM-010) mixed with PVMS formed the crosslinked PVMS networks.[25,28] The amount of crosslinker varied according to the molecular weight of the polymer; a typical network consisted of 10 g PVMS, 0.48 g PVMES, and 0.1 g tin/THF solution (a mole ratio of approximately 1.3 mol PVMES: 1 mol PVMS: 0.042 mol tin catalyst), which after degassing cured in a 60°C oven for an hour against a mold. We made PDMS microfluidic channels with both the standard commercial Sylgard-184 kit (prepared with 10:1 ratio of resin to hardener, as specified by the manufacturer) and an unfilled silanol terminated PDMS (Gelest, DMS-S35-100gm). Network formation with the silanol-terminated PDMS followed the same method as with PVMS; that is, with the tin catalyst and a methoxy crosslinker. All networks cured in an oven at 60°C for an hour (or more) until needed for microchannel fabrication.

Replica molding the polymers against a fluorosilane-treated master mold (SU-8 patterned lithographically on a silicon wafer) produced a molded microfluidic channel.[29] After treating the channels for 20 seconds with oxygen (air) plasma, a molded sheet and flat sheet of siloxane sealed together with the application of gentle pressure. PVMS channels can also be sealed to a glass slide using the same technique with oxygen plasma.

An FTA1000B goniometer determined the contact angles of deionized water and toluene. We recorded at least three contact angles for each sample, and averaged multiple samples for all CA values reported. The drops were 5-6 μL in volume.

A 400W metal halide lamp (Uvitron IntelliRay 400) provided a source of UV light for post-assembly modification of the channels. The lamp used emits primarily at 365 nm, though no optical filter was used to remove other wavelengths (a range of wavelengths are produced between 250 nm and 450 nm). Networks soaked in a solution of photoinitiator (2-hydroxy-2-methylpropiophenone, VWR International) 10 wt% in ethanol (Sigma-Aldrich) for 30-60 minutes before treating with UV light. For microchannels, the solution flowed through the channel for 30 to 60 min at a rate of 1 mL/hr. This process allowed the photoinitiator to diffuse slowly into the channel walls[24] and the time of exposure controls the amount of photoinitiator added, as depicted in Figure 2.1. While UV doses varied from 60 s to 30 min for the purposes of characterization (corresponding to an intensity of 3,500 to 107,000 mJ/cm^2); the more typical exposure doses used in the microchannels were between 18,000 to 36,000 mJ/cm^2 (5-10 min).

We used several analytical techniques to characterize the surface of the siloxane networks. Fourier transform infrared spectroscopy in the attenuated total reflection mode (FTIR-ATR) was employed to characterize chemical changes using a Nicolet 6700 spectrometer equipped with germanium ATR crystal (Ge-ATR). For each sample, 256 scans were collected under constant nitrogen flux.

Dynamic mechanical analysis (Rheometric Scientific, model DMTA-IV) determined the material stiffness with varying UV treatment times. Flat PVMS networks (1mm thick) cut into 20mm×10mm rectangles were immersed in a solution of photoinitiator and ethanol for 30-60 min (the same time as the exposure in microchannels). After drying, the samples

were UV treated with varying exposure times (corresponding to an intensity of 3,500 to 107,000 mJ/cm^2).

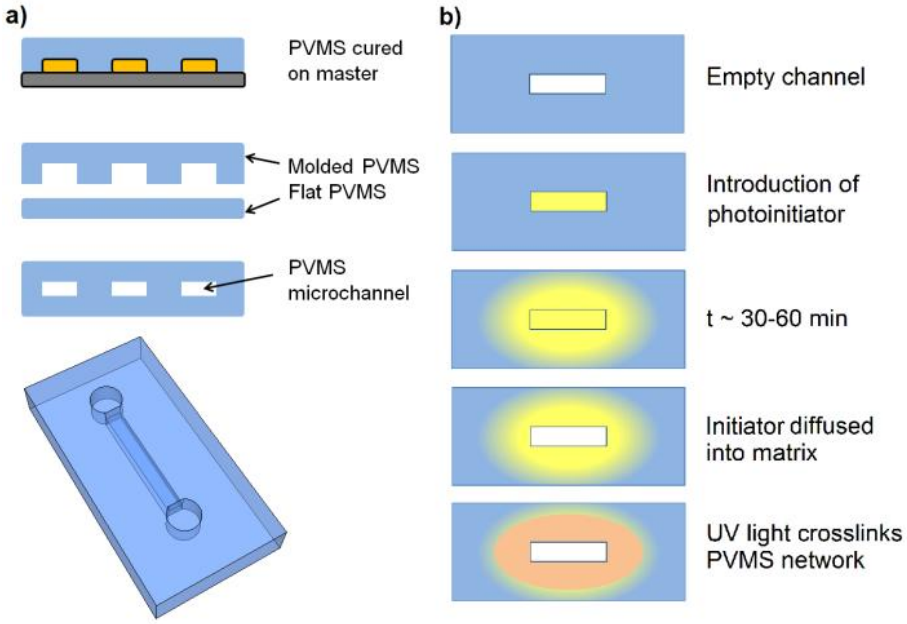

Figure 2.1: A) A cross-sectional depiction of PVMS microchannel fabrication by replica molding. First, the polymer is cured against a lithographically-patterned master substrate. The cured microchannel is then sealed to another sheet of PVMS by exposing both surfaces to oxygen plasma. B) A cross-sectional view of PVMS microchannels depicting the diffusion of initiator into the walls of the channel and subsequent UV treatment to promote resistance to organic solvents. Features not drawn to scale.

Storage modulus (E'), loss modulus (E"), and loss tangent (tan δ) were recorded over frequency range from 1-100 rad/s with 5 points collected per decade at a strain of 0.1% in tensile mode, all within the rubbery plateau region. We collected all data at room temperature (23°C).

2.3. Results and Discussion

We sought to demonstrate some of the advantages of UV treated PVMS relative to Sylgard-184. The images in Figure 2.2 depict the performance of Sylgard-184 and UV-treated PVMS under prolonged periods of exposure to toluene (flow rate of 1 mL/h).

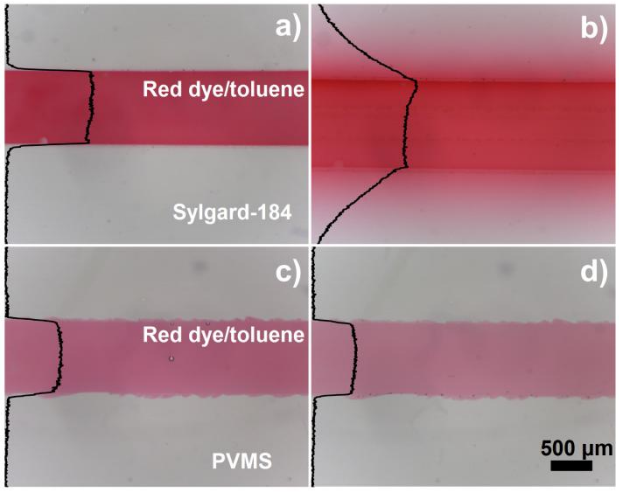

Figure 2.2: Organic solvent leaching in Sylgard-184 and PVMS. The same solution (and therefore the same concentration of red dye) was used for both samples. The black lines represent an average of five line scans of each image showing the intensity of the red color across the channel. A) Sylgard-184 channel at t = 0 min. B) Sylgard-184 channel with extensive leaching and deformation at t = 60 min. C) Treated PVMS channel at t = 0 min. D) Treated PVMS channel at t = 60 min.

We chose toluene as a solvent because toluene diffuses into PDMS and swells it significantly.[30] As toluene loaded with red dye flows through the channel, the dye diffuses into the PDMS matrix around the channel (Figure 2.2a-b). In contrast, the UV-treated PVMS shows essentially no leaching (Figure 2.2c-d), even after two hours (Figure 2.3). Despite the apparent difference in intensity of the red color, the concentration of red dye for both systems

remains the same. The difference in color is likely due to the rapid absorption of red dye into the top and bottom walls of the PDMS channel, which is not seen in the treated PVMS channel even after an hour of exposure. Model PDMS (containing no silica particle fillers) and untreated PVMS channels both show swelling in toluene, behavior indistinguishable from Sylgard-184. Likewise, when we treat Sylgard-184 with photoinitiator and UV light, we see the same swelling behavior as pristine Sylgard-184.

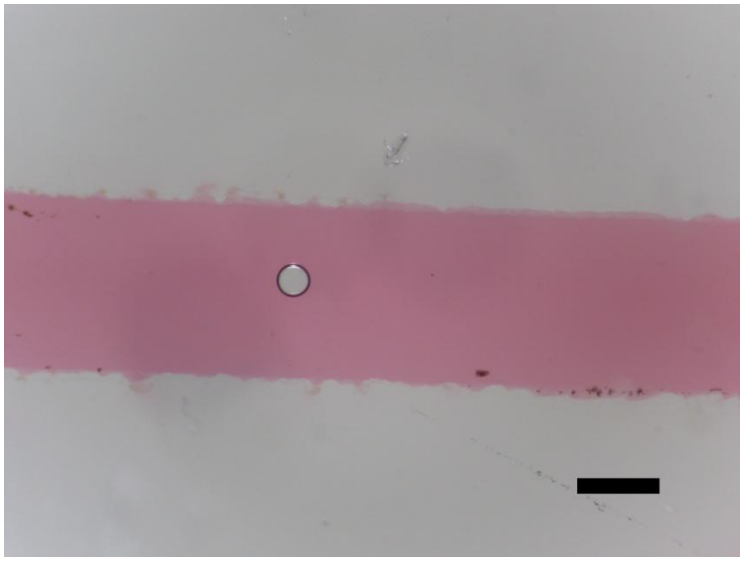

Figure 2.3: PVMS channel after two hours of exposure to toluene/red dye mixture. Scale bar 500 μm.

We used Fourier transform infrared (FTIR) spectroscopy to quantify the chemical changes resulting from UV-induced surface modification of PVMS (Figure 2.4). Because free radical reactions are inhibited by the presence of oxygen,[31] we covered the samples used to produce the FTIR spectra with a quartz slide during UV treatment, limiting oxygen

inhibition at the surface. Other work done on the degradation of silicone rubbers and siloxanes proposes a number of reactions due to UV or oxidation as an effect of UV.[32] However, to our knowledge, little work has been done using a photoinitiator in a system with PVMS. While the exact mechanism of the reaction is unknown, the decrease in IR signal originating from the vinyl groups (1407 and 1598 cm^{-1}) indicates that a primary mechanism is the reaction involving those vinyl groups, resulting in additional crosslinks in the material. The appearance of a shoulder at 930 cm^{-1} is assigned to the formation of a -Si-CH_2-CH=CH- group.[33]

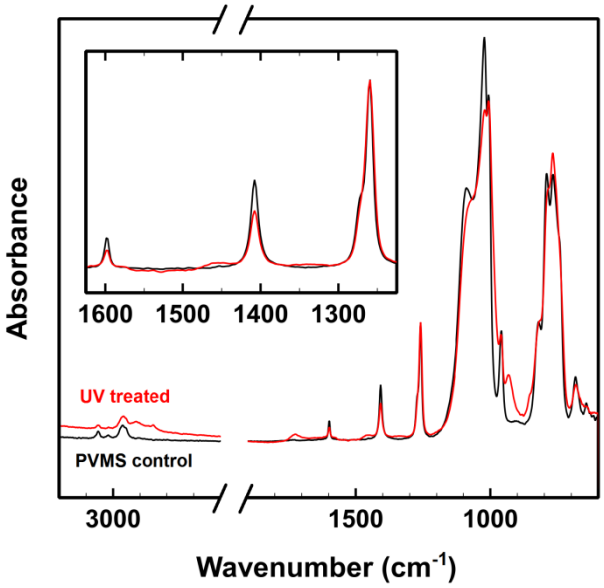

Figure 2.4: Analysis of PVMS by FTIR-ATR after UV treatment (black line = PVMS control; red line = PVMS UV treated 414 J/cm^2). The vinyl peaks at 1407 cm^{-1} and 1598 cm^{-1} decrease in intensity after UV exposure. The IR spectra were normalized relative to the methyl vibration at 1259 cm^{-1}.

Much of the published work involving photocurable siloxanes utilized either acrylate functionality or thiol-ene chemistry; however, work has been done using vinyl methyl siloxanes for free radical reactions and the network crosslinking density was found to depend primarily on the number of vinyl groups available, implying that the methyl side groups are not participating in the free radical crosslinking reaction.[34]

As the polymer network crosslinks through the vinyl side groups, the material stiffens. Dynamical mechanical analysis (DMA) of 1 mm thick PVMS networks shows that infusing the networks with photoinitiator followed by UV exposure increases the storage modulus; this procedure as applied to flat networks is similar to the procedure used for generating solvent resistant channels, as described in the experimental methods section. As seen in Figure 2.5, the modulus increases by two orders of magnitude within ≈10 minutes of UV light exposure.

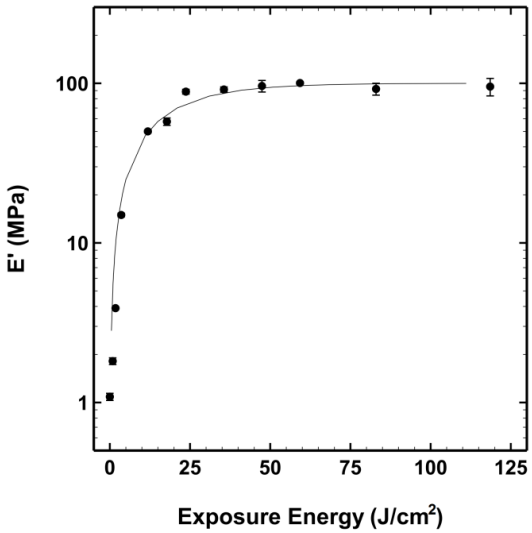

Figure 2.5: Storage modulus as determined by DMA shown as a function of UV exposure energy. Trendline provided to guide the eye.

Variability in the modulus at long UV treatment times is primarily due to the uncontrolled nature of a UV initiated free radical reaction as well as the dependence of the extent of reaction on sample thickness. Because of the variability in mechanical measurements, we caution that the values presented may differ with changes in PVMS molecular weight, UV lamp intensity, photoinitiator concentration, and sample thickness. Nevertheless, the results illustrate that the mechanical properties change significantly with exposure to light. The elastic modulus plateaus after ≈25 J/cm^2 (≈7 min exposure time with our UV lamp for a 10 wt% HMPP photoinitiator solution in ethanol).

The amount of photoinitiator and the dose of UV light determine the extent of reaction inside the microchannel and thus, the mechanical properties and permeability of the PVMS. The amount of photoinitiator embedded in the elastomer depends on the concentration of the HMPP/ethanol solution and the amount of time the solution flows through the channel. This diffusion-based process results in a gradient of photoinitiator from the channel into the surrounding matrix, similar to work done in PDMS channels.[24] In a typical experiment, the UV-modified area extends into the surrounding matrix for ≈500-600 μm (Figure 2.6), as determined by optical microscopy of a cross-section of the channel.

Although the geometry of a PDMS microchannel changes with absorption of organic solvent,[4] we did not see a corresponding deformation in UV-treated PVMS channels. To further demonstrate this effect, we observed the deformation of wells of both PDMS and PVMS in the presence of solvent (Figure 2.7).

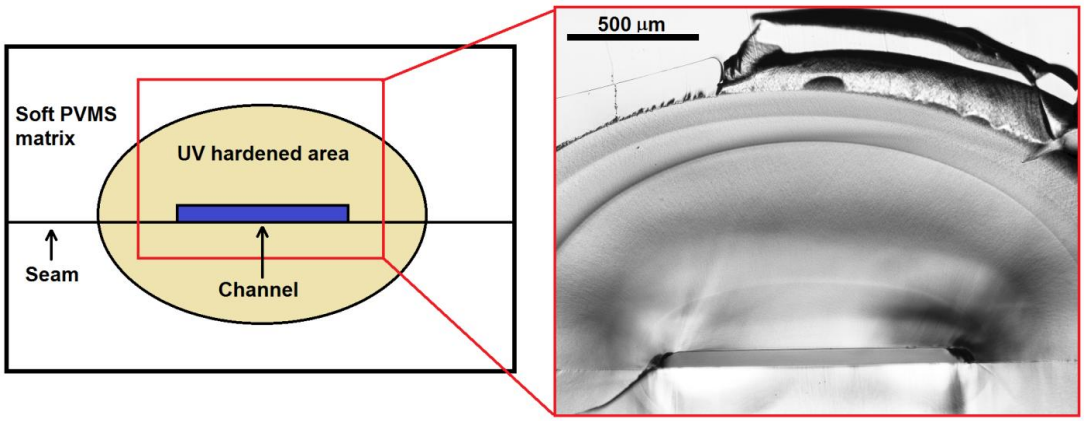

Figure 2.6: Cross-section of UV treated channel prepared by cutting a channel with a razor blade.

The features deform with solvent absorption in PDMS, swelling over 100% by volume, and untreated PVMS (swelling of untreated PVMS not shown), but the UV-treated PVMS features do not change significantly in dimensions with exposure to toluene. After UV modification of the PVMS surface, the siloxane networks maintain organic solvent wettability (Figure 2.8); yet they do not swell in the presence of the organic solvent. A microfluidic chemical synthesis channel could make use of organic solvents without the concern that the solvent will leach into the surrounding network, thus changing the geometry of the channels (and therefore the flow profile) and the concentration of reactants inside the channel.[3]

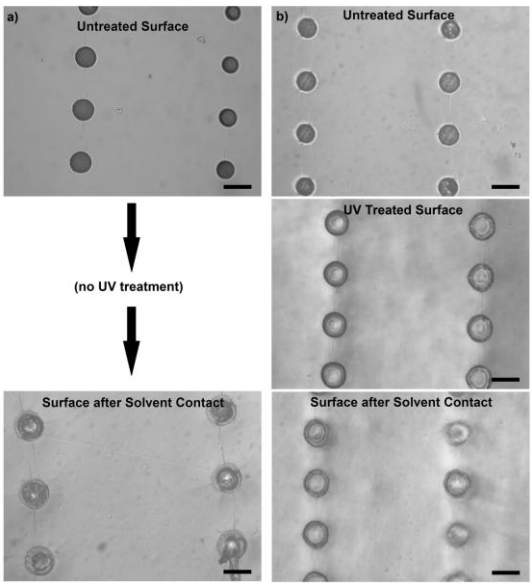

Figure 2.7: Microwells swelling and deforming with exposure to toluene. Scale bar 100 μm. A) PDMS wells before exposure to solvent (top) and after swollen with toluene (bottom). Swelling shown is approximately 200% by volume. B) Untreated PVMS wells (top), UV treated PVMS wells before exposure to solvent (middle) and after exposure to toluene (bottom). The UV treatment results in the change in appearance of PVMS seen in B) moving from the top to the middle image.

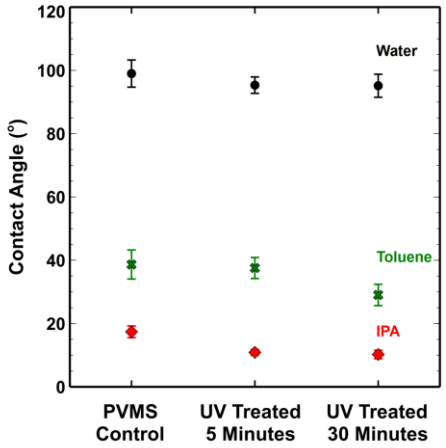

Figure 2.8: Static contact angles using DI water (black circles), toluene (green crosses), and IPA (red diamonds) on pristine PVMS and UV-treated PVMS.

During replica molding, the PVMS occasionally tears due to the lack of filler. Commercial PDMS kits, such as Sylgard-184, contain as much as 30-60 wt% silica particle fillers[35] that are employed to increase the tear strength. We chose to use the PVMS as is, although it is well known that adding fillers reinforces the network and increases tear strength.[36] Tearing can sometimes be observed around the edges of the features (2.9 a and c), although this can also be seen with features reproduced with Sylgard-184 (Figure 2.9 d), as well as with the pure PDMS system (Figure 2.9 b). Based on our preliminary results, adding fillers to the PVMS prevents tearing and increase tear strength to improve replica molding of PVMS channels.

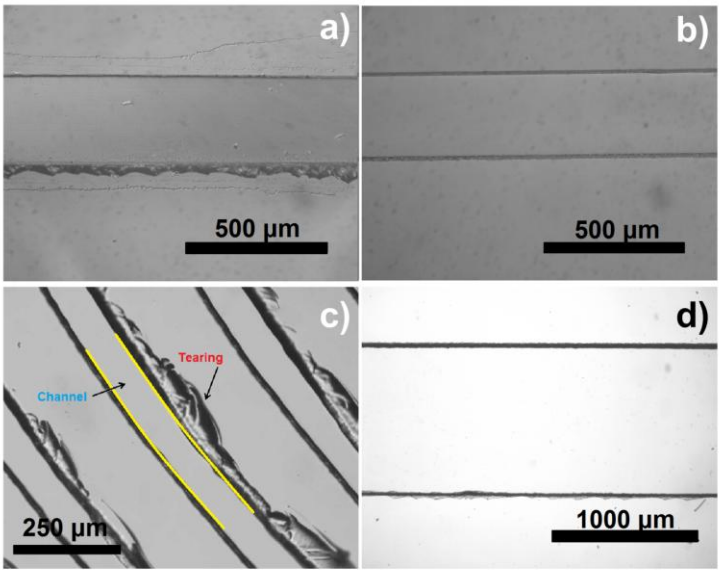

Figure 2.9: Various degrees of tearing in pure PVMS, pure PDMS, and Sylgard-184 channels. Microchannel composed of A) PDMS (no fillers) and B) PVMS (no fillers). C) Tearing on a PVMS channel. Edges of the channel are highlighted with yellow lines. Significant tearing can be seen outside the channel walls. D) Sylgard-184 channel with some tearing on the edges.

We further evaluate the impact of reinforcing nanoparticles on PVMS networks in Chapter 3 of this dissertation.

Additionally, we investigated the use of other organic solvents with our UV treated PVMS microchannel system. The formidable challenge in this case was the tubing rather than the PVMS networks, as most softer tubing swells in organic solvents, and solvent resistant tubing is stiff, resulting in punctures and tears during insertion. We did have limited success with other solvents, however, as indicated in Figure 2.10.

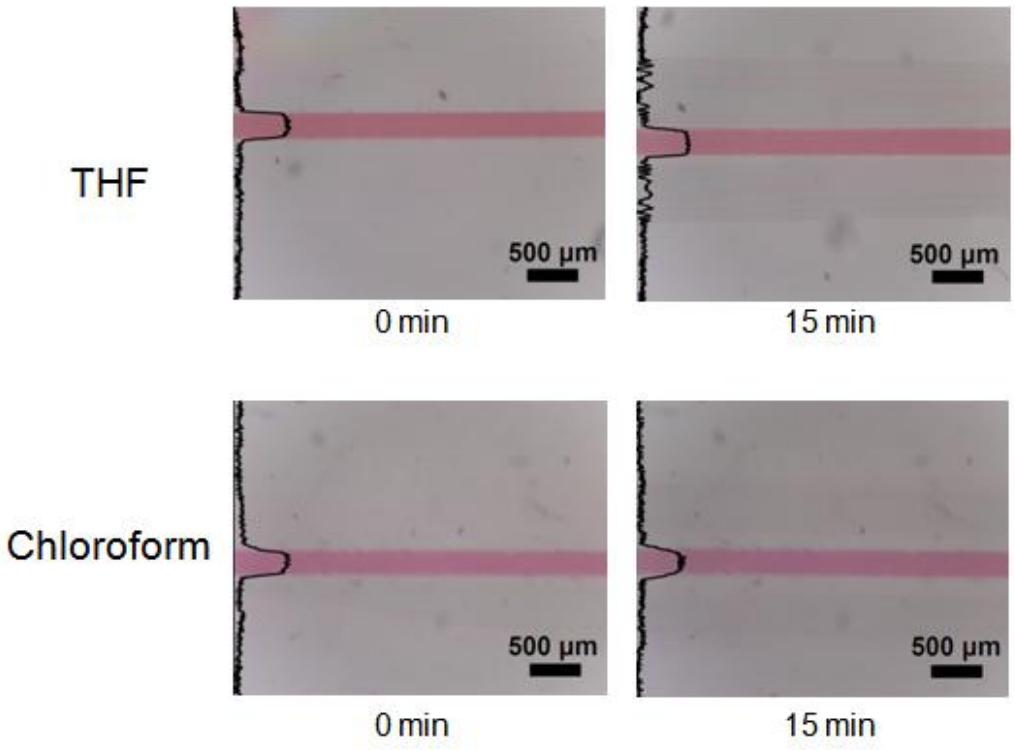

Figure 2.10: UV-treated PVMS microchannel during exposure to THF and chloroform.

With both chloroform and tetrahydrofuran (THF), the UV-treated PVMS microchannel appears to resist swelling and leaching of red dye for short times. Due to issues with the Tygon tubing swelling and blocking the inlet and the solvent resistant tubing (perfluoroalkoxy tubing or PFA tubing) being too stiff and breaking the channel or falling and preventing flow, we were unable to test a microchannel for times longer than 15 minutes. With a thicker PVMS network, the problems with solvent resistant tubing may be avoided. Our UV-treated PVMS networks did not successfully resist leaching when exposed to red dye dissolved in acetone, however, as shown in Figure 2.11. It is unclear why this would be the case, but with future testing or modifications to the UV-treatment procedure, these issues with acetone may be overcome.

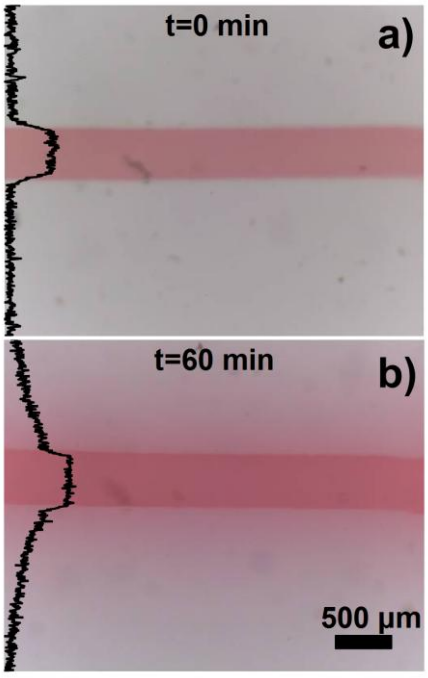

Figure 2.11: UV-treated PVMS microchannel during exposure to acetone.

2.4. Conclusions and Outlook

PVMS is an attractive alternative material for microchannel fabrication that offers several benefits in comparison with PDMS. Like PDMS, PVMS is optically transparent, easy to process, and flexible. However, unlike PDMS, the ability to UV-modify the PVMS interface (e.g., the walls of microchannels, as shown here) allows the user to create flexible, transparent, molded elastomers that are compatible with organic solvents. The UV treatment is also capable of tuning the modulus by two orders of magnitude using light, which may be useful for other applications.

The most significant drawback of PVMS, however, is the lack of a commercially available material. We synthesized the materials used in this study in house; although the synthesis is straightforward, this additional step may be a deterrent to rapid implementation of PVMS devices. Another consideration is the poor tear strength of unfilled silicone rubbers (both PDMS and PVMS); commercial PDMS products are often loaded with silica particles to overcome this problem. Future work will focus on the improvement of mechanical properties for replica molding by including silica fillers like those used in commercial PDMS kits.

The UV treatment in this work is used primarily to modify the mechanical and diffusive properties of the material around the channel. However, it may be possible to introduce other chemical functionality by grafting molecules to the vinyl functional groups on the surface for further tailoring of the properties of PVMS microchannels. For example, grafting of dynamic covalent groups to the vinyl side groups of PVMS would provide an alternate route for mechanical modification of network properties. Using siloxane polymers

with dynamic covalent acylhydrazone groups, rigid and flexible repeat units engage in monomer exchange, altering the mechanical properties of the film.[37] Additionally, grafting groups with hydrophilicity or stimuli-reponsive behavior to the vinyl side groups of a PVMS microchannel will expand the utility of this technology. The versatility and tunability of PVMS shows great promise for use in microfluidics or other soft lithographic applications.

2.5. References

[1] McDonald, J. C. & Whitesides, G. M. Poly(dimethylsiloxane) as a Material for Fabricating Microfluidic Devices. Acc. Chem. Res. 35, 491–499 (2002).

[2] Regehr, K. J. et al. Biological implications of polydimethylsiloxane-based microfluidic cell culture. Lab. Chip 9, 2132 (2009).

[3] Toepke, M. W. & Beebe, D. J. PDMS absorption of small molecules and consequences in microfluidic applications. Lab. Chip 6, 1484 (2006).

[4] Dangla, R., Gallaire, F. & Baroud, C. N. Microchannel deformations due to solvent-induced PDMS swelling. Lab. Chip 10, 2972 (2010).

[5] Rolland, J. P., Van Dam, R. M., Schorzman, D. A., Quake, S. R. & DeSimone, J. M. Solvent-Resistant Photocurable 'Liquid Teflon' for Microfluidic Device Fabrication. J. Am. Chem. Soc. 126, 2322–2323 (2004).

[6] Yang, Y.-W. et al. 'Clicked' fluoropolymer elastomers as robust materials for potential microfluidic device applications. J. Mater. Chem. 22, 1100 (2012).

[7] Carlborg, C. F., Haraldsson, T., Öberg, K., Malkoch, M. & van der Wijngaart, W. Beyond PDMS: off-stoichiometry thiol–ene (OSTE) based soft lithography for rapid prototyping of microfluidic devices. Lab. Chip 11, 3136 (2011).

[8] Kuo, J. S. & Chiu, D. T. Disposable microfluidic substrates: Transitioning from the research laboratory into the clinic. Lab. Chip 11, 2656–2665 (2011).

[9] Zhou, J., Ellis, A. V. & Voelcker, N. H. Recent developments in PDMS surface modification for microfluidic devices. ELECTROPHORESIS 31, 2–16 (2010).

[10] Makamba, H., Kim, J. H., Lim, K., Park, N. & Hahn, J. H. Surface modification of poly(dimethylsiloxane) microchannels. ELECTROPHORESIS 24, 3607–3619 (2003).

[11] Seo, M., Paquet, C., Nie, Z., Xu, S. & Kumacheva, E. Microfluidic consecutive flow-focusing droplet generators. Soft Matter 3, 986–992 (2007).

[12] Logtenberg, H., Lopez-Martinez, M. J., Feringa, B. L., Browne, W. R. & Verpoorte, E. Multiple flow profiles for two-phase flow in single microfluidic channels through site-selective channel coating. Lab. Chip 11, 2030 (2011).

[13] Abate, A. R. et al. Photoreactive coating for high-contrast spatial patterning of microfluidic device wettability. Lab. Chip 8, 2157 (2008).

[14] Rossier, J., Reymond, F. & Michel, P. E. Polymer microfluidic chips for electrochemical and biochemical analyses. ELECTROPHORESIS 23, 858–867 (2002).

[15] Wong, I. & Ho, C.-M. Surface molecular property modifications for poly(dimethylsiloxane) (PDMS) based microfluidic devices. Microfluid. Nanofluidics 7, 291–306 (2009).

[16] Ahmed, S. et al. Poly(vinylmethylsiloxane) Elastomer Networks as Functional Materials for Cell Adhesion and Migration Studies. Biomacromolecules 12, 1265–1271 (2011).

[17] Crowe, J. A. & Genzer, J. Creating Responsive Surfaces with Tailored Wettability Switching Kinetics and Reconstruction Reversibility. J. Am. Chem. Soc. 127, 17610–17611 (2005).

[18] Yang, H.-K., Evren Özçam, A., Efimenko, K. & Genzer, J. Photochromic materials with tunable color and mechanical flexibility. Soft Matter 7, 3766 (2011).

[19] Crowe-Willoughby, J. A., Weiger, K. L., Özçam, A. E. & Genzer, J. Formation of silicone elastomer networks films with gradients in modulus. Polymer 51, 763–773 (2010).

[20] Abdellah, L., Boutevin, B. & Youssef, B. Synthesis and applications of photocrosslinkable poly(siloxanes). Prog. Org. Coat. 23, 201–236 (1994).

[21] Tsougeni, K., Tserepi, A. & Gogolides, E. Photosensitive poly(dimethylsiloxane) materials for microfluidic applications. Microelectron. Eng. 84, 1104–1108 (2007).

[22] Jothimuthu, P. et al. Photodefinable PDMS thin films for microfabrication applications. J. Micromechanics Microengineering 19, 045024 (2009).

[23] Martínez Rivas, A. et al. Simplified and direct microchannels fabrication at wafer scale with negative and positive photopolymerizable polydimethylsiloxanes. Microfluid. Nanofluidics 9, 439–446 (2009).

[24] Schneider, M. H., Tran, Y. & Tabeling, P. Benzophenone Absorption and Diffusion in Poly(dimethylsiloxane) and Its Role in Graft Photo-polymerization for Surface Modification. Langmuir 27, 1232–1240 (2011).

[25] Efimenko, K. et al. Rapid formation of soft hydrophilic silicone elastomer surfaces. Polymer 46, 9329–9341 (2005).

[26] Boehm, P., Mondeshki, M. & Frey, H. Polysiloxane-Backbone Block Copolymers in a One-Pot Synthesis: A Silicone Platform for Facile Functionalization. Macromol. Rapid Commun. 33, 1861–1867 (2012).

[27] Battjes, K. P., Kuo, C.-M., Miller, R. L. & Saam, J. C. Strain-Induced Crystallization in Poly[methyl(3,3,3-trifluoropropyl)siloxane] Networks. Macromolecules 28, 790–792 (1995).

[28] Mark, J. E. & Sullivan, J. L. Model networks of end-linked polydimethylsiloxane chains. I. Comparisons between experimental and theoretical values of the elastic modulus and the equilibrium degree of swelling. J. Chem. Phys. 66, 1006-1011 (1977)

[29] Qin, D., Xia, Y. & Whitesides, G. M. Soft lithography for micro- and nanoscale patterning. Nat. Protoc. 5, 491–502 (2010).

[30] Lee, J. N., Park, C. & Whitesides, G. M. Solvent Compatibility of Poly(dimethylsiloxane)-Based Microfluidic Devices. Anal. Chem. 75, 6544–6554 (2003).

[31] Decker, C. & Jenkins, A. D. Kinetic approach of oxygen inhibition in ultraviolet- and laser-induced polymerizations. Macromolecules 18, 1241–1244 (1985).

[32] Hillborg, H. & Gedde, U. W. Hydrophobicity changes in silicone rubbers. Dielectr. Electr. Insul. IEEE Trans. On 6, 703–717 (1999).

[33] Petrarch Systems, I. Silicon compounds: register and review. (Petrarch Systems, 1987).

[34] Müller, U., Timpe, H.-J., Häusler, K.-G., Peters, K. & Wagner, R. Lichtinitiierte Polymer- und Polymerisationsreaktionen. 36. Mitt.: Photovernetzung vinlygruppenhaltiger Poly(dimethylsiloxane). Acta Polym. 41, 54–59 (1990).

[35] Sylgard 184 Material Safety Data Sheet (MSDS). Retrieved 1/30/2015. at <http://www.dowcorning.com/applications/search/default.aspx?r=131en>

[36] Schaefer, D. W., Vu, B. T. N. & Mark, J. E. The effect of interphase coupling on the structure and mechanical properties of silica-siloxane composites. Rubber Chem. Technol. 75, 795–810 (2002).

[37] Ono, T., Fujii, S., Nobori, T. & Lehn, J.-M. Soft-to-hard transformation of the mechanical properties of dynamic covalent polymers through component incorporation. Chem. Commun. 46 (2007). doi:10.1039/b612035k

CHAPTER 3. Nanoparticles for PVMS Reinforcement

3.1. Reinforced Siloxane Rubbers

Elastomeric materials are frequently reinforced mechanically to improve extensibility, modulus, and toughness.[1,2] Composite materials consisting of organic polymers and inorganic nanoparticles (NPs) demonstrate both the processability and flexibility of polymers as well as the magnetic, electrical, or catalytic behaviors of the inorganic materials.[1] Several researchers have successfully developed flexible iron NP/polymer composites which demonstrate magnetic response,[2,3] which is notable because magnetic materials are usually rigid. If the additional NPs added are more thermally conductive than the polymer matrix, the composite will usually have a higher thermal conductivity than the polymer itself.[4] Organic nanomaterials with interesting electrical and mechanical properties, including carbon nanotubes, can also be used as reinforcing agents.[5]

Commercial siloxane polymers crosslinked into elastomeric networks are usually a mixture of polymer chains and a reinforcing agent such as fumed silica, carbon black, or other nanoparticles; this field of research dates back over fifty years.[8,9] While fumed silica acts primarily as a mechanical reinforcing additive, other fillers such as nanotubes or clay particles can be used to alter electrical and optical properties of the network.[8] The chemical nature and length scale of the additive determines enthalpic and entropic interactions of the polymer chain with the filler.[10] Fillers which are less than 1000 nm in size show the best reinforcing properties, with the ideal particles being between 10-100 nm.[11] In nanocomposite systems, there is an entropic penalty to the polymer chain as the NPs take up void space between chains (excluded volume effect[12]), and the way that fillers affect the movement of each polymer chain alters the mechanical properties of the elastomeric matrix.[13]

For a typical silicone rubber filled with fumed silica, particle-particle interactions and particle-polymer interactions both contribute to the increase in tear strength.[14] Hydrogen bonds between hydroxyl groups on the surface of silica particles are responsible for strong particle-particle interactions. The silica particles act as additional crosslink points between siloxane chains, limiting their extension.[15] Polymer molecules tend to interact through adsorption onto the silanol groups on the surface of the silica particles;[15] these interactions depend on the particle concentration, specific surface area of the particles, and the molecular weight of the polymer.[14] The phenomenon of a polymer chain strongly interacting with a filler particle forming an insoluble complex is referred to as "bound rubber".[6]

The mechanical properties of elastomers and rubber composites can be determined by applying tensile, compressive, flexural, or dynamic stresses, though most frequently tensile or dynamic tests are used.[16] The notable properties are Young's modulus, elongation at break, and ultimate stress. The sample toughness is determined by the area under the stress-strain curve: the rupture energy is the force required to break the sample over the initial volume of the sample (initial cross-sectional area times initial length).[17] Brittle materials may withstand a high stress but a low extension, whereas soft materials easily extend but break under a low stress. Tough polymers undergo both high stress and high strain before failure. Some example stress-strain profiles are demonstrated in Figure 3.1.[16]

The modulus increase of filled rubbers depends on the volume fraction of fillers in the rubber. The modulus of rubber filled with dilute suspensions of particles show a linear correlation with filler volume fraction, whereas the modulus of rubber filled with higher concentrations of particles, in which particle-particle interactions as well as polymer-particle

interactions are important, show a quadratic correlation with volume fraction.[18] If there is a repulsive force between the particles and the polymer chains due to particle surface chemistry, the mechanical reinforcement depends only on filler volume fraction.[19] In addition, smaller particulate sizes correlate with improved reinforcement, even for energetically unfavorable interactions between polymer chains and particle surface.[20]

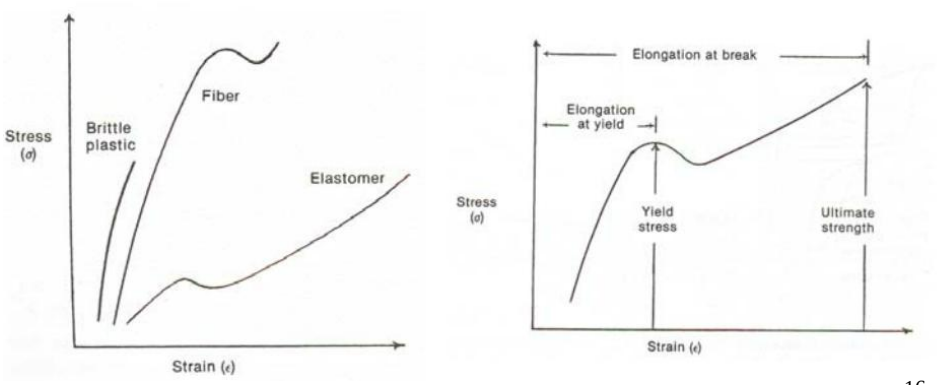

Figure 3.1: Polymer stress-strain curves (constant temperature).[16] A) Examples of stress-strain curves for brittle materials, fibers, and elastomers. B) A thermoplastic stress-strain curve with important characteristics labeled.

The preparation method of a polymer/filler composite material has a significant impact on the ultimate material properties of the composite. Particles can be incorporated in a polymer melt (during extrusion), a polymer solution, or can be present as the polymers are being synthesized.[1] When NPs are incorporated early in the processing steps, the rheological changes in the filler/polymer melt composite make other processing steps difficult.[11] The linear viscoelastic regime seen at low shear stress disappears once a significant weight percent of fillers is incorporated.[11] At low filler concentrations the preparation method has less influence on the final mechanical strength of the composite.[19] Surprisingly,

agglomeration of particles during incorporation into the polymer matrix does not negatively impact the mechanical properties significantly, and in fact these agglomerates may dissipate energy efficiently.[15] Nanoparticles are also thought to dissipate energy even after failure has occurred, thus preventing ultimate failure despite microscopic damage.[21]

Previous researchers have incorporated fillers into silicone networks by either *in situ* generation of particles or by *ex situ* mixing of particles into the liquid polymer prior to crosslinking. Using a silica (or titania) precursor, a hydrolysis reaction will both crosslink hydroxyl end group functionalized polysiloxanes and precipitate particles within the network, thus creating particles *in situ*.[22–25] Mechanically blending *ex situ* generated reinforcing particles into siloxanes requires processing time and energy.[14] Incorporation of small amounts (5 wt%) of *ex situ* generated silica fillers in siloxane networks can increase the Young's modulus and the ultimate break strength, assuming strong chemical compatibility between the particles and the polymer chains.[26]

Siloxanes have also been filled with other functional NPs, including boron nitride, aluminum oxide, iron oxide, and zinc oxide.[4,27] Though most conductive materials are rigid, flexible conductive PDMS composites are being developed and tested.[28–31] There is also a growing interest in silicone/magnetic NP composites for microfluidic actuation or other responsive devices.[32] Because magnetic NP filled silicones have a relatively low Young's modulus with a high magnetization ($M > 10^4$ A/m), application of a magnetic field significantly deforms these composites.[33] By crosslinking magnetic NP filled PDMS in the presence of a magnetic field, the resulting elastomer network shows mechanical anisotropy, even with spherical particles.[34]

The commercial silicone elastomer most commonly used, Sylgard 184®, has a tensile modulus between 1.3–3 MPa and an elongation at break of more than 140% when cured at room temperature[35,36] due to its incorporation of 30-60 wt% silica particles.[37] Curing Sylgard 184® above room temperature reduces the elongation at break and increases the Young's modulus of the network.[35] Although the high weight percentage of silica fillers may be related more to the manufacturer's cost or processing requirements, these particles certainly influence the mechanical properties of the final networks.

Because for the microfluidic work discussed in Chapter 2 of this dissertation we observed tearing of our microchannels at the edges of the features once removed from master molds, we decided to investigate the effects of silica fillers on PVMS networks. Tear strength is defined as the energy required to propagate a tear through a polymer sample until the sample has torn through. Evaluating tear strength can be difficult to reproduce in nanocomposite materials, as the fillers often create erratic crack propagation behavior,[38] so we first decided to study simple stress-strain behavior to learn about the mechanical properties of PVMS composites. We were motivated to improve not only the tear strength of our networks, but also to increase the extensibility and modulus of the networks.

There do not appear to be many studies investigating PVMS nanocomposites,[39] even though the interactions with fillers will be different due to chemical interactions of the vinyl group. For PDMS networks, it is known that the elastic modulus decreases with increasing chain length and increases with crosslinking density;[12] both chain length and crosslink density relate to the distance between crosslink points in the network. For our work with filled PVMS networks, we primarily worked with only one MW of PVMS.

3.2. Nanoparticle filled PVMS Networks

3.2.1. Method

PVMS was synthesized as discussed in Chapter 2 of this dissertation. Hydroxyl-terminated PDMS was purchased from Gelest (DMS-S35-100gm) and used as received. Several techniques were evaluated for strengthening the PVMS networks, including the addition of silica nanoparticles (NPs) and the *in situ* generation of particles. A methyl functionalized fumed silica filler, Aerosil® R104, was added to PVMS in varying weight amounts from 5 wt% up to 25 wt%. At 25 wt% and beyond, the incorporation of additional silica NPs became too difficult with the techniques available in our lab.

The silica particles and PVMS were agitated on a stand mixer for at least five minutes or until well incorporated into the liquid polymer. While sufficient mixing is necessary for uniform incorporation of the NPs into the polymer, further mixing may reduce the silica particle chain structures between the polymer chains; these interparticle associations are thought to play an essential role in the strengthening mechanism of the fillers.

Following the addition of fumed silica particles, a crosslinker (vinylmethoxysiloxane, or VMOS) was added at a weight ratio of 0.48g VMOS for every 10g PVMS used. This was stirred by hand and then degassed for 30 minutes to remove bubbles introduced during the particle addition step. Finally, a tin catalyst (ethyl tin hexanoate) diluted in THF (at a concentration of 1 mL catalyst for 9 mL THF) was added and quickly stirred in. The mixture would immediately begin to crosslink, so the contents would be poured into a petri dish or over a microchannel mold and placed in a 60°C oven to cure overnight.

We also evaluated the *in situ* generation of particles as a method of strengthening PVMS networks. For this method, the crosslinking agent also generates silica NPs as a by-product of the condensation reaction taking place within the network. In order to form particles, we had to use excess amounts of tetraorthosilicate (TEOS), and evaluated a 1:1, 2:1 and 4:1 mass ratio of TEOS to PVMS.[24] First, TEOS and PVMS were thoroughly mixed with the stand mixer for ten minutes. Next, a small amount of dibutyltin dilaurate or DBTDL (0.17 mL per 10g of PVMS) was mixed into the polymer mixture for an additional ten minutes. We then cured this mixture at room temperature for 48 h followed by 24 h in a 60°C oven in a petri dish before evaluating the mechanical properties.

A UV-vis determined transparency of the elastomeric networks. All samples measured had approximately the same thickness (~2 mm).

Samples tested on the Instron were poured into molds with dimensions for specimen type 5B as specified in the ISO 527 standards: gauge length 10 mm, thickness 1-2 mm, and width 2-4 mm. The Instron tested samples at a constant rate of extension of 5 mm/min until the samples broke. Stress was calculated as force over the initial cross-sectional area of the samples. Percentage strain was calculated as the change in sample length divided by the original length.

3.2.2. Results

We first characterized hydroxyl-terminated PDMS with fillers, generating stress-strain behavior predicted from the literature, i.e. increased tensile stress and strain % at break

(Figure 3.2). Even with a small amount of silica fillers, 1% by weight, the modulus and elongation at break increased significantly.

As predicted by filler-reinforcement results in PDMS, even a modest amount of filler increased the strength of PVMS networks (Figure 3.3). The modulus of an unfilled PVMS network is similar to PDMS: for this system, we got a modulus of roughly 2.3 MPa. From the stress-strain results, it is also noticeable that both the modulus and ultimate break stress increased for all filled samples.

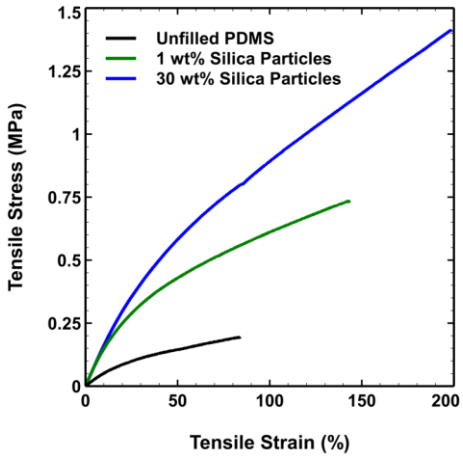

Figure 3.2: Hydroxyl terminated PDMS stress-strain results. Filled PDMS contains functionalized fumed silica.

For the sample with the highest amount of silica fillers, 25 wt%, the sample shows a significant increase in Young's modulus, but also appears to be the most brittle sample of all those tested. This could be related to poor mixing of the filler with the liquid PVMS rather than a theoretical maximum weight percent. The PVMS filled with 20 wt% silica fillers

extended nearly 100%, but this falls far short of the typical Sylgard-184 elongation. Again, without repetition it is difficult to draw definitive conclusions regarding the differences between filled PDMS and filled PVMS. Because we only tested networks made with one MW, this elongation may simply be reflective of the MW of the network.

Next, we evaluated PVMS networks reinforced with *in situ* generated particles. For the highest amount of TEOS:PVMS, we found that the network never fully cured, as after a week at room temperature and more than 24 h in the oven, the mixture was still tacky to the touch.

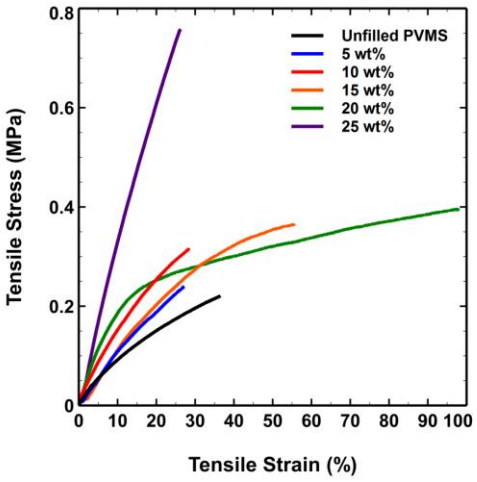

Figure 3.3: Fumed silica reinforced PVMS networks. All filled samples show increased Young's modulus as compared to unfilled PVMS, but elongation and ultimate stress at break are not necessarily improved.

We were able to test the samples with 1:1 and 2:1 ratio of TEOS:PVMS and found improved elongation at break as well as toughness (Figure 3.4). By calculating the amount of SiO_2

added as TEOS molecules, the final filler weight can be estimated to be roughly 20% for the 1:1 ratio and 30% for the 2:1 ratio.[24]

Sol-gel methods for making nanoparticles with the procedure we describe result in various structures based on several reaction conditions such as catalyst, pH, and temperature.[40] We therefore would need to optimize this process if we intended to use only *in situ* generated nanoparticles. Unfortunately, the TEOS filled networks also showed reduced optical transparency, ultimately making their use in microfluidics unlikely (Figure 3.5). One of the advantages of siloxane networks for microfluidic devices is the inherent transparency.

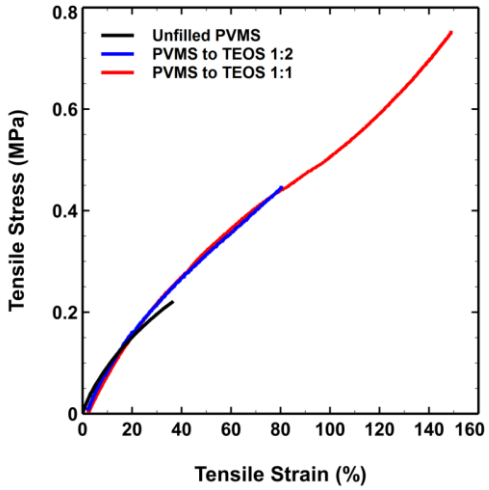

Figure 3.4: PVMS strengthened with *in situ* generated silica particles. The ratios of PVMS to TEOS are mass ratios; the blue curve represents approximately 30 wt% silica particles and the red curve represents approximately 20 wt% silica particles. The Young's modulus is similar for all three samples, but the toughness (the area under the stress-strain curve) is improved for both TEOS-filled samples.

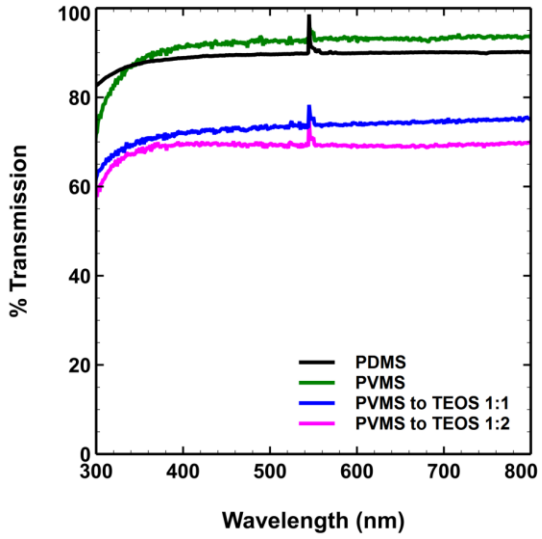

Figure 3.5: PVMS strengthened with *in situ* generated silica particles. The ratios of PVMS to TEOS are mass ratios. The TEOS filled PVMS shows a significant decrease in transparency. These samples were visibly grey in appearance.

Because the value of filling PVMS networks is the increased tear strength for removing networks from master molds, we also prepared several test microchannels to evaluate tearing along the edges of the features. As seen in Figure 3.6, increasing the amount of fillers does appear to improve the fidelity the replica to the master mold by decreasing tearing of the network along the mold edges. For the networks with significant amounts of filler, we were not always able to seal microchannels using oxygen plasma. It is unclear why silica fillers in PVMS would have this effect considering that Sylgard 184® channels contain a great deal of fillers and seal quite easily.

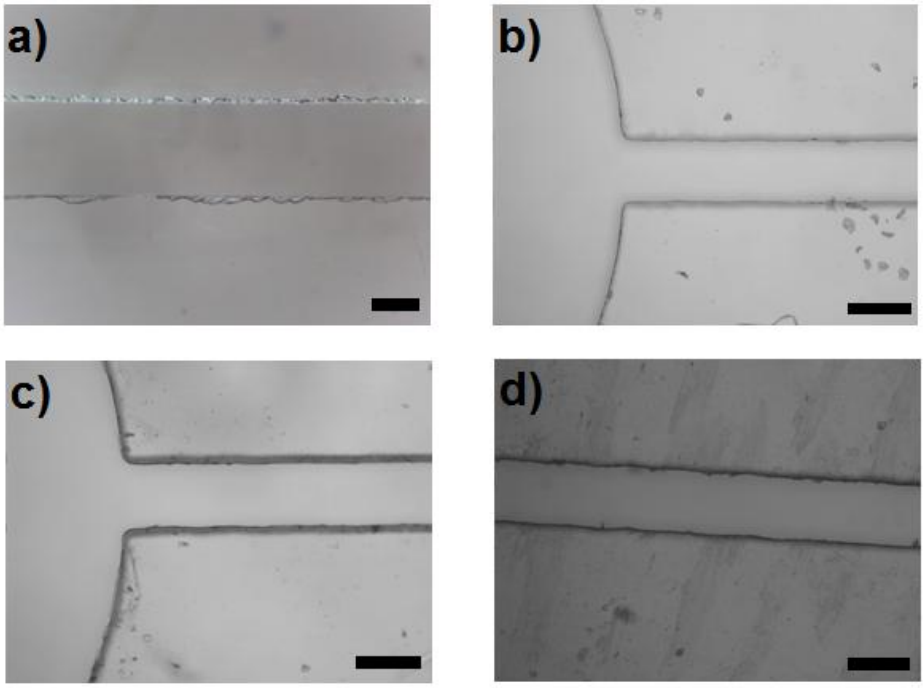

Figure 3.6: Images of PVMS microchannel replicas with varying amounts of silica filler. A) Pure PVMS with no silica fillers; b) 10 wt% filled; c) 15 wt% filled; d) 20 wt% filled. All scale bars are 500 μm.

3.3. Alternate Reinforcement Mechanisms

Although we crosslinked our elastomeric networks through the hydroxyl end groups, there are alternate chemical reactions that are useful for crosslinking siloxanes. Siloxane networks can also be crosslinked through the backbone if the side groups attached to the silicon atom are functional groups, e.g. vinyl groups or silicon hydride groups. Because the molecular weight between crosslink points (M_c) decreases with this method, the rigidity of the network increases. Backbone crosslinking is difficult to control, however, so in order to create a rigid siloxane network, shorter oligosiloxanes are often used in place of

polysiloxanes.[41–46] These networks are useful for optical applications such as encapsulation materials for light-emitting diodes (LEDs)[41] or coatings for optical fibers.[47] Using cyclic siloxanes results in a glassy transparent polymer due to the extremely short distance between crosslinks.[48]

Interpenetrating networks (IPNs) consisting of a siloxane network and another polymeric network may demonstrate beneficial properties of both networks. For example, an IPN of PDMS and a polyfluorinated acrylate demonstrated stronger mechanical properties than PDMS, a lower refractive index, and a more hydrophobic surface.[49] PDMS has also been combined with epoxy resin,[50,51] ethylene oxide,[52,53] N-isopropyl acrylamide,[54] and urethane.[55] These IPNs are more useful if the two networks used are compatible, which can be a challenge when combining a siloxane with an organic polymer.

Siloxane networks cured by thiol-ene mechanisms, as an alternative to platinum-based hydrosilylation or condensation curing methods, have been reported in the literature.[42,56,57] End-group functional PDMS chains which are thiol-ene cured behave similarly to hydrosilylation cured networks,[57] largely because the molecular weight of the polymer dominates the mechanical properties. While a typical PDMS network displays a storage modulus (as determined by dynamic mechanical analysis) of less than 10 MPa,[58] a thiol-ene cured oligosiloxane network at room temperature may have a storage modulus as high as 2000 MPa.[42] Several reports of modifying PVMS or copolymers of PDMS and PVMS by thiol-ene reactions exist in the literature.[59–61] Luminescent thiol-ene cured siloxane materials were also reported recently, made by incorporating lanthanide ions into a PVMS network.[62]

We made a thiol-ene network by combining hydroxyl-terminated PVMS, a photoinitiator, and a multi-functional thiol. Approximately 10g of PVMS was mixed with 0.25g pentaerythritol tetrakis(3-mercaptopropionate) (PETMP) and 0.17g 2-hydroxy-2-methyl-1-phenyl-propan-1-one. The resulting mixture, which was cloudy due to some phase separation of the thiol crosslinker and the polymer, was UV treated for 5 to 10 minutes. PVMS networks made using this technique had a high Young's modulus (over 800 MPa) but demonstrated no elasticity, as shown in Figure 3.7.

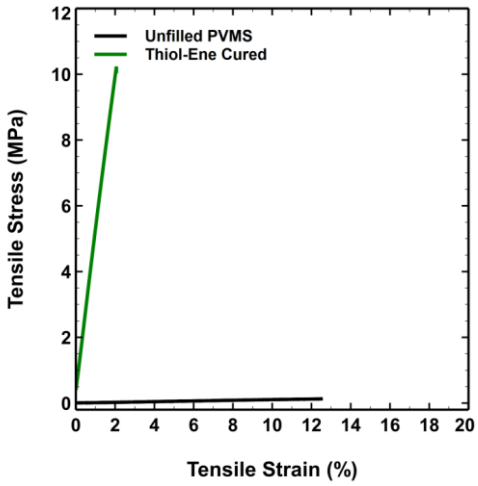

Figure 3.7: Stress-strain curves for end-group crosslinked PVMS (through hydroxyl end groups, using a condensation reaction with tin catalyst) and backbone crosslinked PVMS using a tetra-functional thiol compound. Because the thiol-ene cured PVMS networks breaks at such a high stress, the curve for the end-group PVMS is difficult to distinguish (it appears to be a flat line).

Immediately after UV curing, the networks had a slightly pink color, as seen in Figure 3.8. This color is likely due to an excitation of the photoinitiator byproducts, and could be

removed by washing the network in solvent. Thiol-ene networks which were not rinsed with solvent returned to the pink color with UV excitation.

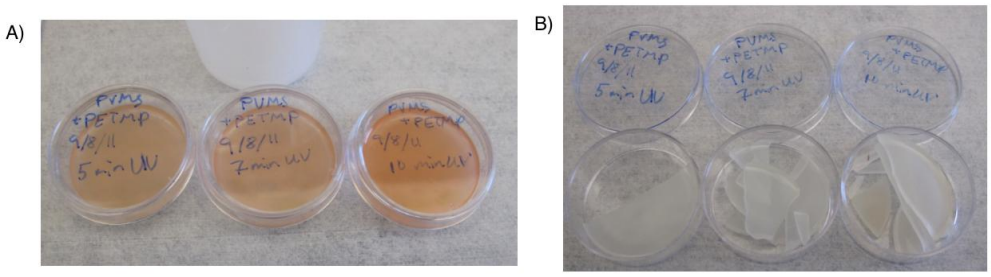

Figure 3.8: Photographs of thiolene cured PVMS networks A) immediately after curing and B) several hours after curing. The pink/orange color is evident in the image on the left (A) which is the result of a by-product of the photoinitiator.

3.4. Conclusion

We have demonstrated the mechanical reinforcement of a PVMS network by the incorporation of functionalized fumed silica particles. The elongation at break and Young's modulus improve with moderate weight percent particles in PVMS. We also observed reduced tearing at the edges of our microchannels with the incorporation of NPs. Additionally, we demonstrated a rigid thiol-ene cured PVMS network, which could potentially be useful for applications requiring a rapidly curing stiff material.

While we only tested a limited number of samples, replicating these results would confirm that silica nanoparticle filled PVMS networks demonstrate improved mechanical properties as compared to unfilled PVMS networks. Because we are primarily interested in increasing the tear strength of our networks, future work in this area includes the

quantification of tear strength with the addition of silica fillers in PVMS. The Instron extensometer used for stress-strain curves can also be used for determining tear strength as depicted in Figure 3.9.

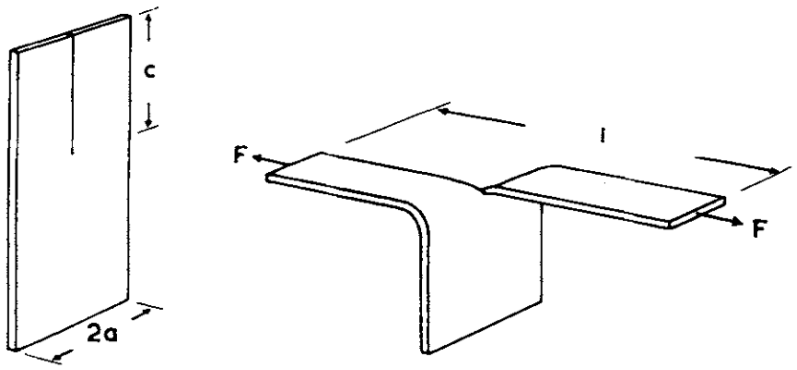

Figure 3.9: Schematic of a tear strength test.[38] A tearing force (*F*) is applied to the arms of a sample (width *2a*) on either side of a cut of length *c*.

We also demonstrated thiol-ene cured PVMS networks with a modulus orders of magnitude higher than traditional siloxane elastomeric networks. While thiol-ene cured polysiloxanes have been reported in the literature, our PVMS has both silanol end groups as well as vinyl side groups, giving our system dual functionality. Feasibly, a PVMS network could be both end-group cured and then additionally hardened with thiol groups, similar to the method used for the UV-hardened microchannels in Chapter 2 of this dissertation.

3.5. References

[1] Boonstra, B. B. Role of particulate fillers in elastomer reinforcement: a review. Polymer 20, 691–704 (1979).

[2] Bokobza, L. Elastomeric composites. I. Silicone composites. J. Appl. Polym. Sci. 93, 2095–2104 (2004).

[3] Althues, H., Henle, J. & Kaskel, S. Functional inorganic nanofillers for transparent polymers. Chem. Soc. Rev. 36, 1454 (2007).

[4] Gray, B. L. A Review of Magnetic Composite Polymers Applied to Microfluidic Devices. J. Electrochem. Soc. 161, B3173–B3183 (2014).

[5] Evans, B. A. et al. A highly tunable silicone-based magnetic elastomer with nanoscale homogeneity. J. Magn. Magn. Mater. 324, 501–507 (2012).

[6] Kong, S. M., Mariatti, M. & Busfield, J. J. C. Effects of types of fillers and filler loading on the properties of silicone rubber composites. J. Reinf. Plast. Compos. 30, 1087–1096 (2011).

[7] Coleman, J. N., Khan, U. & Gun'ko, Y. K. Mechanical Reinforcement of Polymers Using Carbon Nanotubes. Adv. Mater. 18, 689–706 (2006).

[8] Paul, D. R. & Mark, J. E. Fillers for polysiloxane ('silicone') elastomers. Prog. Polym. Sci. 35, 893–901 (2010).

[9] Warrick, E. L. & Lauterbur, P. C. Filler Phenomena in Silicone Rubber. Ind. Eng. Chem. 47, 486–491 (1955).

[10] Crosby, A. J. & Lee, J. Polymer Nanocomposites: The 'Nano' Effect on Mechanical Properties. Polym. Rev. 47, 217–229 (2007).

[11] Leblanc, J. L. Rubber–filler interactions and rheological properties in filled compounds. Prog. Polym. Sci. 27, 627–687 (2002).

[12] Yue, Y., Zhang, H., Zhang, Z. & Chen, Y. Tensile properties of fumed silica filled polydimethylsiloxane networks. Compos. Part Appl. Sci. Manuf. 54, 20–27 (2013).

[13] Mark, J. E., Abou-Hussein, R., Sen, T. Z. & Kloczkowski, A. Some simulations on filler reinforcement in elastomers. Polymer 46, 8894–8904 (2005).

[14] Camenzind, A., Schweizer, T., Sztucki, M. & Pratsinis, S. E. Structure & strength of silica-PDMS nanocomposites. Polymer 51, 1796–1804 (2010).

[15] Bokobza, L. The Reinforcement of Elastomeric Networks by Fillers. Macromol. Mater. Eng. 289, 607–621 (2004).

[16] Stevens, M. P. Polymer chemistry: an introduction. (Oxford University Press, 1999).

[17] Llorente, M. A., Andrady, A. L. & Mark, J. E. Model networks of end-linked polydimethylsiloxane chains. XI. Use of very short network chains to improve ultimate properties. J. Polym. Sci. Polym. Phys. Ed. 19, 621–630 (1981).

[18] Heinrich, G., Klüppel, M. & Vilgis, T. A. Reinforcement of elastomers. Curr. Opin. Solid State Mater. Sci. 6, 195–203 (2002).

[19] Le Strat, D., Dalmas, F., Randriamahefa, S., Jestin, J. & Wintgens, V. Mechanical reinforcement in model elastomer nanocomposites with tuned microstructure and interactions. Polymer 54, 1466–1479 (2013).

[20] Edwards, D. C. Polymer-filler interactions in rubber reinforcement. J. Mater. Sci. 25, 4175–4185 (1990).

[21] Gersappe, D. Molecular Mechanisms of Failure in Polymer Nanocomposites. Phys. Rev. Lett. 89, 058301 (2002).

[22] Sur, G. S. & Mark, J. E. Elastomeric networks cross-linked by silica or titania fillers. Eur. Polym. J. 21, 1051–1052 (1985).

[23] Sun, C.-C. & Mark, J. E. Comparisons among the reinforcing effects provided by various silica-based fillers in a siloxane elastomer. Polymer 30, 104–106 (1989).

[24] Alexandru, M., Cristea, M., Cazacu, M., Ioanid, A. & Simionescu, B. C. Composite materials based on polydimethylsiloxane and in situ generated silica by using the sol-gel technique. Polym. Compos. 30, 751–759 (2009).

[25] McCarthy, D. W., Mark, J. E. & Schaefer, D. W. Synthesis, structure, and properties of hybrid organic–inorganic composites based on polysiloxanes. I. Poly(dimethylsiloxane) elastomers containing silica. J. Polym. Sci. Part B Polym. Phys. 36, 1167–1189 (1998).

[26] Schaefer, D. W., Vu, B. T. N. & Mark, J. E. The effect of interphase coupling on the structure and mechanical properties of silica-siloxane composites. Rubber Chem. Technol. 75, 795–810 (2002).

[27] Yurkov, G. Y. et al. Fe-Containing nanoparticles in siloxane rubber matrices. Inorg. Mater. 42, 496–502 (2006).

[28] Cong, H. & Pan, T. Photopatternable Conductive PDMS Materials for Microfabrication. Adv. Funct. Mater. 18, 1912–1921 (2008).

[29] Liu, C. X. & Choi, J. W. Patterning conductive PDMS nanocomposite in an elastomer using microcontact printing. J. Micromechanics Microengineering 19, 085019 (2009).

[30] Kujawski, M., Pearse, J. & Smela, E. PDMS/graphite stretchable electrodes for dielectric elastomer actuators. in 76420R–76420R–9 (2010). doi:10.1117/12.847249

[31] Niu, X. Z., Peng, S. L., Liu, L. Y., Wen, W. J. & Sheng, P. Characterizing and Patterning of PDMS-Based Conducting Composites. Adv. Mater. 19, 2682–2686 (2007).

[32] Nguyen, V. Q., Ahmed, A. S. & Ramanujan, R. V. Morphing Soft Magnetic Composites. Adv. Mater. 24, 4041–4054 (2012).

[33] Thévenot, J., Oliveira, H., Sandre, O. & Lecommandoux, S. Magnetic responsive polymer composite materials. Chem. Soc. Rev. 42, 7099–7116 (2013).

[34] Sohoni, G. B. & Mark, J. E. Anisotropic reinforcement in elastomers containing magnetic filler particles. J. Appl. Polym. Sci. 34, 2853–2859 (1987).

[35] Johnston, I. D., McCluskey, D. K., Tan, C. K. L. & Tracey, M. C. Mechanical characterization of bulk Sylgard 184 for microfluidics and microengineering. J. Micromechanics Microengineering 24, 035017 (2014).

[36] Schneider, F., Fellner, T., Wilde, J. & Wallrabe, U. Mechanical properties of silicones for MEMS. J. Micromechanics Microengineering 18, 065008 (2008).

[37] Sylgard 184 MSDS (downloaded 1/30/2015). at <http://www.dowcorning.com/applications/search/default.aspx?r=131en>

[38] Greensmith, H. W. & Thomas, A. G. Rupture of rubber. III. Determination of tear properties. J. Polym. Sci. 18, 189–200 (1955).

[39] Meng, Y., Chu, J., Liu, C., Wei, Z. & Zhang, L. Oil resistance and mechanical properties of polysiloxane nanocomposites prepared by in situ reaction of reactive polar monomers. J. Appl. Polym. Sci. 131, n/a–n/a (2014).

[40] Breiner, J. M. & Mark, J. E. Preparation, structure, growth mechanisms and properties of siloxane composites containing silica, titania or mixed silica–titania phases. Polymer 39, 5483–5493 (1998).

[41] Bae, J., Kim, Y., Kim, H.-Y., Lim, Y. & Bae, B.-S. Sol–gel synthesized linear oligosiloxane-based hybrid material for a thermally-resistant light emitting diode (LED) encapsulant. RSC Adv. 3, 8871–8877 (2013).

[42] Kim, J.-S., Yang, S., Park, H. & Bae, B.-S. Photo-curable siloxane hybrid material fabricated by a thiol–ene reaction of sol–gel synthesized oligosiloxanes. Chem. Commun. 47, 6051 (2011).

[43] Jacobine, A. F. & Nakos, S. T. in Radiation Curing (ed. Pappas, S. P.) 181–240 (Springer US, 1992).

[44] Eo, Y.-J., Kim, J. H., Ko, J. H. & Bae, B.-S. Optical characteristics of photo-curable methacryl-oligosiloxane nano hybrid thick films. J. Mater. Res. 20, 401–408 (2011).

[45] He, J., Zhou, L., Soucek, M. D., Wollyung, K. M. & Wesdemiotis, C. UV-curable hybrid coatings based on vinylfunctionlized siloxane oligomer and acrylated polyester. J. Appl. Polym. Sci. 105, 2376–2386 (2007).

[46] Abe, Y. & Gunji, T. Oligo- and polysiloxanes. Prog. Polym. Sci. 29, 149–182 (2004).

[47] Masson, F., Decker, C., Andre, S. & Andrieu, X. UV-curable formulations for UV-transparent optical fiber coatings: I. Acrylic resins. Prog. Org. Coat. 49, 1–12 (2004).

[48] Zheng, P. & McCarthy, T. J. Rediscovering Silicones: Molecularly Smooth, Low Surface Energy, Unfilled, UV/Vis-Transparent, Extremely Cross-Linked, Thermally Stable, Hard, Elastic PDMS. Langmuir 26, 18585–18590 (2010).

[49] Darras, V., Fichet, O., Perrot, F., Boileau, S. & Teyssié, D. Polysiloxane–poly(fluorinated acrylate) interpenetrating polymer networks: Synthesis and characterization. Polymer 48, 687–695 (2007).

[50] Sung, P. H. & Lin, C. Y. Polysiloxane modified epoxy polymer networks—I. Graft interpenetrating polymeric networks. Eur. Polym. J. 33, 903–906 (1997).

[51] Jia, L.-Y., Zhang, C., Du, Z.-J., Li, C.-J. & Li, H.-Q. A novel approach to interpenetrating networks of epoxy resin and polydimethylsiloxane. J. Appl. Polym. Sci. 105, 2663–2669 (2007).

[52] Oh, B. et al. New interpenetrating network type poly (siloxane-g-ethylene oxide) polymer electrolyte for lithium battery. J. Power Sources 119, 442–447 (2003).

[53] Oh, B., Hyung, Y.-E., Vissers, D. R. & Amine, K. New Interpenetrating Network-Type Siloxane Polymer Electrolyte. Electrochem. Solid-State Lett. 5, E59–E61 (2002).

[54] Erbil, C., Kazancıoğlu, E. & Uyanık, N. Synthesis, characterization and thermoreversible behaviours of poly(dimethyl siloxane)/poly(N-isopropyl acrylamide) semi-interpenetrating networks. Eur. Polym. J. 40, 1145–1154 (2004).

[55] Byczyński, Ł., Dutkiewicz, M. & Maciejewski, H. Thermal degradation kinetics of semi-interpenetrating polymer network based on polyurethane and siloxane. Thermochim. Acta 560, 55–62 (2013).

[56] Müller, U., Kunze, A., Herzig, C. & Weis, J. Photocrosslinking of Silicones. Part 13. Photoinduced Thiol-Ene Crosslinking of Modified Silicones. J. Macromol. Sci. Part A 33, 439–457 (1996).

[57] Goswami, K., Skov, A. L. & Daugaard, A. E. UV-Cured, Platinum-Free, Soft Poly(dimethylsiloxane) Networks. Chem. – Eur. J. 20, 9230–9233 (2014).

[58] Glaser, R. H. & Wilkes, G. L. Structure property behavior of polydimethylsiloxane and poly(tetramethylene oxide) modified TEOS based sol-gel materials. Polym. Bull. 19, 51–57 (1988).

[59] Xue, L. et al. Facile, versatile and efficient synthesis of functional polysiloxanes via thiol–ene chemistry. Eur. Polym. J. 49, 1050–1056 (2013).

[60] Abdellah, L., Boutevin, B. & Youssef, B. Synthesis and applications of photocrosslinkable poly(siloxanes). Prog. Org. Coat. 23, 201–236 (1994).

[61] Cole, M. A. & Bowman, C. N. Evaluation of thiol-ene click chemistry in functionalized polysiloxanes. J. Polym. Sci. Part Polym. Chem. 51, 1749–1757 (2013).

[62] Zuo, Y. et al. Preparation and characterization of luminescent silicone elastomer by thiol–ene ‘click’ chemistry. J. Mater. Chem. C 2, 2724–2734 (2014).

CHAPTER 4. Elastin-like Peptides for PVMS Surface Modification

4.1. Introduction

As discussed in Chapter 1 of this dissertation, stimuli-responsive materials exhibit changes in one or more physical or chemical property in response to various internal or external stimuli, such as pH, temperature, light, magnetic or electric field, or chemical agents.[1–3] Polymers comprising two or more distinct chemical moieties offer opportunities for tailoring responsiveness if the responsive building blocks of the heteropolymer respond in a reversible fashion to different stimuli or respond differently to the same stimulus.[1,4] Stimuli-responsive materials can effectively manipulate and monitor biological compounds in microfluidic and bioanalytical devices.[5] For example, control over cellular or biomolecular interactions on surfaces or at interfaces can prevent undesirable adsorption while encouraging intended cellular attachment.[6] Additionally, the interface between biological systems and nanomaterials involves complex dynamic physicochemical and thermodynamic interactions; understanding these interactions is critical for the use of nanomaterials in biological applications.[7] Many polypeptides self-assemble into complex nanomaterials.[8] Thus, synthetic polypeptides are being explored for applications in drug delivery,[9] biomedical engineering,[10] and biomolecular purification.[11]

We have chosen to study elastin-like polypeptides (ELPs), or elastin-like recombinamers,[12] for their highly controlled amino acid composition, sequence, and length. These attributes endow ELPs with tunable and well defined physicochemical characteristics, such as a temperature trigger to transition from the coil to the globule conformation in aqueous environments.[13] Additionally, ELPs are biodegradable,[14] so they are excellent candidates for biomedical applications and are considered environmentally friendly

materials. Recombinantly synthesized ELPs consist of the repeat unit (Xaa-Gly-Val-Pro-Gly), where Xaa can be replaced with any amino acid residue except proline. Most ELPs exhibit a lower critical solution temperature (LCST). Adjustments to the guest residue and the sequence of the pentapeptides tune the LCST of the ELP, giving fine control over the responsiveness.[15] Additionally, changes to pH and salt concentration may increase or decrease the LCST of an ELP by several degrees, increasing the parameter space for controlling ELP solutions.

ELPs with a diblock copolymer architecture (diblock ELPs) exhibit two transition temperatures, one associated with the collapse of each block. Thus, a diblock ELP will pass through a micelle stage before completely collapsing.[16,17] Because micelle assembly is reversible in solution, stable nanoparticles are created through chemical crosslinking[18] or through manipulation of the environment to favor stable aggregates. For example, if the ELP contains lysine, crosslinking can be carried out with glutaraldehyde, and there is some evidence that naturally occurring tropoelastin undergoes irreversible aggregation[19] under certain conditions (such as incubation at elevated pH), even in the absence of crosslinking agents. However, in the absence of these stabilizing conditions, irreversible micelle formation or aggregation of ELPs has not been reported previously.

Although the covalent grafting of polymer chains onto surfaces is a rich field,[20] many studies investigating the interaction of polypeptides with surfaces rely only on physical adsorption rather than covalent grafting.[21,22] Surfaces modified with ELPs by other research groups may rely on adsorption[23] or π-π stacking,[24] and when covalently bound to the surface may rely on crosslinking through lysine groups.[25] These previous reports indicate that when

ELPs are adsorbed onto a surface they do not interact with strongly, they rearrange and form aggregates on the surface over time.[23] When adsorbed onto a more strongly interactive surface, however, ELPs will behave as "grafting-to" brushes, demonstrating temperature responsiveness.[24] Research on polymer brushes exhibiting LCST behavior reveals that classical models do not necessarily fully describe the behavior of the brushes,[26] so ELP brushes also may behave in unexpected ways. Other research groups also have investigated the adsorption of conventional diblock copolymer micelles on surfaces, studying the resulting features with TEM and AFM.[27–30] Micelles typically adsorb onto an attractive surface in a sparsely populated monolayer due to surface exclusion effects.[30] Over time, however, if the outer block of the micelle has a large affinity for the surface, the micelle can slowly break apart, allowing the outer block to spread over the surface, rearranging and forming a polymer-brush like layer.[29]

4.1.1. ELPs for PVMS Modification

Developing bioassays and biosensors on substrates such as glass, gold, silicon, or polymers requires chemical modification through attachment of small molecules or proteins.[31–33] When grafted onto a gold surface or other rigid surface, ELPs demonstrate responsive capture and release of targeted cells or proteins,[34,35] but ELPS have not yet been utilized on softer elastomeric substrates. PDMS is often used for microfluidic bioassays[36] because it is so easy to work with, though it is not particularly easy to modify chemically. Nevertheless, many researchers chose to work with PDMS for their biological devices and modify the surface using acids,[37,38] plasma,[39] UV light,[38,40] or other techniques.[41–43]

Some examples of biological applications using modified PDMS include cell adhesion,[44,45] prevention of non-specific adsorption,[46] or attachment of bioactive monolayers for biosensing.[47] For example, researchers attempting to create an anti-microbial surface attached arginine−tryptophan-rich peptides to a PDMS surface using UV grafting.[48] In another example, the uncured PDMS was doped with undecylenic acid to provide an anchoring group to attach a thiol-based monolayer, onto which they grafted DNA.[49] While these PDMS modification techniques are innovative and useful for exploring this area, many approaches require several steps (five or more) to generate the desired functionalization.[50]

Our motivation was to create a temperature responsive ELP film on a polymer surface for applications in bio-microfluidics. By attaching ELPs to the simple-to-modify PVMS vinyl side groups, we are enabling the rapid generation of bioactive surfaces. First using thiol-ene chemistry to attach a mercapto-acid to the vinyl-rich surface, we could then generate a carboxylic acid monolayer. The desired molecule or peptide can then be easily grafted with EDC/NHS chemistry, resulting in a simple two-step modification. Because of the complicated nature of the diblock polypeptide, we first chose to perform control grafting experiments on simple substrates, namely silicon wafers.

In this work, we covalently grafted ELPs to silicon surfaces from solution temperatures that corresponded to fully solvated, micellar, or fully collapsed ELPs. Thus, we considered conditions comparable to the typical "grafted-to" polymer brush system as well as systems in which diblock copolymer micelles are attached to surfaces. The surface morphologies of our grafted ELP assemblies as characterized by AFM revealed significant differences between our system and typical grafted polymer assemblies. Specifically, we

found that depositing ELPs at high temperatures formed stable aggregates on silicon surfaces modified with carboxylic acid functional monolayers. We sought to expand our understanding of these deviations in phase behavior in several ways: by reversing which block grafted to the surface, comparing chemically grafted and physically adsorbed assemblies, and using surfactants to probe the stability of the surface-grafted ELP assemblies. We believe these findings will be important considerations for future design of responsive surfaces.

4.2. Experimental Methods

Elastin-like peptides were synthesized as described elsewhere.[51] The two diblock ELPs used had the following sequences: G-$(SGVPG)_{40}$-$(VGVPG)_{40}$, called the "G-Diblock", and G-$(VGVPG)_{40}$-$(SGVPG)_{40}$, called the "Reversed Diblock" or "R-Diblock". The blocky copolypeptides had the following sequences: "alternating" SKGPG-$(SGVPGVGVPG)_{40}$-WPC, "blocky-5" SKGPG-$[(SGVPG)_5$-$(VGVPG)_5]_8$-WPC, "blocky-10" SKGPG-$[(SGVPG)_{10}$-$(VGVPG)_{10}]_{40}$-WPC, and "diblock" SKGPG-$(SGVPG)_{40}(VGVPG)_{40}$-WPC. We also had two homopolymers, "L1 4-80" SKGPG-$(VGVPG)_{80}$-Y, and "L1 S-80" SKGPG-$(SGVPG)_{80}$-WPC.

2-(N-morpholino)ethanesulfonic acid buffer (BupH MES Buffered Saline, Thermo Scientific) was prepared by dissolving a packet of MES buffer solution in deionized (DI) water, resulting in a pH of 4.7. A solution of 1 N NaOH (Fisher) was diluted in DI water to prepare a 0.1 N solution of NaOH. This diluted NaOH was added to the MES buffer solution to bring the final pH up to 6.0. Phosphate-buffered saline (PBS pH 7.4, Sigma-Aldrich) was

used to dissolve the ELPs for deposition. The concentration of the deposition solution was 25 μM of peptide in PBS.

Peptide solutions were prepared by dissolving 41.39 mg peptide in 5 mL filtered PBS. The solution was mixed with a touch mixer and then centrifuged (Thermo Scientific, SORVALL ST-16R) at 13000 rpm for 30 s. The mixing/centrifugation was repeated three times. The solution was then divided into 1 mL aliquots (250 μM) for future use. An aliquot was diluted in 9 mL PBS before being used for depositions, bringing the concentration of ELPs in PBS to 25 μM.

Silicon wafers were cleaned with UV-ozone exposure (Model No. 2 UVO Cleaner, Jelight Co, Inc.) for 20 minutes. Wafers were immediately immersed into a solution of 10-undecenyltrichlorosilane (UDTS, Gelest) in anhydrous toluene (Sigma-Aldrich) and stored overnight (or until needed) at 5°C. UDTS treated wafers were rinsed with fresh toluene, dried with nitrogen, and the UDTS layer was evaluated with ellipsometry (VASE, J.A. Woollam) at three angles of incidence (65, 70, 75°) over wavelength range 400~800 nm and water contact angle (WCA, model 100-00, Rame-Hart). Wafers were then covered in a solution of 11-mercaptoundecanoic acid (MUA, Aldrich) in IPA (Sigma-Aldrich) (concentration of 0.1 g MUA/ 1 mL isopropanol) and covered with a quartz slide for UV treatment. Exposure to 254 nm light (Model ENF-260C, Spectroline) lasted for 30 minutes. The UV light grafted the MUA groups onto the UDTS by thiol-ene chemistry, providing a carboxylic acid terminated surface for further modification by ELPs. Wafers were then rinsed with methanol and isopropanol, and thickness was checked with ellipsometry (and WCA). Wafers were used immediately or stored in DI water until needed.

The MUA-coated wafers were activated for peptide coupling with a solution of 1-ethyl-3-[3-dimethylaminopropyl]carbodiimide hydrochloride (EDC, Thermo Scientific Pierce) and N-hydroxysulfosuccinimide (sulfo-NHS, Thermo Scientific Pierce) in MES buffer and stored in 5°C for 4-6 hours (0.015 g/5mL of EDC and 0.015 g/5mL of sulfo-NHS in MES buffer). Activated wafers were rinsed with DI water to remove EDC/sulfo-NHS and submerged into peptide solutions for deposition of peptides. Heated peptide depositions were performed by dropping an activated wafer into a test tube of peptide/buffer solution (concentration 25 μM or 0.83 mg/mL) and then placed in a pre-heated heating bath. All depositions were carried out overnight (at least 12 hrs).

Wafers were sonicated post-deposition in a bath sonicator in ice water for 30 minutes to remove physically adsorbed peptides. For control experiments, some wafers were additionally sonicated in sodium dodecyl sulfate (SDS) solutions of varying concentrations for an additional 20 minutes, then left in SDS solutions overnight before being thoroughly rinsed with DI water. Wafers were also analyzed with ellipsometry and WCA and then stored in DI water at 5°C until needed for studies using atomic force microscopy (AFM). AFM images (Bruker Cantilevers: ScanAsyst-Fluid tips with nominal radius of 20 nm and spring constant 0.7 N/m, Bruker Multimode 8, Nanoscope 9.0) were recorded in air and DI water at room temperature using a fluid cell. The fluid cell was cleaned with ethanol and dried with nitrogen prior to scans. DI water was used for fluid images. Water contact angle was recorded using a goniometer at room temperature.

4.3. Elastin-like Polypeptide Characterization

ELPs were characterized by dynamic light scattering and SDS-PAGE by our collaborators at Duke Unversity as follows in Figures 4.1-4.8.

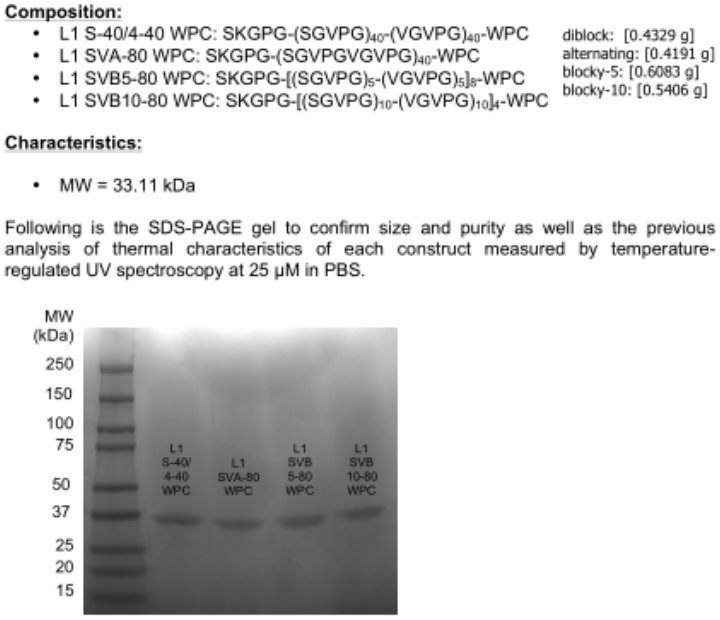

Figure 4.1: Blocky peptide sequence, molecular weight, and SDS-PAGE gel results.

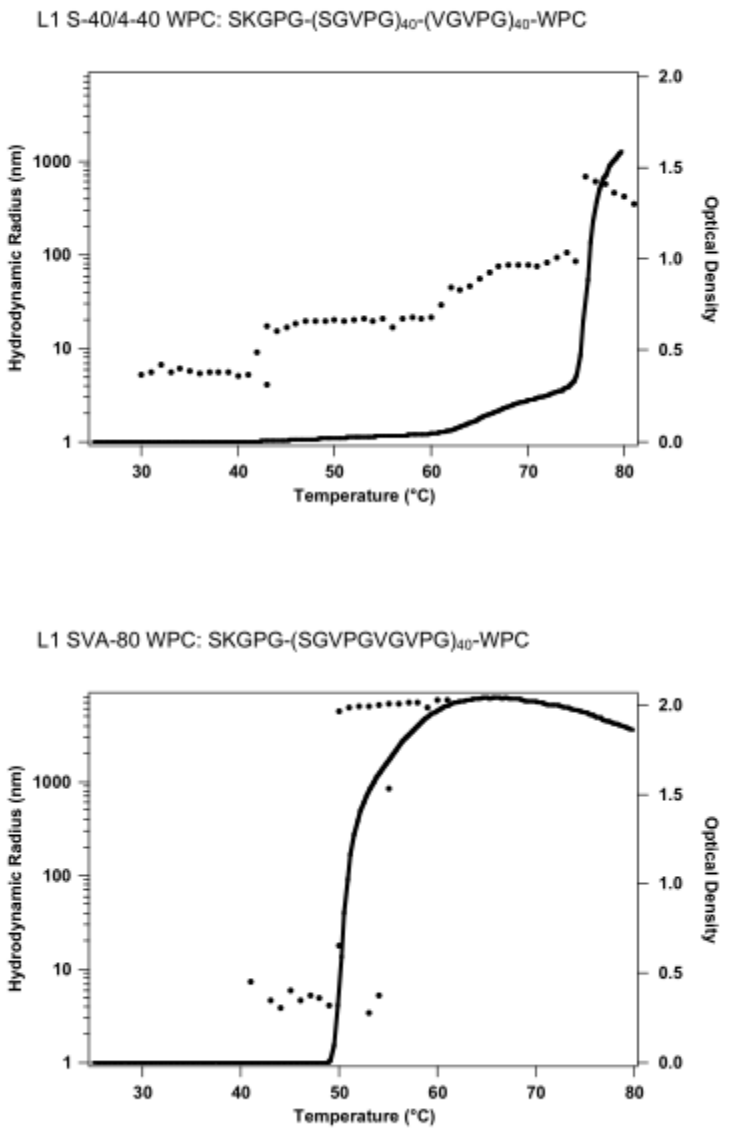

Figure 4.2: Dynamic light scattering results for diblock (top) and alternating (bottom) ELPs.

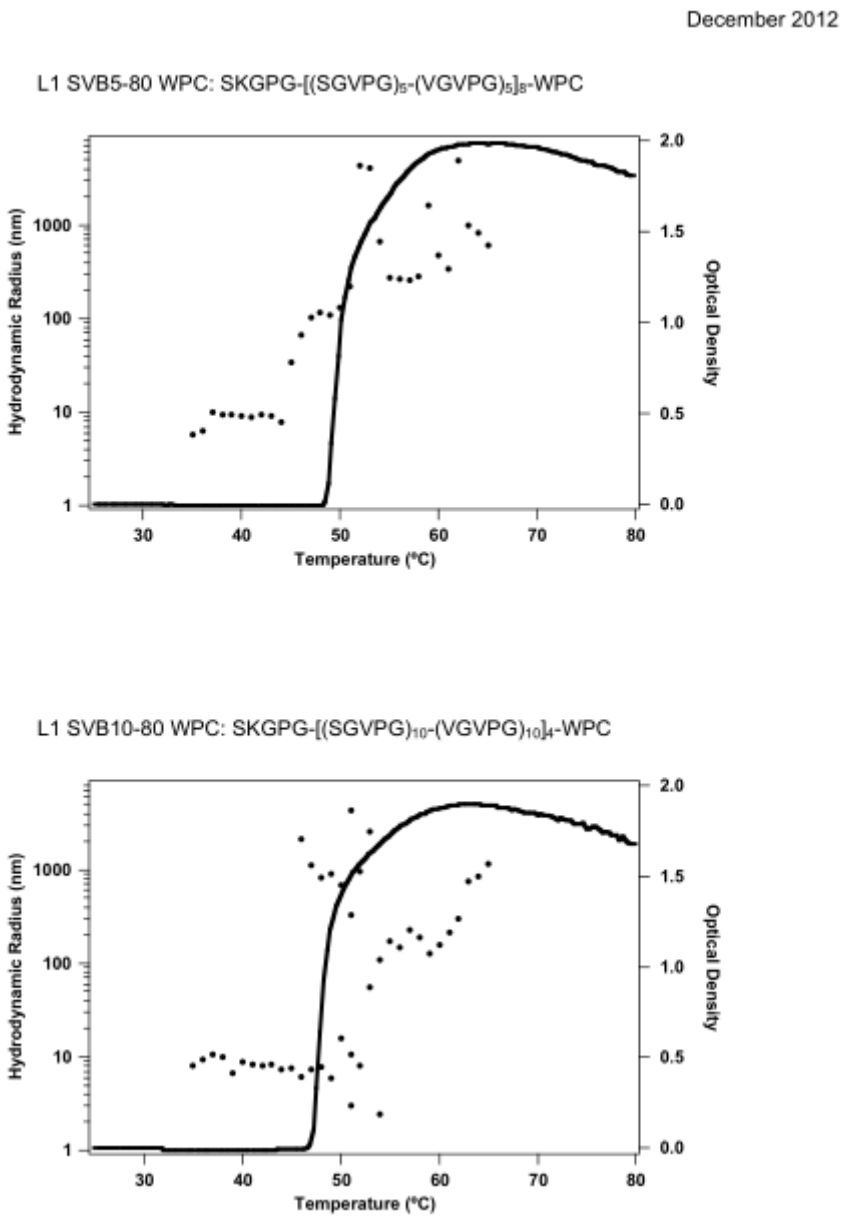

Figure 4.3: Dynamic light scattering results for blocky-5 (top) and blocky-10 (bottom) ELPs.

The following ELP_{BC}s have "flipped" sequences based on the order of their encoded hydrophobic and hydrophilic ELP domains. The ELP sequences are always written from N- to C-terminus. I've included schematics to help orient the position of the amine and carboxyl terminal groups inherent to each polypeptide when they are in their soluble unimer or self-assembled micelle state – I show the hydrophobic block in black and the hydrophilic block in grey. Thermal characterization is at 25 μM in PBS.

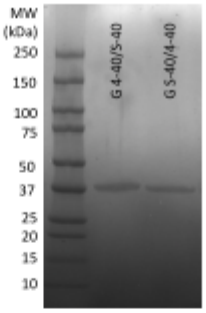

Sample: G 4-40/S-40
ELP sequence: G-$(VGVPG)_{40}$-$(SGVPG)_{40}$
MW: 32.35 kDa

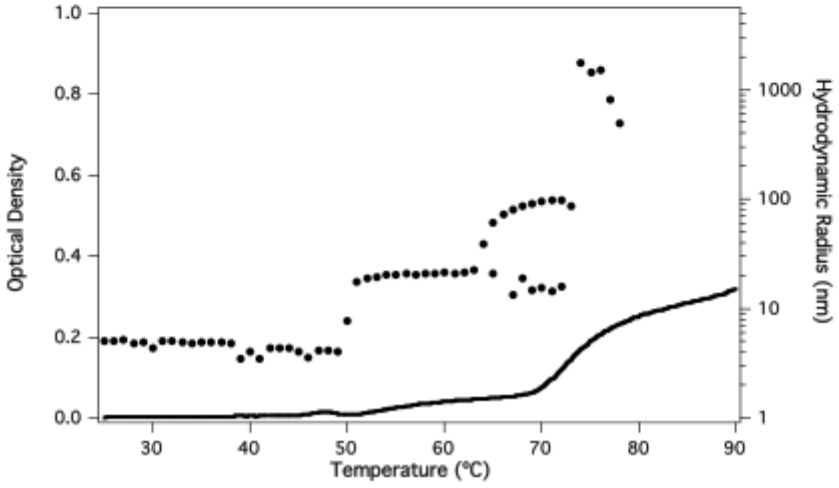

Figure 4.4: SDS-PAGE results for G-Diblock and R-Diblock. Dynamic light scattering results for R-diblock ELP.

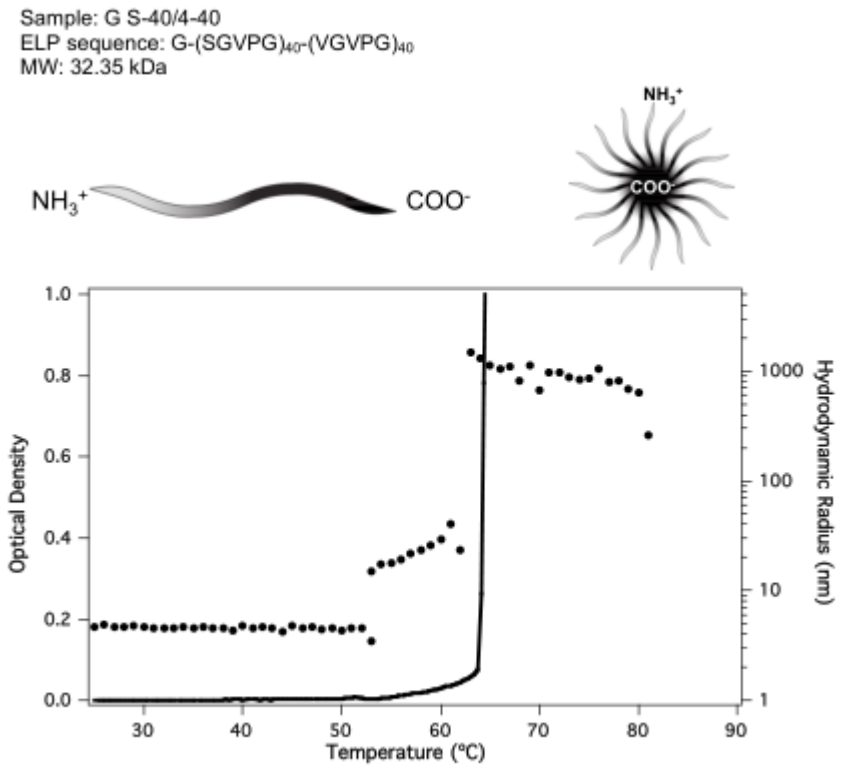

Figure 4.5: Dynamic light scattering results for the G-diblock ELP.

This homopolymer control is composed of the hydrophilic ELP sequence (serine guest residue) and size matched to the other constructs (80 pentapeptides). This ELP is very hydrophilic – we cannot detect its T_t in PBS. If we measure its T_t over a range of NaCl concentrations we can extrapolate to its approximate T_t in PBS. By this method we can approximate that the T_t in PBS at 25 µM is 105 °C.

Sample: L1 S-80 WPC
ELP sequence: SKGPG-$(SGVPG)_{80}$-WPC
MW: 32.63 kDa

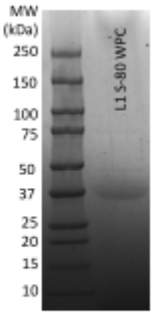

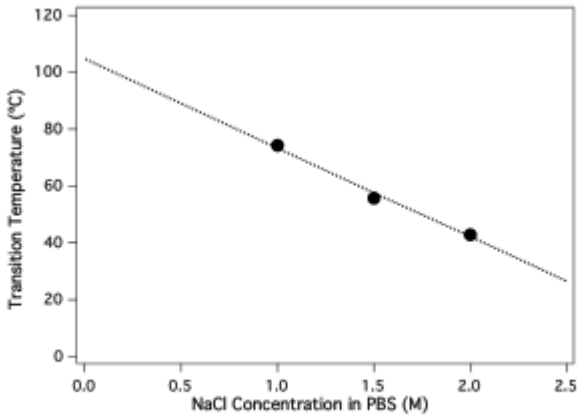

Figure 4.6: SDS-PAGE results for the hydrophilic L1 S-80 homopolymer. Transition temperature plotted as a function of NaCl concentration.

December 2012

Storage:
Store lyophilized ELPs at -20 °C upon arrival. Once resuspended, store ELPs in solution at -20 °C, aliquoting in volumes to minimize freeze-thaw events of the solution.

Resuspension:
- To resuspend lyophilized ELPs weigh desired amount of dried sample and add buffer to create desired concentration.
- Once the buffer is added, centrifuge the solution (the ELP will not likely yet be solubilized) at 13,000g for 30 seconds.
- Pipette the solution to help dissolve the resulting pellet.
- Centrifuge again at 13,000g for 30 seconds and pipette the solution to help dissolve the pellet, if there is one.
- Centrifuge a final time at 13,000g for 1 minute to ensure no pellet is formed and the ELP is completely solubilized.

Composition:
- L1 4-80: SKGPG-$(VGVPG)_{80}$-Y
- L1 36-80: SKGPG-$(VGVPGVGVPGAGVPGVGVPGVGVPG)_{16}$-Y

Characteristics:

- L1 4-80
  MW = 33.37 kDa
  Transition temperature ~ 29-35 °C at 5-100 µM in PBS
- L1 36-80
  MW = 32.92 KDa
  Transition temperature ~ 34-42 °C at 5-100 µM in PBS

Following is the SDS-PAGE gel to confirm size and purity as well as the analysis of thermal properties by temperature-regulated UV spectroscopy at 5-100 µM in PBS.

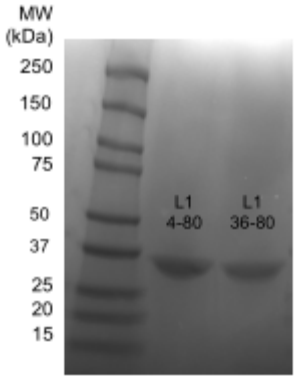

Figure 4.7: SDS-PAGE results for hydrophobic L1 4-80 homopolymer.

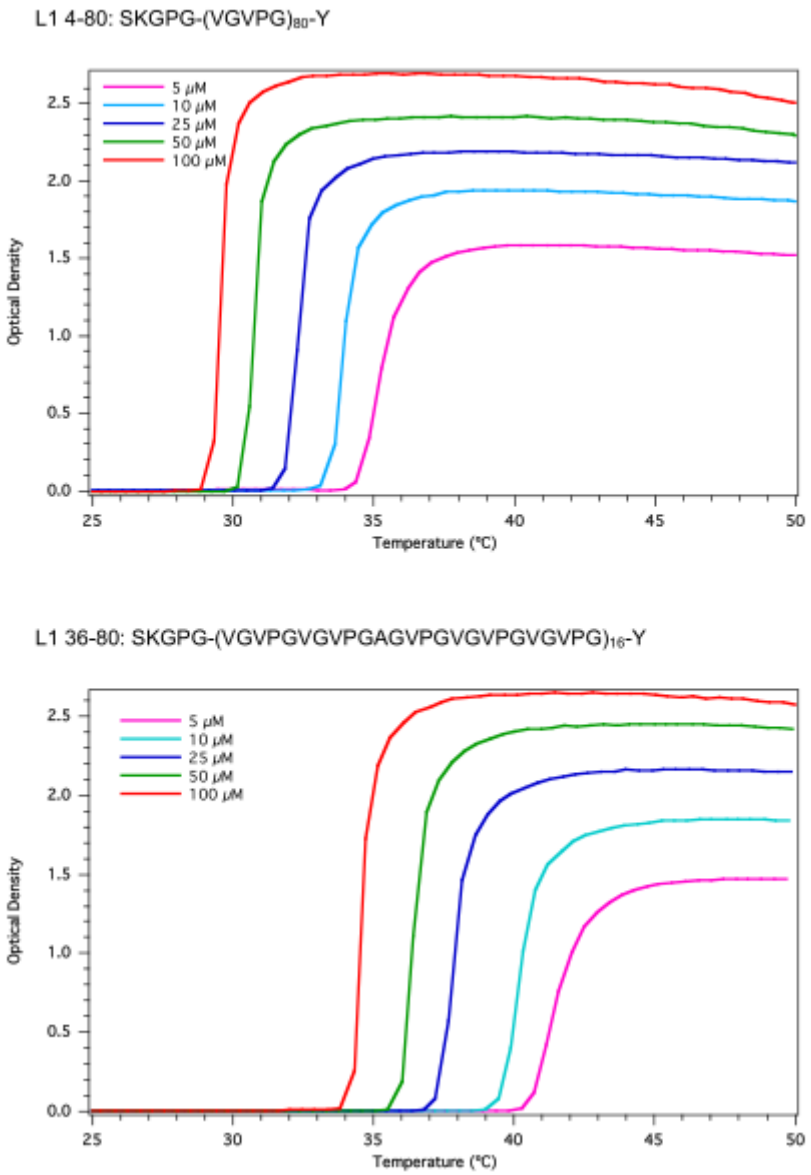

Figure 4.8: Dynamic light scattering results for L1 4-80 and L1 36-80 ELPs.

4.4. Results

4.4.1. Diblock Copolypeptides

Our initial hypothesis was that by partially collapsing diblock ELPs, we would be able to increase the grafting density at the surface, as indicated by the schematic in Figure 4.9. By covalently grafting fully or partially collapsed diblock polypeptides, we theorized that the volume exclusion effects that normally prevent grafting-to polymer brushes from generating densely packed brushes would be minimized. Once cooled, the grafted ELP micelles or aggregates would ideally resolubilize. We found, however, that after deposition, the aggregates and micelles did not resolubilize as anticipated.

The behavior of ELPs in bulk was assessed by measuring the cloud points and hydrodynamic radius. The ELP deposition on surfaces was carried out at 25, 40, 50, 55, 60, 65, 70, and 80°C, with these temperatures corresponding to the various transitions of the ELPs in bulk. After sonication to remove physically adsorbed ELPs on the surface, we employed AFM and ellipsometry to characterize thickness and morphology, respectively, of the grafted ELPs on silicon surfaces (Figures 4.10-4.12). For all ELPs and deposition temperatures, a MUA surface that had not undergone EDC/s-NHS activation served as a control. These controls were treated the same way as the grafted surfaces (i.e. sonicated in fresh DI water in an ice bath after deposition and then stored in DI water). Through both ellipsometric measurements and AFM results (Figures 4.10-4.14), it is clear that less peptide remains on the surface of controls after sonication than in the grafted case. Some peptide will remain physically adsorbed to the surfaces after sonication due to hydrogen bonding

between the carboxylic acid groups on the surface and the peptides, as will be discussed below.

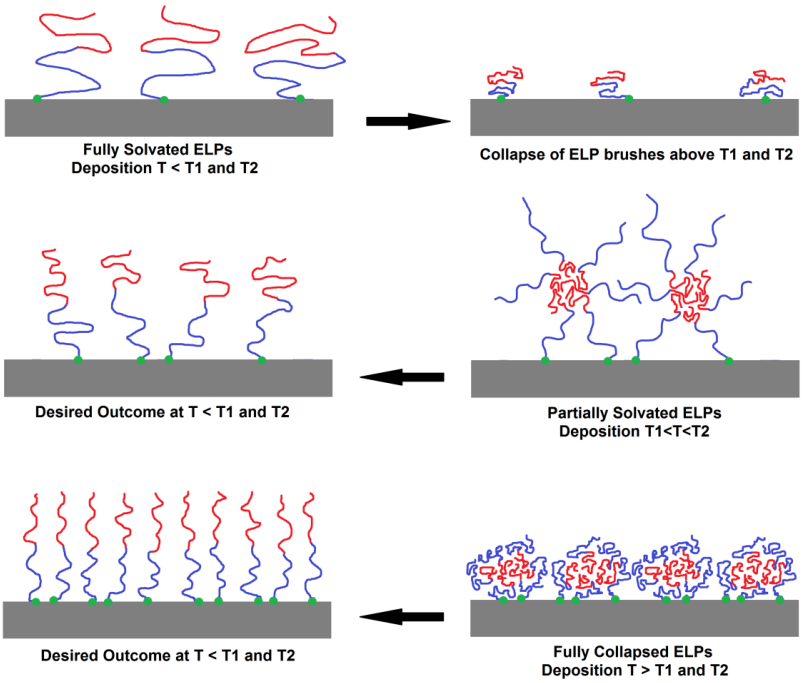

Figure 4.9: Desired result of deposited ELPs above either one or both transition temperatures. A) Deposition of ELPs while fully solvated should result in a sparsely populated "mushroom" type polymer brush. Once heated, ELP chains presumably collapse. B) Hypothetical case when depositing ELPs above transition temperature of one block (while in micellar state). A desirable outcome would be for the ELPs to re-solubilize when cooled. D) Hypothetical case when depositing ELPs above both transition temperatures, when fully collapsed. The desirable outcome once cooled would be a densely grafted polymer brush.

In some cases, the grafted film demonstrated in-plane structural heterogeneity which made thickness determination by ellipsometry difficult. Thickness values shown in Figure 4.10 represent averages of 3 measurements per sample, for 3 or more samples at each

temperature. At low temperatures (23°C), the thicknesses as measured by ellipsometry indicate that the grafted peptide layer is roughly 20-30 Å (subtracting the MUA and UDTS thickness). Considering that our peptides have 401 amino acids per chain, we can approximate the radius of gyration in solution to be ≈30 Å in a good solvent, or ≈15 Å in a poor solvent (using calculations from Rubinstein's *Polymer Physics*[56]).

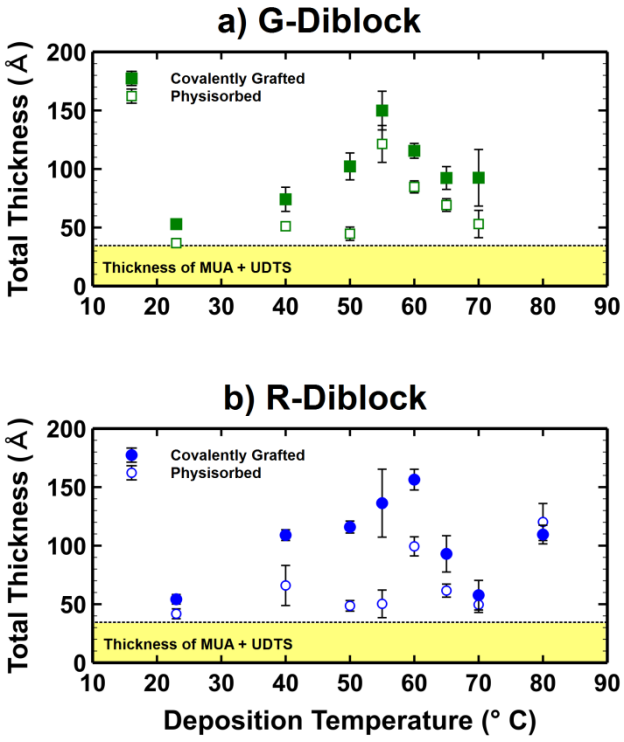

Figure 4.10: Ellipsometric results for heated depositions of G- and R-diblock. Both covalently grafted g-diblock ELPs (filled symbols) and physically adsorbed (hollow symbols) data are shown.

For both G-diblock and R-diblock systems, the thicknesses of grafted films reach a maximum at 55°C, trailing off at higher temperatures. This is likely due to the fact that the grafting end

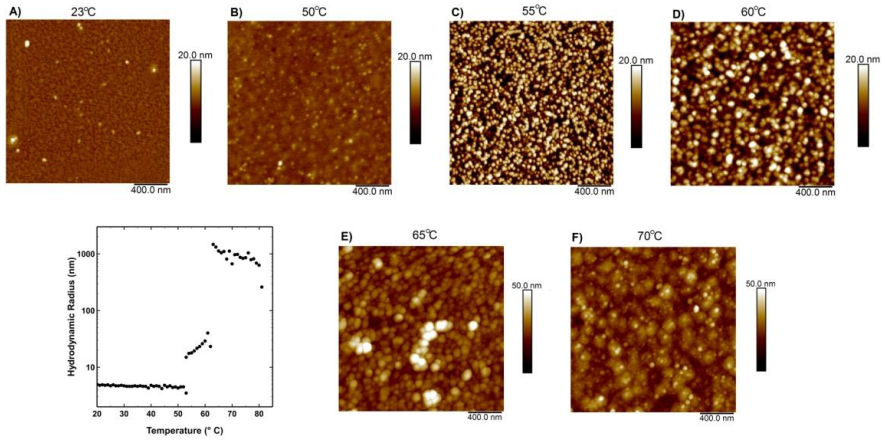

Figure 4.11: AFM results for heated deposition and covalent grafting of the g-diblock. Images A-F are labeled with the deposition temperature. Hydrodynamic radius as determined by dynamic light scattering for the g-diblock in a bulk phosphate buffer solution are shown.

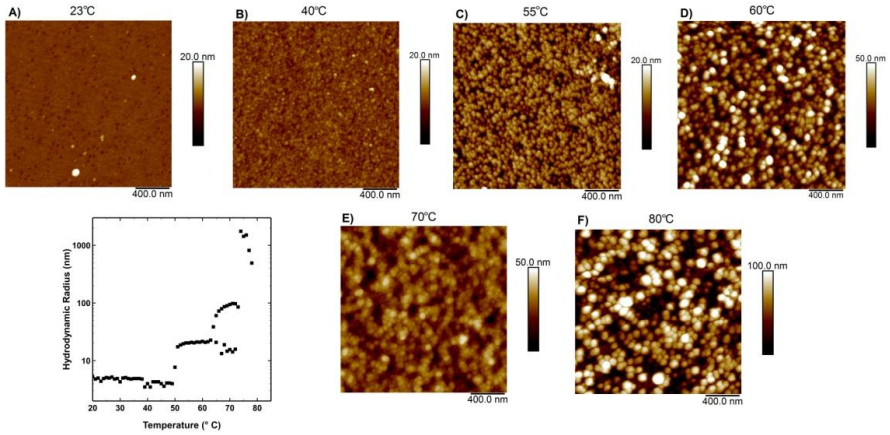

Figure 4.12: AFM results for heated deposition and covalent grafting of the r-diblock. Images A-F are labeled with the deposition temperature. Hydrodynamic radius as determined by dynamic light scattering for the r-diblock in a bulk phosphate buffer solution are shown.

of the peptides becomes less available as the grafting block collapses. At high deposition temperatures, both blocks are collapsed, reducing mobility and preventing attachment. One exception is at 80°C for the R-diblock, though the physically adsorbed control shows approximately the same thickness as the grafted case, indicating that the grafted sample is mostly physically adsorbed material rather than a covalently grafted brush.

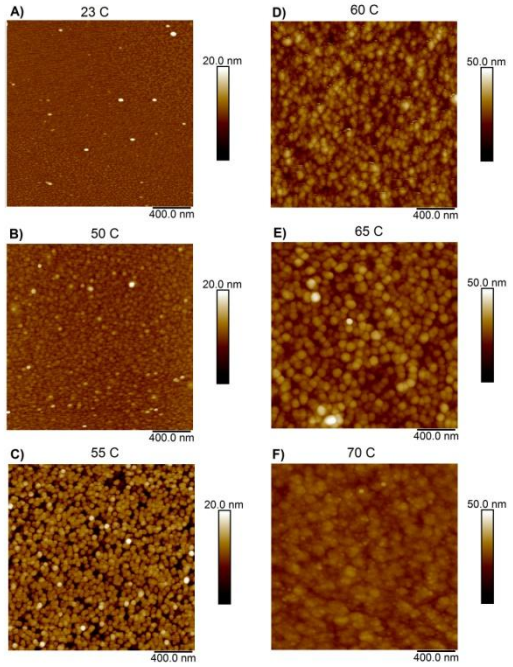

Figure 4.13: AFM results for heated deposition of the g-diblock, with physical adsorption only. Images A-F were taken at room temperature and are labeled with the deposition temperature.

AFM elucidates the morphology and thickness variability seen in the deposited ELP layers. Significant roughness exists in the depositions done above LCST (roughness values reported in Figure 4.15), presumably due to the aggregation of ELPs precipitating out of

solution during the heated deposition process. Although the feature sizes found in the AFM scans do not correlate perfectly with those from the DLS scans done in bulk, we do see a systematic increase in feature size with increasing temperature. The unpredictable nature of the collapse of the chains resulted in varying features sizes and surface morphology at high temperature depositions. We note that particle size determination from AFM scans is prone to errors for closely packed features, as the tip cannot penetrate fully between particles.

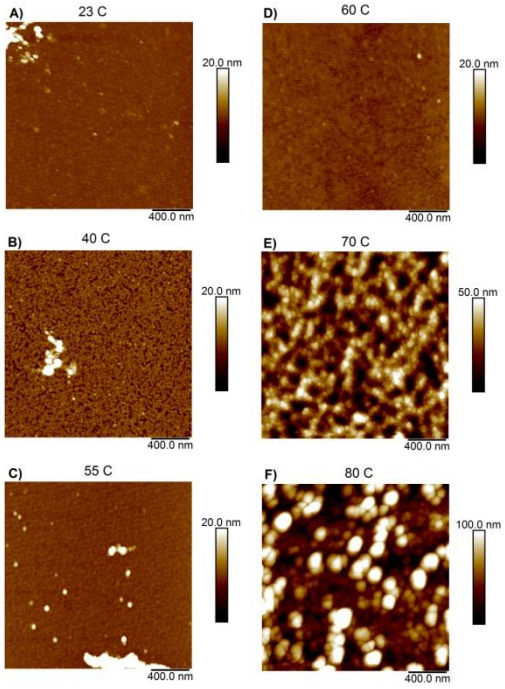

Figure 4.14: AFM results for heated deposition of the r-diblock, with physical adsorption only. Images A-F were taken at room temperature and are labeled with the deposition temperature.

As seen in Figure 4.11, at low temperatures for the g-diblock, we see a fairly homogeneous surface with few evident features. As we increase the deposition temperature

for the g-diblock, we see densely packed aggregates on the silicon surface in AFM starting at 55°C, with increasing aggregate size correlating with increasing temperature. Similar patterns are evident for the r-diblock, shown in Figure 4.12. Starting with the 40°C deposition, we see packed aggregates. Once again, as we increase the deposition temperature for the r-diblock, the size of surface aggregates appears to increase in AFM.

AFM images of the peptide surfaces in water demonstrate that the peptides partially resolubilize at room temperature even after grafting to the surface (Figure 4.16). This is indicated in the softening of features seen in AFM, especially at lower deposition temperatures. However, in spite of resolubilizing, the aggregates stay attached to the substrate. The aggregates deposited at higher temperatures for the diblock do not break apart in the presence of room temperature (RT) water.

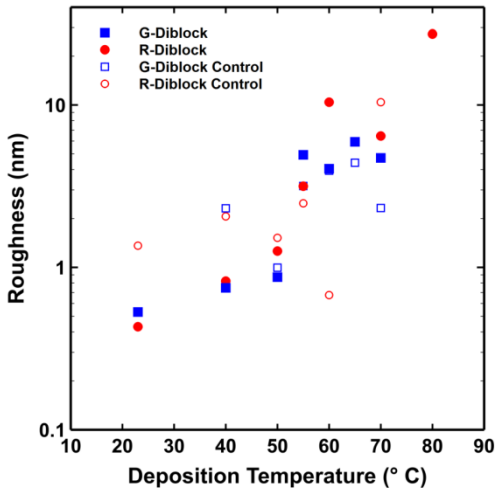

Figure 4.15: RMS roughness of AFM images for chemically grafted samples (filled symbols) and physically adsorbed samples (hollow symbols).

The irreversibility of aggregates on the surface is in contrast to previous work with ELPs.[52] Once the ELPs have deposited on the surface, the local concentration is higher than that of the bulk solution. Because increasing concentration decreases the transition temperature,[53] it is difficult to know whether room temperature is sufficiently low enough to disrupt these aggregates. We note, however, that we keep wafers in water at ~4°C before imaging, which implies that if the stability of aggregates is due to a concentration related drop in LCST, the new transition temperature would be below 4°C.

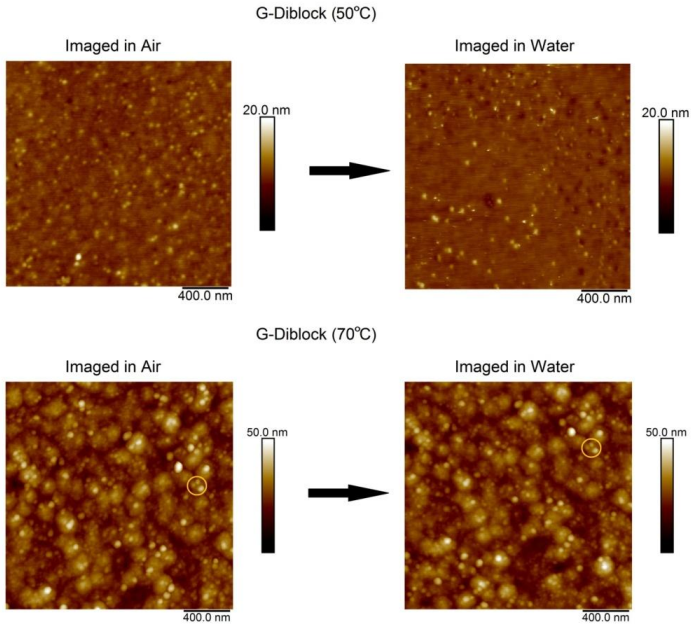

Figure 4.16: Comparison of air and water AFM images for select deposition temperatures. The circled feature in the second set of images is the same in both images.

To determine if the features we see are due merely to physical adsorption rather than covalent attachment, we carried out several control experiments. First, we evaluated the possibility that micelles or peptide aggregates are merely adsorbing onto grafted ELPs. To test this, we carried out a two-step deposition process. We started by grafting a layer of ELPs at room temperature followed by a second deposition by submerging the room temperature brush in a heated peptide solution (Figure 4.17). We found that neither the thickness nor the morphology matched that of our heated deposition case, eliminating this hypothesis.

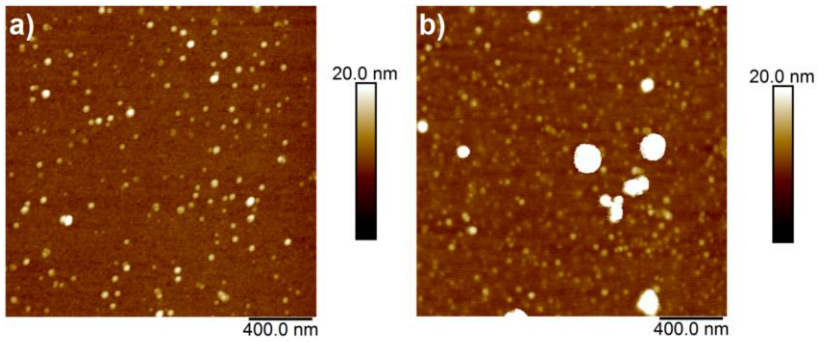

Figure 4.17: A) G-diblock RT covalently grafted brush followed by 55°C micelles deposition, total thickness 77Å (as compared to 150 Å for heated deposition). B) R-diblock RT covalently grafted brush followed by 55°C micelles deposition, total thickness 90Å (as compared to 130 Å for heated deposition)

Next, we considered the role the substrate material played in ELP adsorption. To test this, we used UDTS-coated silicon wafers as a control, and found that much less peptide adsorbed onto UDTS substrates relative to the UDTS-MUA substrates (ELPs were roughly

20-40Å thinner on UDTS than MUA). These findings reveal that the UDTS-modified substrate alone is not responsible for adsorption of peptides, rather the carboxylic acid groups present in the MUA play a role in attaching the ELPs. We also created an analogue system with MUA grafted on gold, and saw significant adsorption of ELPs. This observation further elucidates that the MUA layer acts as a source of physical binding to the ELP.

We attempted to disrupt the ELP aggregates with an ionic surfactant, sodium dodecyl sulfate (SDS) (Figures 4.18 and 4.19). As demonstrated by the images shown in Figure 4.19 exposure to a 4 mM SDS solution did not break up the surface ELP aggregates even after 30 minutes during *in situ* AFM experiments.

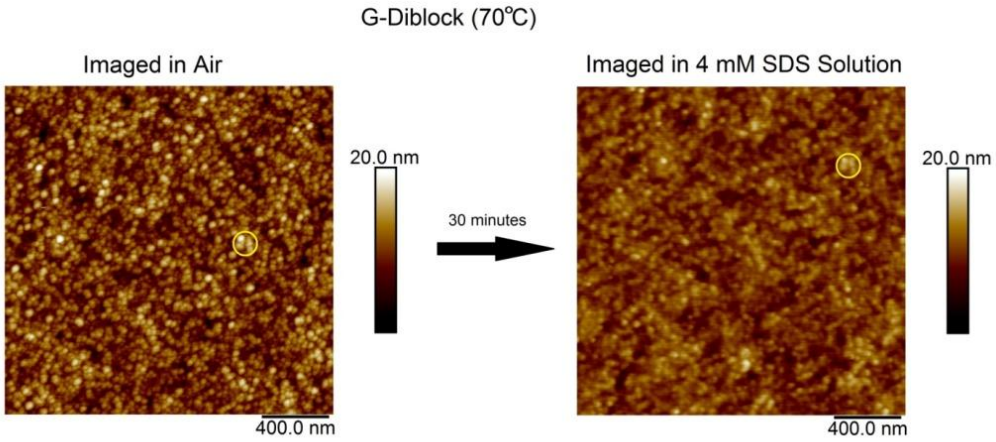

Figure 4.18: Comparison of AFM images for G-diblock after exposure to SDS solution. The circled feature in the image is the same in both images.

We also performed overnight exposure to varying concentrations of SDS solutions, and found no thickness changes in our samples after rinsing with DI water. While the

morphology of the ELPs was somewhat altered, the consistency of film thicknesses indicates that there was merely surface rearrangement rather than removal of physically adsorbed ELPs (Figure 4.18).

Additionally, we deposited ELPs in the presence of SDS at varying concentrations. Depositions of the G-diblock ELP carried out at 55°C in the presence of 4 mM SDS showed a significant decrease in thickness and surface roughness (Figure 4.20).

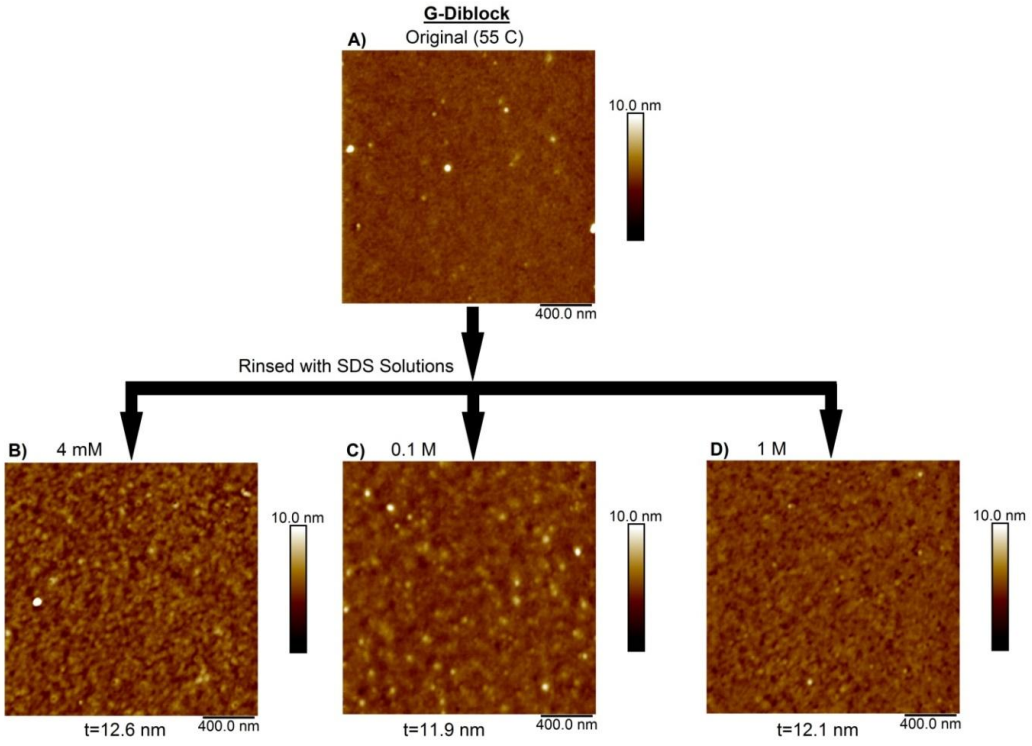

Figure 4.19: Deposited ELPs after overnight rinsing with SDS. Under each image is the corresponding total thickness after rinsing. Original thickness (corresponding to the top image) was 12 nm (120 Å), which includes the MUA/UDTS thickness. A) Original image, after rinsing with B) 4 mM, C) 0.1 M, and D) 1 M SDS solutions, followed by DI water rinse.

Once the concentration of SDS reached its critical micelle concentration (CMC, 7-8 mM), the thickness of the ELP layer attained a normal thickness (~160 Å) and the surface morphology matched that of our typical deposition case. For the 4 mM concentration, the SDS is not concentrated enough to form micelles. Instead, it is most likely interacting with the ELP chains, preventing their aggregation, which has been demonstrated previously.[54] For the 8 mM SDS case, the SDS should be assembled into micelles, presumably less able to interact with the polypeptides, and therefore it does not prevent their aggregation.

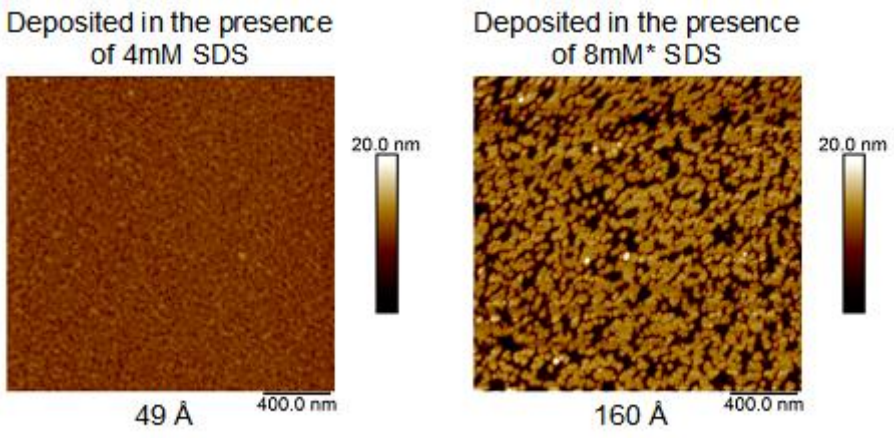

Figure 4.20: 55°C G-diblock depositions in the presence of SDS Thicknesses as measured by ellipsometry shown below images. The thickness of the 5 mM deposition was 40Å and the 6 mM deposition was 96Å. *8mM SDS is above the CMC.

Helpful comparisons can be made between the imaging of traditional polymer diblock micelles adsorbed on surfaces[28] and the aggregate features we report here resulting from covalent grafting of diblock ELPs. By adjusting the concentration of polymers in solution,

diblocks will adsorb either as individual chains or as micelles. Before reaching the CMC, single diblock polymer chains adsorb onto the surface. At concentrations greater than the CMC, most copolymer chains in solution get incorporated into micelles and only a few chains are present in a non-micellar form. Under these conditions, the entire micelle, rather than individual polymer chains, will adsorb onto the surface. A similar phenomenon may explain the irreversible aggregation of ELPs in our case, but with increasing temperature being the critical variable rather than concentration. As temperature increases, more ELPs exist as either micelles or collapsed aggregates instead of single chains. Other researchers have demonstrated that physically adsorbed ELPs exhibit dynamic behavior on silicon, rearranging to form fibrils or nanoclusters.[55] Flamia et al. used AFM to study the dynamic behavior of P(VGGVG) deposited on silicon and found that ELP suspensions from methanol rearranged over several days, whereas aqueous suspensions did not evolve towards other structures after several days. Our results correlate with these prior reports. Even with our physically adsorbed ELPs, we do not see evidence of dynamic behavior in our AFM scans. Is it unclear whether this is due to strong bonding with the carboxylic acid groups at the surface or kinetic trapping.

In order to understand the stability of ELP aggregates on our surfaces compared to the reversibility of ELP aggregates in solution, we turn to conventional polymer physics. Polymers which collapse in a poor solvent tend to stick together due to the high cost of the surface energy of the polymer globules.[56] Looking at the thermally responsive polymer poly(N-isopropylacrylamide) (PNIPAM) in particular, altering grafting density of the brush influences the collapse behavior of the polymer.[57] Lateral domain structures are not always

observed above the LCST of PNIPAM brushes, depending on the molecular weight of the polymer as well as the grafting density.

Work has also been done investigating the physisorption of PNIPAM regarding the differences of layer formation while above or below the LCST.[58] While swollen PNIPAM deposited below its LCST resulted in only monolayers, collapsed PNIPAM appeared to deposit multilayers. This was partially due to the interactions of the swollen polymer coils with the solvent. Once the chains collapse, the chemical potential of PNIPAM in solution increases, which favors the deposition of additional chains on the surface.[58] Similar to results found from the physisorption of swollen vs collapsed PNIPAM, we found that our collapsed ELP adsorption resulted in thicker layers.[58]

Because other researchers have found that longer times at elevated pH can create irreversible coacervation of tropoelastin,[19] we investigated the time dependence of the features we saw in heated depositions (Figure 4.21). We found that after a relatively short time (60 minutes), the thickness of the grafted R- and G-diblock layers deposited at 55°C leveled off at around 100 and 150 Å, respectively. Although the morphology in AFM scans shows some changes with increasing deposition time, we do see spherical surface aggregates early on, especially for the R-diblock samples. These results indicate that the phenomenon responsible for the results we see is not simply the degradation of the polypeptides at high temperatures.

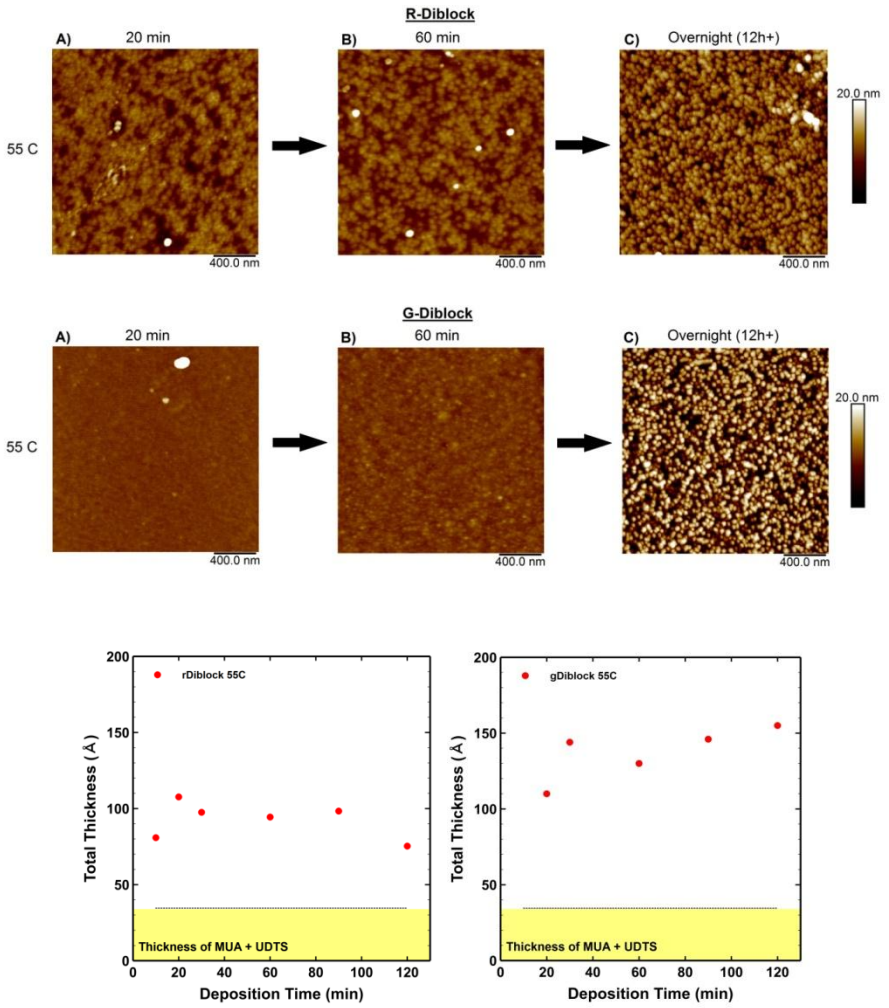

Figure 4.21: Time trials for both G-diblock and R-diblock. AFM images are taken at various time points as noted above the scans. Thickness plots correspond to additional time points performed; each data point represents 3 measurements on 1 sample.

Although it appears that we have successfully grafted our diblock ELPs to the UDTS-MUS modified silicon surface, it is difficult to distinguish between physical adsorption and covalent grafting based on morphology. The thickness data presented in Figure 4.10 suggest that we have more ELPs in all of our grafted cases (except the 80°C R-diblock case) than our

adsorbed controls. Also, though we attempted to remove any adsorbed ELPs in our grafted samples, we found that cold temperatures, sonication, and exposure to SDS did not significantly decrease the thickness of our layers. Because it would be difficult to correctly assess through FTIR or other chemical analysis tool whether our MUA is covalently attached to our ELP chains, we must rely on controls, ellipsometry, and AFM data to support the assertion that the polypeptides are not merely laying on the silicon surface.

4.4.2. Blocky Copolypeptides

We also performed experiments using polypeptides with varying "blockiness", as indicated in Figure 4.1. In this study, we sought to characterize the effect of blockiness on ELP copolymers grafted to a silicon surface. The recombinant synthesis of ELPs carefully controls for molecular weight, chemical composition of pentapeptide repeat units, and order and number of pentapeptide units. The chemical composition of our blocky peptides was constant for all ELPs; only the order of the 80 pentapeptide repeat units was altered. These "blocky" ELPs, with the exception of the diblock, had one transition temperature rather than two distinct transitions (as seen in Figure 4.2-4.3), although the transitions were not as sharp as with homopolymers. The existence of only one transition temperature is consistent with other researchers' work using varying sequences and distributions of amino acids along the ELP chain.[53] The morphology of blocky ELPs deposited above and below LCST demonstrates poorly ordered aggregates (Figures 4.22-4.23); these ELPs are not likely to transition through an ordered micellar or other nanostructured phase. The alternating copolymer in particular is rough and disordered, which may reflect a more complicated

collapse behavior due to the solubility of the Serine-containing pentapeptide repeat unit and the hydrophobicity of the Valine-containing repeat unit.

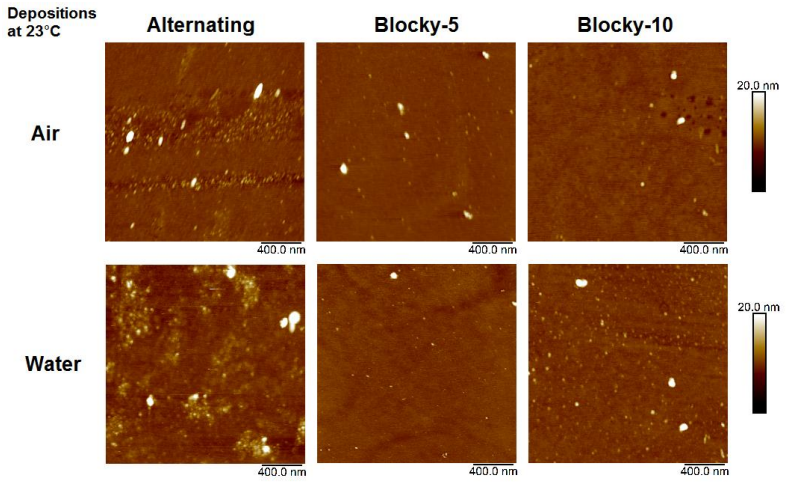

Figure 4.22: Blocky ELPs deposited at room temperature, AFM images performed in air and water.

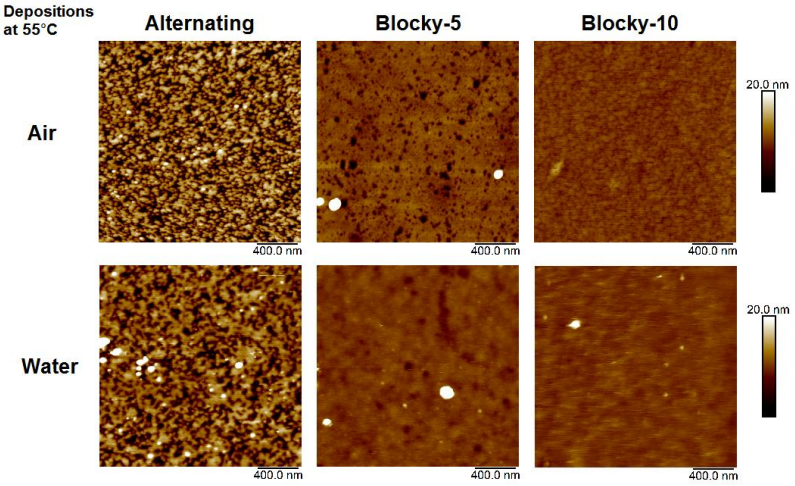

Figure 4.23: Blocky ELPs deposited at 55°C, AFM images performed in air and water.

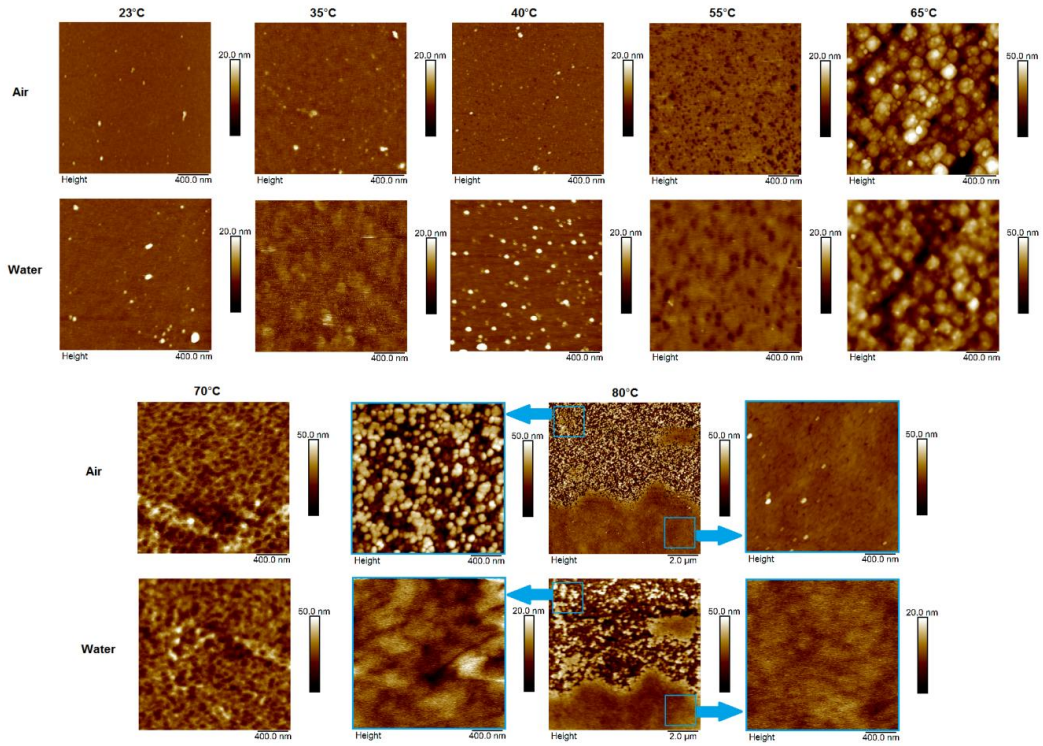

Figure 4.24: Diblock room temperature and heated ELP depositions imaged in air and water.

The diblock ELP demonstrates more complex behavior both in solution (Figure 4.2) and when grafted to the silicon wafer (Figure 4.24) than the blocky ELPs. At lower grafting temperatures, the diblock does not form large aggregates on the silicon surface. Once exposed to water, the peptides appear to resolubilize, particularly in the 35°C case in which the AFM image in water appears to have lost any well defined spherical structures. In contrast, the depositions at higher temperatures such as 65°C and 70°C resulted in large, stable aggregates which did not completely break apart once submerged in water. Particularly in the 65°C case, the diameter of the diblock aggregates corresponds to the feature sizes seen in DLS and are not disrupted by exposure to cold water.

As another technique for investigating the impact of grafting density on surface morphology, we created gradients in MUA grafting density and therefore in ELP grafting density. Using a shutter during the UV-based thiol-ene reaction moving at a speed of 1.33 cm/min, we created a gradient in MUA thickness that extended over 2-3 cm of a 5 cm long silicon wafer. The remaining reactive vinyl groups on the UDTS layer were backfilled with an inert small chain (a polyethylene glycol short chain with a thiol terminal group) before ELP grafting. The resulting thickness of the MUA layer and the ELP layer are plotted versus position on the wafer as shown in Figures 4.25-4.27. We investigated both room temperature deposited blocky-ELPs as well as heated ELPs.

For the RT deposition using blocky-10 ELP on an MUA gradient sample (Figure 4.25), we see a gradual thickness change across the wafer in the MUA and ELP layers. The morphological characteristics of the ends of the gradient reflect a gradual increase in packing of peptides on the surface. In particular, the AFM image at 32.5 mm on the wafer indicates an increase in roughness and more packing of spherical features. We also generated several samples using gradient MUA substrates and a heated grafting deposition process. Using both blocky-5 and diblock ELPs, we performed depositions at 55°C and recorded the resulting thicknesses and morphological characteristics with ellipsometry and AFM, respectively. In Figure 4.26, the AFM scan shown at position 43 mm reflects the PEG-modified surface primarily, which we conclude from the very low thickness of the peptide layer. At 39 mm on the wafer, scattered grafted peptides are evident on the surface as spherical features.

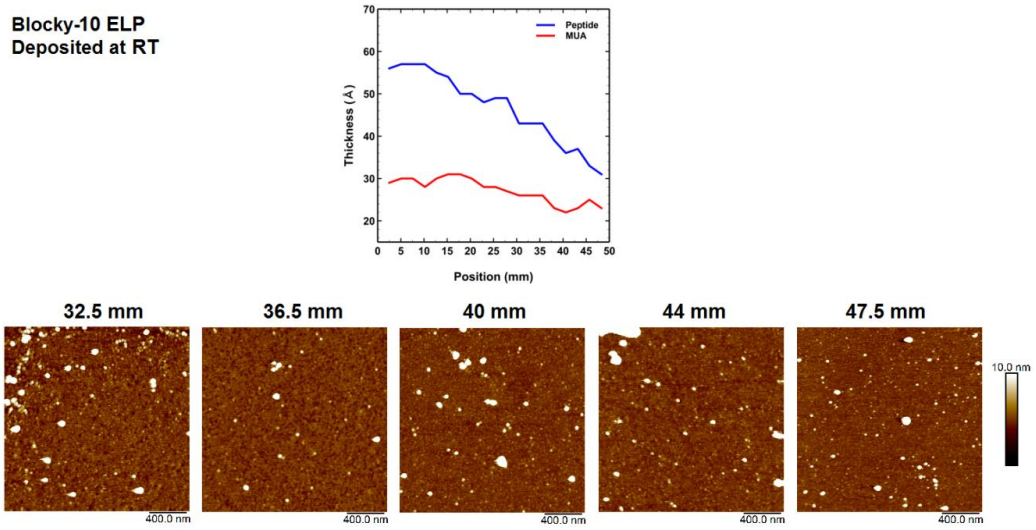

Figure 4.25: Room temperature deposition of Blocky-10 ELP on a gradient MUA surface. The thickness of the MUA layer before ELP grafting is shown in the plot (red line), and the ELP thickness after grafting is shown in blue. The corresponding AFM images are labeled with the position on the sample which corresponds to the x axis of the plot.

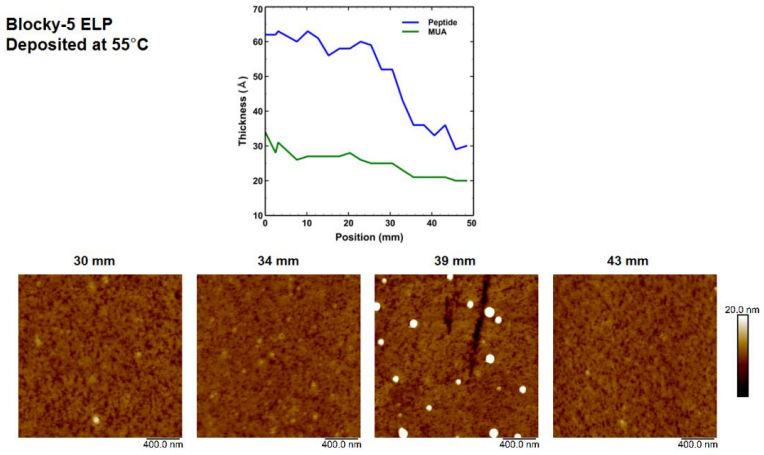

Figure 4.26: 55°C deposition of Blocky-5 ELP on a gradient MUA surface. The thickness of the MUA layer before ELP grafting is shown in the plot (green line), and the ELP thickness after grafting is shown in blue. The corresponding AFM images are labeled with the position on the sample which corresponds to the x axis of the plot.

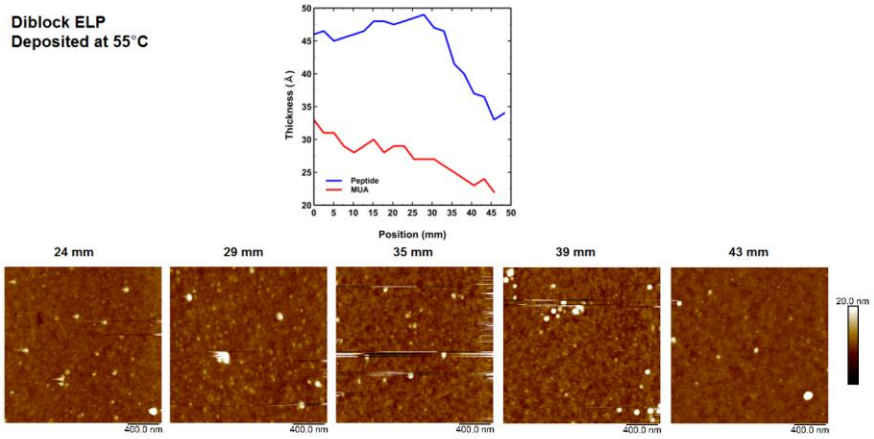

Figure 4.27: 55°C deposition of Diblock ELP on a gradient MUA surface. The thickness of the MUA layer before ELP grafting is shown in the plot (red line), and the ELP thickness after grafting is shown in blue. The corresponding AFM images are labeled with the position on the sample which corresponds to the x axis of the plot.

4.5. Preliminary Results on PVMS

The ultimate goal for studying the behavior of ELPs on surfaces is to graft temperature responsive peptides onto PVMS for use in microfluidic channels or for biological applications. To that end, we used the same basic procedure for grafting MUA to a PVMS network as we have outlined for grafting to a UDTS-modified silicon wafer. Initial attempts attaching MUA directly onto PVMS through UV-triggered thiol-ene chemistry proved difficult due to wrinkling of the PVMS surface, as shown in Figure 4.28. Longer treatment times were associated with increased buckling on the PVMS surface, as seen in the network treated for 18 minutes.

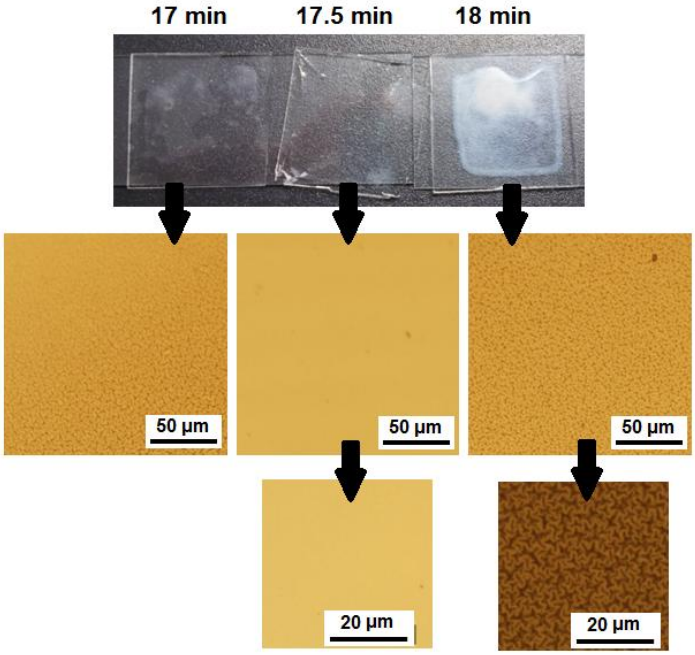

Figure 4.28: Optical microscopy images of MUA treated PVMS networks. Time indicated above photographs of images is UV treatment time.

Because of the consistent buckling of the PVMS network surface during MUA treatment, we were unable to study the grafting of ELPs to PVMS networks as initially intended. However, it is expected that with optimization of the MUA grafting procedure or with the grafting of an alternate carboxylic acid group, PVMS modification with ELPs will be practical. Furthermore, previous work with PVMS successfully demonstrated the attachment of small molecules through thiol-ene chemistry for the purposes of responsive surfaces and for cell adhesion studies.[59,60]

4.6. Conclusions and Outlook

We were motivated in this work to create and study a densely grafted ELP surface for stimuli-responsive applications. We found, however, that by attempting to pack more polypeptides onto a surface, we lost the beneficial responsive properties. This work is relevant to researchers designing a stimuli-responsive surface, as considerations need to be made in the balance of full surface coverage versus optimal stimulus response. Although it is unclear what the optimal grafting density of ELPs on a surface may be, grafting of polypeptides in mushroom-regime, sparsely-populated brushes demonstrates responsive behavior and should be sufficient for surface modification and functionalization.

One potential future direction for the grafting of ELPs onto a soft PVMS network rather than silicon wafers would be the introduction of nanoparticles into the PVMS networks in order to stabilize the network and potentially prevent wrinkling. There have also been reports of modifying PDMS for peptide attachment, though this path would be more difficult chemically, as has been discussed throughout this dissertation. Additionally, it may be possible to modify a PVMS microchannel *in situ* by flowing through the channel in sequence: first MUA in the presence of UV light, followed by EDC/s-NHS, and finally ELP solution. A PVMS surface which has been constrained as a microchannel may suffer from less buckling than a free network of PVMS.

4.7. References

[1] Schattling, P., Jochum, F. D. & Theato, P. Multi-stimuli responsive polymers – the all-in-one talents. Polym. Chem. 5, 25–36 (2013).

[2] Meng, H. & Jinlian Hu. A Brief Review of Stimulus-active Polymers Responsive to Thermal, Light, Magnetic, Electric, and Water/Solvent Stimuli. J. Intell. Mater. Syst. Struct. 21, 859–885 (2010).

[3] Stuart, M. A. C. et al. Emerging applications of stimuli-responsive polymer materials. Nat. Mater. 9, 101–113 (2010).

[4] Kelley, E. G., Albert, J. N. L., Sullivan, M. O. & Thomas H. Epps, I. I. I. Stimuli-responsive copolymer solution and surface assemblies for biomedical applications. Chem. Soc. Rev. 42, 7057–7071 (2013).

[5] Gulati, S. et al. Opportunities for microfluidic technologies in synthetic biology. J. R. Soc. Interface 6, S493–S506 (2009).

[6] Cole, M. A., Voelcker, N. H., Thissen, H. & Griesser, H. J. Stimuli-responsive interfaces and systems for the control of protein–surface and cell–surface interactions. Biomaterials 30, 1827–1850 (2009).

[7] Nel, A. E. et al. Understanding biophysicochemical interactions at the nano–bio interface. Nat. Mater. 8, 543–557 (2009).

[8] Ray, J. G., Johnson, A. J. & Savin, D. A. Self-assembly and responsiveness of polypeptide-based block copolymers: How 'Smart' behavior and topological complexity yield unique assembly in aqueous media. J. Polym. Sci. Part B Polym. Phys. 51, 508–523 (2013).

[9] Chilkoti, A., Christensen, T. & MacKay, J. A. Stimulus responsive elastin biopolymers: applications in medicine and biotechnology. Curr. Opin. Chem. Biol. 10, 652–657 (2006).

[10] Deming, T. J. Synthetic polypeptides for biomedical applications. Prog. Polym. Sci. 32, 858–875 (2007).

[11] Meyer, D. E. & Chilkoti, A. Purification of recombinant proteins by fusion with thermally-responsive polypeptides. Nat. Biotechnol. 17, 1112–1115 (1999).

[12] Rodríguez-Cabello, J. C., Martín, L., Alonso, M., Arias, F. J. & Testera, A. M. 'Recombinamers' as advanced materials for the post-oil age. Polymer 50, 5159–5169 (2009).

[13] Floss, D. M., Schallau, K., Rose-John, S., Conrad, U. & Scheller, J. Elastin-like polypeptides revolutionize recombinant protein expression and their biomedical application. Trends Biotechnol. 28, 37–45 (2010).

[14] Shah, M. et al. Biodegradation of elastin-like polypeptide nanoparticles. Protein Sci. 21, 743–750 (2012).

[15] Urry, D. W. Physical Chemistry of Biological Free Energy Transduction As Demonstrated by Elastic Protein-Based Polymers†. J. Phys. Chem. B 101, 11007–11028 (1997).

[16] Kim, W., Thévenot, J., Ibarboure, E., Lecommandoux, S. & Chaikof, E. L. Self-Assembly of Thermally Responsive Amphiphilic Diblock Copolypeptides into Spherical Micellar Nanoparticles. Angew. Chem. Int. Ed. 49, 4257–4260 (2010).

[17] Carlsen, A. & Lecommandoux, S. Self-assembly of polypeptide-based block copolymer amphiphiles. Curr. Opin. Colloid Interface Sci. 14, 329–339 (2009).

[18] Osborne, J. L., Farmer, R. & Woodhouse, K. A. Self-assembled elastin-like polypeptide particles. Acta Biomater. 4, 49–57 (2008).

[19] Mithieux, S. M., Tu, Y., Korkmaz, E., Braet, F. & Weiss, A. S. In situ polymerization of tropoelastin in the absence of chemical cross-linking. Biomaterials 30, 431–435 (2009).

[20] Zhao, B. & Brittain, W. J. Polymer brushes: surface-immobilized macromolecules. Prog. Polym. Sci. 25, 677–710 (2000).

[21] Castle, J. E., Salvi, A. M., Flamia, R. & Satriano, G. Surface science aspects of supramolecular conformation in elastin-like polypeptides. Surf. Interface Anal. 44, 246–257 (2012).

[22] Rodriguez-Hernandez, J., Ibarboure, E. & Papon, E. Surface segregation of polypeptide-based block copolymer micelles: An approach to engineer nanostructured and stimuli responsive surfaces. Eur. Polym. J. 47, 2063–2068 (2011).

[23] Yang, G., Woodhouse, K. A. & Yip, C. M. Substrate-Facilitated Assembly of Elastin-Like Peptides: Studies by Variable-Temperature in Situ Atomic Force Microscopy. J. Am. Chem. Soc. 124, 10648–10649 (2002).

[24] Wang, E., Desai, M. S., Heo, K. & Lee, S.-W. Graphene-Based Materials Functionalized with Elastin-like Polypeptides. Langmuir 30, 2223–2229 (2014).

[25] Blit, P. H., Battiston, K. G., Woodhouse, K. A. & Santerre, J. P. Surface immobilization of elastin-like polypeptides using fluorinated surface modifying additives. J. Biomed. Mater. Res. A 96A, 648–662 (2011).

[26] Toomey, R. & Tirrell, M. Functional Polymer Brushes in Aqueous Media from Self-Assembled and Surface-Initiated Polymers. Annu. Rev. Phys. Chem. 59, 493–517 (2008).

[27] Peng, B. et al. Adsorption kinetics and stability of poly(ethylene oxide)-block-polystyrene micelles on polystyrene surface. Polymer 54, 5779–5789 (2013).

[28] Hamley, I. W., Connell, S. D. & Collins, S. In Situ Atomic Force Microscopy Imaging of Adsorbed Block Copolymer Micelles. Macromolecules 37, 5337–5351 (2004).

[29] Glynos, E., Pispas, S. & Koutsos, V. Amphiphilic Diblock Copolymers on Mica: Formation of Flat Polymer Nanoislands and Evolution to Protruding Surface Micelles. Macromolecules 41, 4313–4320 (2008).

[30] Gensel, J. et al. Surface immobilized block copolymer micelles with switchable accessibility of hydrophobic pockets. Soft Matter 7, 11144–11153 (2011).

[31] Samanta, D. & Sarkar, A. Immobilization of bio-macromolecules on self-assembled monolayers: methods and sensor applications. Chem. Soc. Rev. 40, 2567–2592 (2011).

[32] Goddard, J. M. & Hotchkiss, J. H. Polymer surface modification for the attachment of bioactive compounds. Prog. Polym. Sci. 32, 698–725 (2007).

[33] Falconnet, D., Csucs, G., Michelle Grandin, H. & Textor, M. Surface engineering approaches to micropattern surfaces for cell-based assays. Biomaterials 27, 3044–3063 (2006).

[34] Hyun, J., Lee, W.-K., Nath, N., Chilkoti, A. & Zauscher, S. Capture and Release of Proteins on the Nanoscale by Stimuli-Responsive Elastin-Like Polypeptide 'Switches'. J. Am. Chem. Soc. 126, 7330–7335 (2004).

[35] Pierna, M., Santos, M., Arias, F. J., Alonso, M. & Rodríguez-Cabello, J. C. Efficient Cell and Cell-Sheet Harvesting Based on Smart Surfaces Coated with a Multifunctional and Self-Organizing Elastin-Like Recombinamer. Biomacromolecules 14, 1893–1903 (2013).

[36] Sia, S. K. & Whitesides, G. M. Microfluidic devices fabricated in Poly(dimethylsiloxane) for biological studies. ELECTROPHORESIS 24, 3563–3576 (2003).

[37] Sui, G. et al. Solution-Phase Surface Modification in Intact Poly(dimethylsiloxane) Microfluidic Channels. Anal. Chem. 78, 5543–5551 (2006).

[38] Yang, L. et al. Photocatalyzed Surface Modification of Poly(dimethylsiloxane) with Polysaccharides and Assay of Their Protein Adsorption and Cytocompatibility. Anal. Chem. 82, 6430–6439 (2010).

[39] Makamba, H., Kim, J. H., Lim, K., Park, N. & Hahn, J. H. Surface modification of poly(dimethylsiloxane) microchannels. ELECTROPHORESIS 24, 3607–3619 (2003).

[40] Hu, S. et al. Tailoring the surface properties of poly (dimethylsiloxane) microfluidic devices. Langmuir 20, 5569–5574 (2004).

[41] Tu, Q. et al. Surface modification of poly(dimethylsiloxane) and its applications in microfluidics-based biological analysis. Rev. Anal. Chem. 31, (2012).

[42] Zhou, J., Khodakov, D. A., Ellis, A. V. & Voelcker, N. H. Surface modification for PDMS-based microfluidic devices. ELECTROPHORESIS 33, 89–104 (2012).

[43] Zhou, J., Ellis, A. V. & Voelcker, N. H. Recent developments in PDMS surface modification for microfluidic devices. ELECTROPHORESIS 31, 2–16 (2010).

[44] Mikhail, A. S. et al. Rapid and Efficient Assembly of Functional Silicone Surfaces Protected by PEG: Cell Adhesion to Peptide-Modified PDMS. J. Biomater. Sci. Polym. Ed. 21, 821–842 (2010).

[45] Wu, Y., Coyer, S. R., Ma, H. & García, A. J. Poly(dimethylsiloxane) elastomers with tethered peptide ligands for cell adhesion studies. Acta Biomater. 6, 2898–2902 (2010).

[46] Boxshall, K. et al. Simple surface treatments to modify protein adsorption and cell attachment properties within a poly(dimethylsiloxane) micro-bioreactor. Surf. Interface Anal. 38, 198–201 (2006).

[47] Fujii, Y., Henares, T. G., Kawamura, K., Endo, T. & Hisamoto, H. Bulk- and surface-modified combinable PDMS capillary sensor array as an easy-to-use sensing device with enhanced sensitivity to elevated concentrations of multiple serum sample components. Lab. Chip 12, 1522–1526 (2012).

[48] Lim, K. et al. Immobilization Studies of an Engineered Arginine–Tryptophan-Rich Peptide on a Silicone Surface with Antimicrobial and Antibiofilm Activity. ACS Appl. Mater. Interfaces 5, 6412–6422 (2013).

[49] Zhou, J., Voelcker, N. H. & Ellis, A. V. Simple surface modification of poly(dimethylsiloxane) for DNA hybridization. Biomicrofluidics 4, 046504 (2010).

[50] Séguin, C., McLachlan, J. M., Norton, P. R. & Lagugné-Labarthet, F. Surface modification of poly(dimethylsiloxane) for microfluidic assay applications. Appl. Surf. Sci. 256, 2524–2531 (2010).

[51] Dreher, M. R. et al. Temperature Triggered Self-Assembly of Polypeptides into Multivalent Spherical Micelles. J. Am. Chem. Soc. 130, 687–694 (2008).

[52] Frey, W., Meyer, D. E. & Chilkoti, A. Thermodynamically Reversible Addressing of a Stimuli Responsive Fusion Protein onto a Patterned Surface Template†. Langmuir 19, 1641–1653 (2003).

[53] Meyer, D. E. & Chilkoti, A. Quantification of the Effects of Chain Length and Concentration on the Thermal Behavior of Elastin-like Polypeptides. Biomacromolecules 5, 846–851 (2004).

[54] Pinedo-Martín, G., Castro, E., Martín, L., Alonso, M. & Rodríguez-Cabello, J. C. Effect of Surfactants on the Self-Assembly of a Model Elastin-like Block Corecombinamer: From Micelles to an Aqueous Two-Phase System. Langmuir 30, 3432–3440 (2014).

[55] Flamia, R., Zhdan, P. A., Martino, M., Castle, J. E. & Tamburro, A. M. AFM Study of the Elastin-like Biopolymer Poly(ValGlyGlyValGly). Biomacromolecules 5, 1511–1518 (2004).

[56] Rubinstein, M. Polymer physics. (Oxford University Press, 2003).

[57] Choi, B.-C., Choi, S. & Leckband, D. E. Poly(N-isopropyl acrylamide) Brush Topography: Dependence on Grafting Conditions and Temperature. Langmuir 29, 5841–5850 (2013).

[58] Zhu, D.-M. et al. Physisorption of Poly(N-isopropylacrylamide) in Its Swollen and Collapsed States: Effects of Molecular Conformation and Substrate Interaction. J. Phys. Chem. C 111, 18679–18686 (2007).

[59] Crowe-Willoughby, J. A. & Genzer, J. Formation and Properties of Responsive Siloxane-Based Polymeric Surfaces with Tunable Surface Reconstruction Kinetics. Adv. Funct. Mater. 19, 460–469 (2009).

[60] Ahmed, S. et al. Poly(vinylmethylsiloxane) Elastomer Networks as Functional Materials for Cell Adhesion and Migration Studies. Biomacromolecules 12, 1265–1271 (2011).

CHAPTER 5. Thiol-ene Resins for Nanoskiving*

---

* This chapter is partially based on: R. L. Mays, P. Pourhossein, D. Savithri, J. Genzer, R. C. Chiechi, M. D. Dickey, ***J. Mater. Chem. C***, 2013, 1, 121-130

5.1. Introduction

Nanoskiving is a form of edge lithography that uses an ultramicrotome equipped with a diamond knife to section thin films (e.g., gold) embedded in a polymer matrix.[1] The conventional polymer used for embedding these films is typically a liquid pre-polymer that cures with minimal shrinkage to produce a hard bulk polymer that facilitates handling and is necessary for sectioning. Adhesion between the sample (i.e., often a metal film in the case of nanoskiving) and the polymer matrix is important to assure that the final composite does not disintegrate during microtomy sectioning.

Epoxies are popular embedding resins for microtomy because they are hard, shrink minimally during curing, and adhere conformally to most materials. Epoxies, however, do not adhere well to gold (or other smooth, metallic structures). Gold is often used for nanoskiving because it is easy to deposit and section, is not brittle, and does not oxidize readily.

The two most commonly used commercially available epoxides are Araldite and Epofix. Araldite is advantageous because it is easy to trim (a necessary first step in nanoskiving) and forms mechanically stable sections even at very thin (< 100 nm) thicknesses that are common in nanoskiving. However, Araldite is a three-part epoxy with a lengthy curing time (~ 48 hours for optimal mechanical properties) and is optimized for soft materials (e.g., biological specimens). Epofix is a two-part, thermally-curable epoxy that is designed specifically for sectioning hard materials, but it is considerably harder than Araldite which leads to unstable sections and an increased susceptibility to "chattering," in which the diamond knife skips across the surface of the epoxy block leading to non-uniform

thicknesses in the resulting sections. Neither Araldite nor Epofix adhere particularly well to smooth metal surfaces, especially gold.

We hypothesized that incorporating monomers with thiol functionality into the embedding polymer would improve the adhesion between gold and the polymer during sectioning by introducing chemisorption *via* the spontaneous formation of gold-thiolate bonds. We evaluated photocurable thiol-ene polymers because they possess properties that are well suited for microtomy, i.e.: (1) their mechanical properties can be tailored by the choice of monomers, (2) they have low viscosity before curing, which facilitates embedding, (3) they photocure quickly on demand to deep thicknesses, which allows for rapid prototyping, and (4) they cure by step-growth polymerization, which leads to low shrinkage compared to most free-radical polymerizations. We also studied a thiol-epoxy formulation, which has many of the same desirable attributes of the epoxy networks, but includes thiol functionality. We compared the most relevant properties of the new embedding resins such as mechanical behavior, polymerization shrinkage, and adhesion to gold to evaluate the advantages and limitations relative to conventional epoxy resins. We also fabricated gold nanowires of various dimensions and examined the resulting sections by optical microscopy, measured the conductance of the nanowires, and compared the etching rates by plasma oxidation to demonstrate that the thiol-containing embedding resins are superior to conventional epoxy resins for nanoskiving.

Nanoskiving is a simple and convenient edge lithography technique for fabricating nanostructures by sectioning embedded films (typically metal or polymer) using an ultramicrotome.[1] Figure 5.1 outlines the procedure for fabricating nanostructures by

nanoskiving. Preparing the sample (or "block") for sectioning by microtome is a key aspect of nanoskiving. Typically, the fabrication process begins with a substrate consisting of a cured embedding resin that can either be flat or have topography (defined by soft lithography,[2-4] for example).

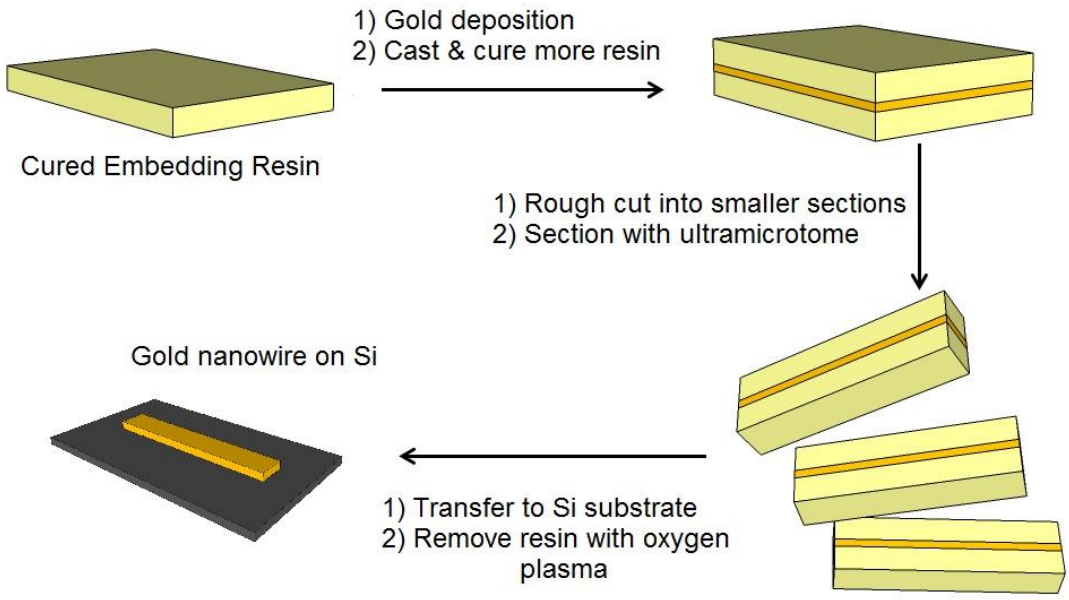

Figure 5.1: A schematic of the fabrication of a gold nanowire by nanoskiving.

Thin films can be deposited onto this substrate with precise thickness by a number of methods (e.g., spin coating, physical vapor deposition, sputtering). The entire substrate is then embedded in additional resin. Prior to sectioning the face of the block is trimmed manually into a trapezoidal shape (~1-15 mm^2) using a razor blade. Sectioning the resulting block with an ultramicrotome equipped with a diamond knife attached to a boat filled with water yields thin polymer slabs that float on the surface of the water and that can be

transferred to a substrate directly (e.g., by dipping a substrate in the boat) or *via* a drop of water. Structures formed by nanoskiving are often composed of gold because it is easy to deposit, does not oxidize, and is soft relative to most metals, which facilitates sectioning and results in stable, electrically continuous nanostructures. Exposure to oxygen (or air) plasma removes selectively the embedding resin and generates freestanding nanostructures. The topography of the original substrate, the thickness of the deposited film, and the thickness of the sections cut by the ultramicrotome (as thin as 15 nm) determine the dimensions of these nanostructures. The ability to control the dimensions of the nanostructures without the use of sophisticated lithographic tools or a clean room makes this technique very attractive for rapid prototyping. Nanostructures can be fabricated from materials that are not compatible with conventional photolithography/etching. Nanoskiving produces hundreds of thousands of identical sections from a single block and the thin polymeric sections can be positioned onto various substrates.[5]

Biologists and material scientists use ultramicrotomy conventionally to produce thin (~100 nm thick) sections of cells, tissues, and materials for analysis by electron microscopy.[6,7] Embedding is done by infiltration of the sample with a liquid embedding medium that polymerizes to produce a solid block that can be handled and sectioned using a microtome. An embedding medium for conventional biological samples should have the following properties: commercial availability, uniformity from one batch to another, solubility in dehydrating agents, low viscosity as a monomer for ease of handling, uniform polymerization, minimal volume change upon polymerization to avoid distortion of the sample, ease of sectioning and stability in an electron beam.[6] Embedding resins for

nanoskiving do not require solubility in dehydrating agents nor stability in an electron beam, but should be able to be etched by oxygen plasma.

None of the embedding media developed so far possesses all the desired qualities for microtomy, although several commercial epoxies (e.g., Araldite and Epofix) work well for most microtome applications.[1,8] Epoxies are generally cross-linked and possess relatively large elastic moduli (Young's modulus, E >1500 MPa), which is well suited for sectioning at room temperature.[9] Hardening of epoxies occurs via an addition reaction that results in very little change of volume. Epoxy resins also adhere well to many materials with polar surfaces (i.e. surface oxides) by hydrogen bonding.[10]

Most nanoskiving work to date relied on Araldite and Epofix epoxy resins, which offer convenience at the expense of performance.[7,11] Unfortunately, epoxy-based embedding resins exhibit poor adhesion to gold, which can lead to catastrophic delamination of the nanostructures from the embedding resin during sectioning or during preparation of the sample blocks. Sectioning is a mechanical cutting process and relies on the smooth and continuous advance of the block past the edge of the knife. Delamination diminishes significantly the quality of the sectioning process and should be mitigated when possible. For applications in which the epoxy matrix is used to electrically isolate the top face of gold nanostructures, delamination is catastrophic.[12] Delamination between the epoxy and gold has been minimized–but not eliminated–previously by careful handling and ensuring that the epoxy completely encapsulates the gold film on all sides.[1]

We sought to evaluate polymeric embedding materials that possess the important material characteristics required for microtoming, while enhancing the binding to gold and

increasing the rate of curing with minimal shrinkage. We chose polymers that contained thiols because they form strong bonds with many metals including gold, silver, palladium, copper, and many others.[13] Although in some circumstances it may be possible to improve adhesion between metal and the embedding resin by modifying the gold films with self-assembled monolayers (SAMs), we have had limited success with epoxide and carboxylate-terminated SAMs with both Epofix and Araldite. Thus, we sought to develop a simpler and more universally useful resin that contained thiols so that no additional steps would be required to improve adhesion to gold. In this paper, we evaluate the critical properties of several thiol-containing resins within the context of microtomy and demonstrate the utility of these materials in nanoskiving.

5.2. Methods

5.2.1. Experimental Design

Thiol-esters: We evaluated two commercially available, photocurable, mercapto-ester systems: NOA 63 and NOA 81. Norland Products sells many photocurable adhesives, but we selected these polymers because they possess elastic moduli similar to that of conventional epoxy resins. The manufacturer does not provide chemical information other than to call these products 'mercapto-esters' and we use the term 'thiol-ester' to be consistent with our other notations. These resins are also sold in smaller quantities than Araldite and Epofix, as they are optical adhesives that are optimized for transparency, not embedding.

Thiol-enes: The photopolymerization of mixtures of thiols and alkenes is an efficient method for the rapid production of crosslinked polymer networks.[14] Thiol-ene

photopolymerization proceeds rapidly by a step-growth free-radical chain transfer reaction.[14] We formulated thiol-ene resins using commercially available monomers, pentaerythritol tetra(3-mercaptopropionate) and triallyl-1,3,5-triazine-2,4,6-trione (referred to as PETMP and TATATO, respectively). PETMP/TATATO has been studied a potential dental restorative material, which also has the requirements of minimal shrinkage and hardness.[15] The properties of this formulation can be tuned by varying the composition and stoichiometry of the reacting monomers. We evaluated 3:4 and 1:1 molar compositions of PETMP/TATATO. The 3:4 molar mixtures have stoichiometric amounts of functional groups, whereas 1:1 mixture has an excess of thiol functional groups but comprises stoichiometric amounts of monomer molecules.

Thiol-epoxies: We also evaluated a thiol-epoxy catalyzed by an amine, which involves a multistep reaction resulting in the opening of the epoxide ring followed by the addition of a thiol anion.[16] The motivation for using these materials is driven by the low shrinkage and mechanical properties enabled by epoxies and by the ease with which a commercial thiol (PETMP) can be added to a commercial epoxy embedding resin (Epofix).[17] These materials are cured thermally at room temperature using the chemistry developed for conventional resins (i.e., using an amine initiator).

Benchmark embedding resins. We selected two conventional epoxy-based resins, Araldite 502 and Epofix, as benchmarks to compare the thiol containing resins. Both embedding resins have been used previously for nanoskiving.[4,12] Araldite cures at 60°C over a 24-48 h period, whereas Epofix cures at room temperature over 8-10 h. The main difference between these two epoxies is the nature of the curing agent that adds across the

epoxy groups of the resin molecules to provide cross linking. In Araldite, the curing agent is an anhydride, whereas in Epofix, it is an aliphatic amine.

Characterization: We sought to measure the properties and compare the performance of the new resins to the benchmark resins. Previous studies have shown that stress-strain tensile measurements provide the best metric for predicting *a priori* whether a material will be a satisfactory embedding resin.[9] Ideal materials are hard enough to prevent sample deformation (i.e., they possess a large modulus), but are not too brittle so as to prevent cracking. We therefore use stress-strain behavior as a primary metric for predicting ideal embedding resins. Of course, the ultimate metric for evaluating new resins is their performance during nanoskiving.

Table 5.1 Materials Studied as Embedding Resins for Nanoskiving.

Material	Polymer Type
Epofix	Epoxy
Araldite 502	Epoxy
NOA 63	Thiol-Ester
NOA 81	Thiol-Ester
PETMP/TATATO (1:1)	Thiol-Ene
PETMP/TATATO (3:4)	Thiol-Ene
PETMP/Epofix	Thiol-Epoxy

There are also some additional fundamental properties of polymer networks that help predict whether a resin will perform well; these include glass transition temperature (T_g),

shrinkage, and adhesion to gold.[9] Thermomechanical analysis provides insight into the glass transition temperature of the polymer networks. The T_g is a physical property of polymers that can indicate the best temperature settings needed for microtomy. As a general rule, polymers that are hard (T_g > room temperature) can be sectioned at room temperature while soft materials (T_g < room temperature) need to be sectioned at lower temperatures.[9] Shrinkage of the resin during preparation of the block should be minimized to avoid sample distortion and adhesion of the resin to gold during sectioning should be maximized to avoid delamination.

5.2.2. Materials and Preparation

Materials and preparation: We purchased Epofix and Araldite 502 as a kit (Electron Microscopy Sciences). The Epofix kit consists of two components, a resin (contains bisphenol-A-diglycidyl ether) and hardener (triethylenetetramine). Following the instructions from the kit, we mixed the resin and hardener in 25:3 (w/w) ratios and stirred rigorously for two minutes, keeping the mixture in vacuum for no longer than 20 min removed visible trapped air bubbles. Epofix cures at room temperature for 8-10 h,[18] though it performs better when cured at 60°C presumably because it lowers the viscosity before hardening. Araldite 502 kits consist of three components, Araldite 502 resin, DDSA (dodecenyl succinic anhydride) and DMP-30 (2,4,6-tri-(dimethylaminomethyl)phenol) and those are mixed in 20:22:0.65 (v/v) ratios, respectively. Araldite cures at 60°C in an oven for 24-48 h.[18]

We purchased PETMP and TATATO (Sigma Aldrich) monomers and mixed all formulations with 0.1 wt% of 2,2-dimethoxy-2-phenylacetophenone (DMPA, Ciba-Geigy) as the photoinitiator. Figure 5.2 depicts the chemical structures of the monomers. All materials were used as received. We purchased NOA 63 and NOA 81 (Norland Optical Adhesive) from Norland Products. We cured the thiol-ene and NOA resins for 60 s (75 mW/cm^2) to ensure thorough curing. The NOA curing time varied with sample thickness as outlined in the technical data sheets.[18] A mercury UV Floodlight (Intelli-Ray 400 from Uvitron International) cured the formulations. To formulate the thiol-epoxy, we mixed PETMP (thiol, 0.6 g), Epofix resin (epoxy, 1.4 g) and DMP-30 (0.1 g, 5 wt%) as the catalyst, resulting in stoichiometric amounts of functional groups (epoxy and thiol). The mixture cured at room temperature for 30 min to 1 h.

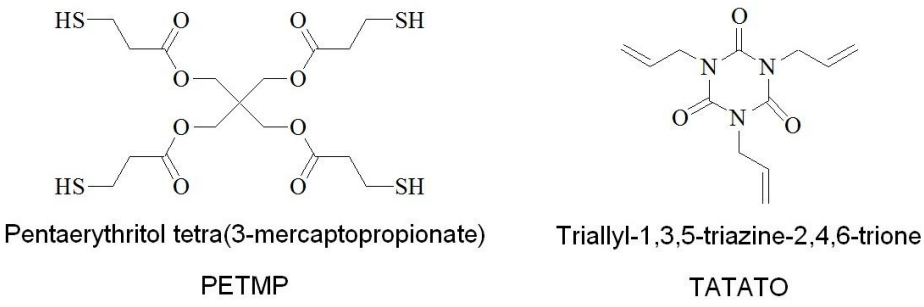

Figure 5.2: Chemical structures of the thiol and ene monomers

Polymerization shrinkage. We analyzed the shrinkage by measuring the density of the resin before and after curing. Equation 1 defines the percentage volumetric shrinkage, ΔV,

$$\Delta V = \frac{\rho_{cured} - \rho_{uncured}}{\rho_{cured}} \times 100\% \quad (1)$$

in which ρ_{cured} and $\rho_{uncured}$ are the densities of the mixtures before and after curing, respectively. This method has been used previously for determining the volumetric shrinkage of cured polymers.[19] We weighed 10 mL of each monomer formulation to determine $\rho_{uncured}$ and averaged 4-5 measurements.

We measured the density of the cured polymer samples by the flotation method in mixed solvents.[20] Cured polymer samples floated on carbon tetrachloride (ρ= 1.594 g/cm^3)[20] in a graduated cylinder with a magnetic stir bar. A burette added dropwise a light solvent – toluene (ρ = 0.8668 g/cm^3)[20] – to the carbon tetrachloride. Aluminum foil covered the container except for a small hole for the toluene to drop through to minimize evaporation. Equation 2 determines the density of the sample at the point when the sample floated halfway in the cylinder:

$$\rho_{sample} = \frac{V_{CT}\rho_{CT} + V_T\rho_T}{V_T + V_{CT}} \quad (2)$$

where ρ is the density, V is the volume of the solvent which is either toluene (T) or carbon tetrachloride (CT). The samples did not swell with exposure to solvent, nor did the weight of the samples change significantly after immersion in solvent.

Tensile Properties. An extensometer (Instron 5943) measured the stress and elongation at the breaking point as well as the elastic modulus. We followed the ISO 527-2 standard using a specimen type 5A. All samples cured in a stainless steel mold coated with a non-stick layer.

Dynamic Mechanical Anaylsis. DMA determined the glass transition temperature of the cured polymers. Curing the pre-polymer formulations in a Teflon Petri dish produced the specimens (6-8 mm wide, 0.6-1.0 mm thick and 15-17 mm long) for analysis. We conducted DMA (TA Q800 DMA, TA instruments) studies over a temperature range of 0-120°C for epoxy and -50-120°C for thiol containing systems, with a ramping rate of 5°C/min using tensile mode (sinusoidal stress of 1 Hz frequency).

Peel test. We evaluated the adhesion of polymer to gold using an extensometer in peel test mode.[21] Figure 5.3 illustrates two approaches used to prepare the samples. To study the adhesion of polymer cured on gold, we used electron beam evaporation to deposit titanium (5 nm) followed by gold (30 nm) onto clean glass slides and then spun cast thin films (15-17 μm thick, as verified by profilometry) of monomer onto the gold surface.

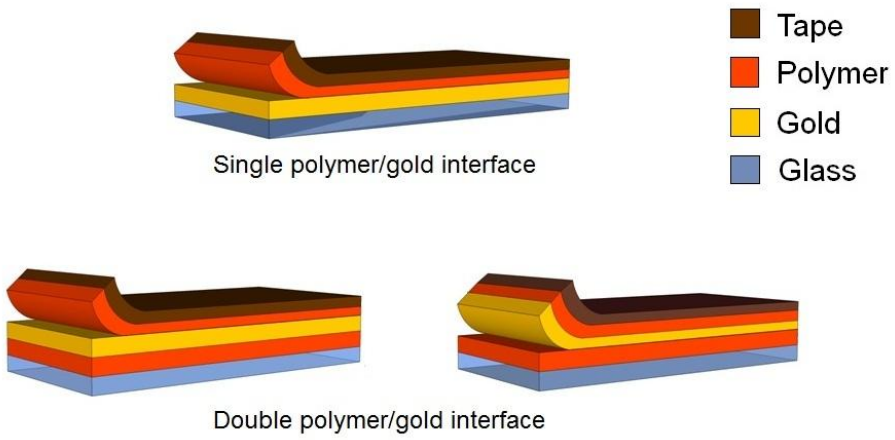

Figure 5.3: Comparison of peeling using glass/Ti/Au/polymer and glass/polymer/Au/polymer substrates. In the first case ("single polymer/gold interface") peeling primarily occurs at the Au/polymer interface. In the second case, peeling could occur at two interfaces, as shown.

An additional set of experiments measured the peel strength of the interface between gold and polymer formed by depositing gold onto cured polymer. We cured a thin film of the polymer on glass and deposited a thin (30 nm) film of gold onto the cured polymer surface by e-beam evaporation. We cast a thin film of the same pre-polymer formulation on the gold surface and cured it against a backing material that can be gripped by the Instron. We pressed a suitable backing material (e.g., Scotch tape) on top of the pre-polymer film and cured the polymer. The backing material had to be thin (so that it could be bent easily) and had to have sufficient adhesion to the polymer to avoid delamination during the peel test. Commercial Scotch tape served as the backing material for most of the measurements, although Kapton film (DuPont) served as the backing material for the Epofix samples because Epofix showed poor adhesion to the Scotch tape. Peeling the backing tape slowly (~5 mm/s by hand) from the substrate provided a qualitative evaluation of the nature of failure. The Instron measured the force required to peel the polymer film (90^o peel angle and a 1.0 mm/s peel rate) from the gold coated substrate at room temperature.

Nanoskiving. We prepared samples for ultramicrotome sectioning by first depositing a thin film of gold (thickness 50 or 100 nm) on a Si-wafer by e-beam evaporation. We spin coated (or drop cast for Epofix) the pre-polymer on the gold surface and cured it. The gold-film adhered to the polymer as it was peeled from the Si surface and cut into small strips of (5-7 mm long, 3 mm wide). Embedding the gold strips in more pre-polymer formulation in a mold produced the block. A razor blade trimmed the edges of the sample block into a trapezoid shape (about 1 X 1 mm) to expose the metal.

A Leica UC-6 Ultramicrotome prepared sections from the blocks containing gold films with thicknesses of 50, 100, 150, and 200 nm using a 2 mm 35° Diatome diamond knife at 1 mm/s except for the 50 nm sections which we sectioned at 0.8 mm/s.

5.3. Results and Discussion

Tensile Testing and Young's modulus. Tensile tests represent the best method for predicting the usefulness of embedding resins.[9] The Young's modulus (i.e., the initial slope of the stress-strain plot) is important in sectioning since mechanical damage by compression can occur in softer samples and cracking occurs in hard, brittle samples. Embedding materials with Young's moduli of 1.5-3 GPa generally provide high quality sections in ultramicrotomy.[9] Softer resins (with moduli < 1.5 GPa) can be cut below room temperature, but so-called "cryo-sectioning" is more challenging than room temperature sectioning. Resins should also undergo minimal plastic flow (i.e., low ductility) to avoid distortions during sectioning. Figure 5.4a shows that the two conventional epoxy resins have all of these desirable features (Figure 5.4a). In contrast, the commercial NOA resins have highly undesirable deformation and ductility, which reduces the usefulness of the NOA resins for nanoskiving.

The PETMP-based resins behave favorably (Figure 5.4b), with limited yielding and low ductility. Notably, the 1:1 PETMP/TATATO has significant variability in its stress-strain curves (Figure 5.5), likely due to the non-stoichiometric nature of the network. This variability limits the utility of this resin for reliable sectioning. The 3:4 PETMP/TATATO showed almost identical behavior to the Araldite resin and therefore appeared to be the most

promising of all the thiol containing resins studied. The PETMP/Epofix sample had the highest yield stress and showed low ductility, which suggests this thiol-epoxy resin may be useful for nanoskiving too.

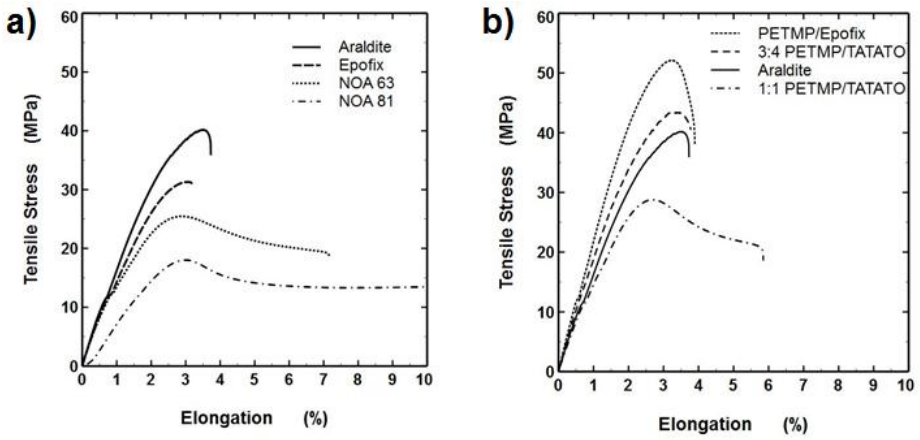

Figure 5.4: (a) Conventional embedding resins and commercial photocurable 'thio-esters' (NOA 63 and 81). Not shown: The break point of NOA 81 occurs at 15.8%. (b) Thiol-ene and thiol-epoxy embedding resins and Araldite (for comparison).

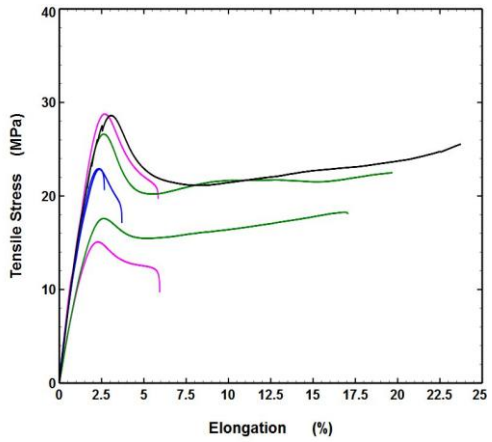

Figure 5.5: Variations in stress-strain behavior for 1:1 PETMP/TATATO. Colors indicate samples from the same batches.

The slope of the initial linear portion of the stress-strain traces provided the modulus values listed in Table II. Using the elastic moduli of Araldite and Epofix as benchmark values (2.01 and 2.15 GPa, respectively), the values for NOA 63 and NOA 81 are low. Although the modulus value of 3:4 PETMP/TATATO is lower than the benchmark values, it is larger than the 1:1 PETMP/TATATO and still acceptable for room temperature sectioning. The value also agrees with modulus values found for similar formulations in the literature[22] and is consistent with the known trend that increasing the amount of ene in the thiol-ene formulation increases hardness.[17] The thiol-epoxy formulation also yielded sample blocks with modulus values slightly greater than the benchmark.

Cure time. The thiol containing polymers evaluated in this study cured rapidly compared to the epoxy based networks (Araldite and Epofix). The benchmark resins require several hours to cure completely. In contrast, the thiol-ene and NOA resins cured within minutes. Previous studies on the curing kinetics of PETMP/TATATO polymerization suggest that 60 s of irradiation (at 5.0 mW/cm^2) resulted in 90% conversion of the TATATO allyl group and 77% conversion of the PETMP thiol functional group.[15] The shorter cure time of the thiol-enes and NOAs offers a potential advantage over conventional epoxy-based embedding resins in terms of rapid prototyping.

The thiol-epoxy system required ~30 min to cure at room temperature, as estimated by the time required to get a non-tacky hard-set polymer. Notably, the polymerization begins almost immediately upon mixing as indicated by the increase in viscosity. This characteristic makes it challenging to process the resin (i.e., mixing it rapidly and uniformly without

entraining air bubbles). Of the approximately twenty-five samples we produced for nanoskiving, three were too soft to section, presumably due to poor mixing.

Polymerization shrinkage. Table 5.2 summarizes the shrinkage measurements. Epoxies are known to undergo a low extent of shrinkage during polymerization; a volume reduction around 4-5% is expected for epoxy resins, but can vary based on filler content (embedding resins usually lack filler because the filler can damage diamond knives) and preparation conditions of the resin such as mixing or initial resin temperature.[10] Araldite 502 shrunk 4.8% and Epofix shrunk ~6%. NOA 63 and NOA 81 underwent 5.7% and 8.8% shrinkage, respectively. PETMP/TATATO formulations undergo 7.7% and 7.5% shrinkage for the 1:1 and 3:4 formulations. The shrinkage reported for a 3:4 stoichiometric PETMP/TATATO resin composition by the static volume change method is 6.2%.[22] We speculate that our shrinkage values are slightly higher than those measured previously because during curing our samples were not confined by the walls of the sample container. We did not observe any adverse effects of shrinkage in the samples prepared by nanoskiving, and the amount of shrinkage is less than some embedding resins that have been used previously (e.g., PMMA which has a 15-20% shrinkage[23]).

Dynamic Mechanical Analysis. Table 5.2 summarizes the T_g. As a general rule, the T_g of an embedding resin must be greater than room temperature if sectioning is to be done at room temperature,[24] and practically, the T_g should be 47°C or greater for proper sectioning.[9] The benchmark epoxy polymers had T_g values between 70-76°C. The T_g of all the thiol-containing polymers studied are lower than the epoxies, but well above room temperature (and all but the NOAs were above 47°C), suggesting that the sectioning can be done at room

temperature. The PETMP/TATATO based networks exhibited a higher glass transition temperature than both NOAs. As the amount of alkene bonds decreases in the PETMP/TATATO formulation (going from 3:4 to 1:1 molar), the T_g decreases.

Table 5.2 T_g, Young's modulus, and percent shrinkage of embedding resins

Materials	T_g (°C)	Young's Modulus (GPa) at 25°C	% Shrinkage
Araldite	76	2.01 ± 0.15	4.8
Epofix	72	2.15 ± 0.22	6.3
NOA 63	44	1.54 ± 0.08	5.7
NOA 81	35	0.85 ± 0.05	8.8
PETMP/TATATO (1:1)	51	1.43 ± 0.09	7.7
PETMP/TATATO (3:4)	73	1.70 ± 0.13	7.5
PETMP/Epofix	60	2.19 ± 0.08	3.0

The inclusion of thiol in epoxy networks also reduces the T_g (from 72 °C for Epofix to 60°C for PETMP/Epofix). The Young's modulus of the thiol-ene cured resins correlates well with similar thiol-ene resins.[25]

Peel tests. Peel tests evaluated the adhesion of the polymers to gold (Figure 5.6). The peeling mechanism differed for the benchmark resins and thiol containing polymers both qualitatively and quantitatively. Epofix and Araldite delaminated primarily at the gold-polymer interface (i.e., adhesive failure), confirming that the adhesion between Au-epoxy is weak. Based on visual inspection of the substrate, we estimate that the epoxy peeled cleanly from at least 90% of the surface area of the gold substrate . Surprisingly, we observed the same behavior for NOA 63 samples despite the presence of thiols (although the technical

data sheet from Norland suggests that NOA 81 binds more strongly to metals than NOA 63). In contrast, NOA 81, PETMP/TATATO, and the thiol-epoxy left polymer on the gold substrate after peeling. This qualitative observation suggests that the adhesion of these polymers to gold is better than that of Epofix, Araldite, and NOA 63.

A 90° peel test quantified the peel force. PETMP/TATATO, NOA 81, and PETMP/Epofix had larger average peel forces than Epofix and NOA 63 as shown in Figure 5.6. It is difficult to assign definitive meanings to the absolute values of the peel force measurements. Regardless, the values obtained provide an insight into relative forces required to induce delamination of polymer from the gold surface.

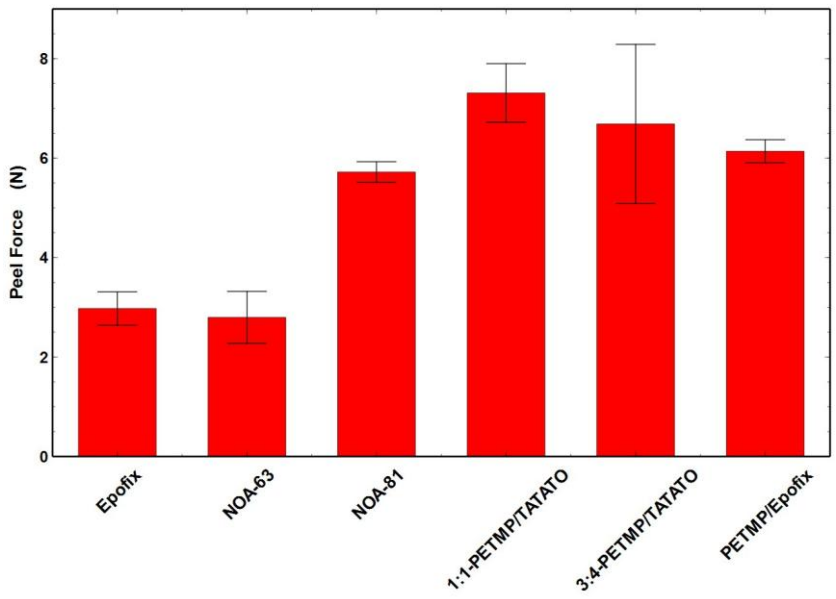

Figure 5.6: The comparison of average load required to peel the polymers from gold surface of glass/Ti/Au/polymer substrates.

Although the benchmark epoxy resins contain amines, which provide some adhesion to gold,[26] thiols are known to bond roughly two times more strongly to gold.[27] Thiol is much more abundant in these resins, too. It is therefore expected that the force required to peel a thiol-containing resin from a gold layer would be higher than for an amine containing resin; indeed, the peel test results confirm this hypothesis. The addition of a thiol group to Epofix approximately doubles the peel force necessary to remove the polymer from the gold layer relative to pure Epofix.

We also evaluated qualitatively the interface between gold and polymer formed by depositing gold onto pre-cured polymer (polymer/Au/polymer sandwiches). We expected this interface to be weaker than the interface created by curing polymer against gold. During the peeling of Epofix samples, the bottom polymer layer (i.e., the pre-cured layer) and gold failed adhesively suggesting that the adhesion of pre-cured polymer to gold is weaker than that formed by curing polymer against a gold film. In all the thiol-containing samples, patches of gold remained attached to both the top and bottom polymer layers, as might be expected due to the presence of thiol on both sides of the gold. According to theoretical models, Au-Au bonds in bulk gold break with a force of 0.8-0.9 nN.[28] It is expected that the S-Au bond, with a strength of 1.4 nN,[27] would break after the Au-Au bond which is consistent with our observations.

Nanoskiving. The sample blocks for each polymer system contained an embedded film of gold (50 or 100 nm-thick). Prior to sectioning with ultramicrotome, we trimmed these specimens to a rough trapezoid shape (~1 x 1 mm) as shown in Figure 5.7.

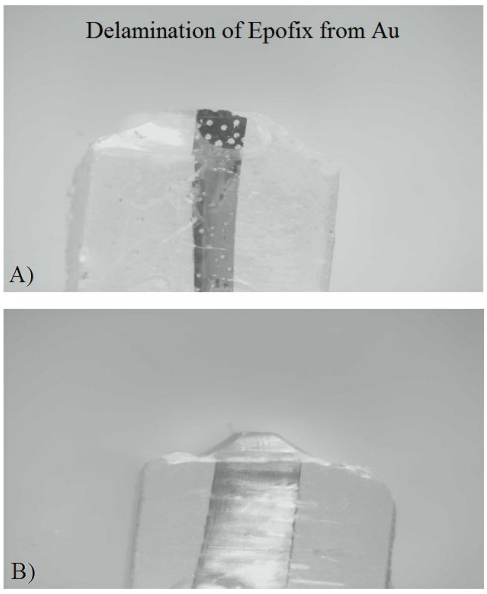

Figure 5.7: Photographs of sample blocks prepared by cutting polymer with a razor blade. A) Epofix does not contain thiol and delaminates from gold in some cases. B) PETMP/TATATO contains thiol and adheres to gold.

We only sectioned the Araldite, Epofix, NOA 81, and PETMP/TATATO 3:4; the mechanical properties of the blocks formed from the other embedding resins precluded trimming and sectioning, primarily because they were too soft and deformed during the trimming process (Figure 5.8). In some cases, the brittle nature of Epofix, combined with its poor adhesion to gold, cause the polymer to delaminate and break away in chips, requiring the block to be rough-cut and re-trimmed. An example of this type of failure is shown in Figure 5.7a, which is contrasted with a block containing thiols (PETMP/TATATO, Figure 5.7b).

The PETMP/Epofix gave the most unexpected result; some of the sample blocks (3 out of 25) were too soft to trim (Figure 5.8**)** and the remaining ones were brittle (they could be snapped into two pieces by hand). Although the macroscopic measurements suggest

PETMP/Epofix has desirable mechanical properties, we believe this inconsistency arises because the addition of PETMP to Epofix initiates a rapid polymerization that precludes effective mixing on the microscale. The relatively small blocks (and extremely small slabs formed during nanoskiving) are sensitive to small, localized variation in mechanical properties arising from the inefficient mixing. This variation manifested itself as block-to-block inconsistencies; some of the blocks could, in fact, be trimmed, (Figure 5.8) but we did not continue the nanoskiving test because of the irreproducibility of the blocks.

Figure 5.9 shows optical micrographs of the resulting sections of thicknesses of 50, 100, 150, and 200 nm. With the exception of NOA 81, we produced sections down to 40 nm (not shown) before they became too fragile to handle, though the technical limit of the ultramicrotome is 15 nm. Although the resolution of these micrographs (250X magnification) is not sufficient to directly image the gold structures, which are 50-100 nm thick, the mismatch in the indices of refraction between the embedding resins and the gold appears as a dark line. The thickness of the sections can be verified by the color of the sections, which results from thickness-dependent interference; 50 nm appears grey, 100 nm turquoise, 150 nm blue, and 200 nm orange-brown. The NOA 81 sections all appear blue-turquoise, however, indicating that the actual thickness of the sections deviated from the set thickness.

Figure 5.8: Photographs of the blocks of the different embedding resins being trimmed with a razor blade prior to sectioning. The photographs marked with a red X indicate blocks that could not be trimmed because the polymers were too soft, causing the block to deform, and/or the stress induced by the razor blade caused macroscopic adhesive failure–i.e., the block fell apart. The photographs marked with a green check mark indicate blocks that could be trimmed, but not necessarily sectioned. Three different blocks of thiol/Epofix are pictured, highlighting the block-to-block variability; one block (bottom-left) was too soft to be trimmed, one (bottom-center) could be trimmed (but was not sectioned), and one (bottom-right) was too flexible to be mounted for trimming.

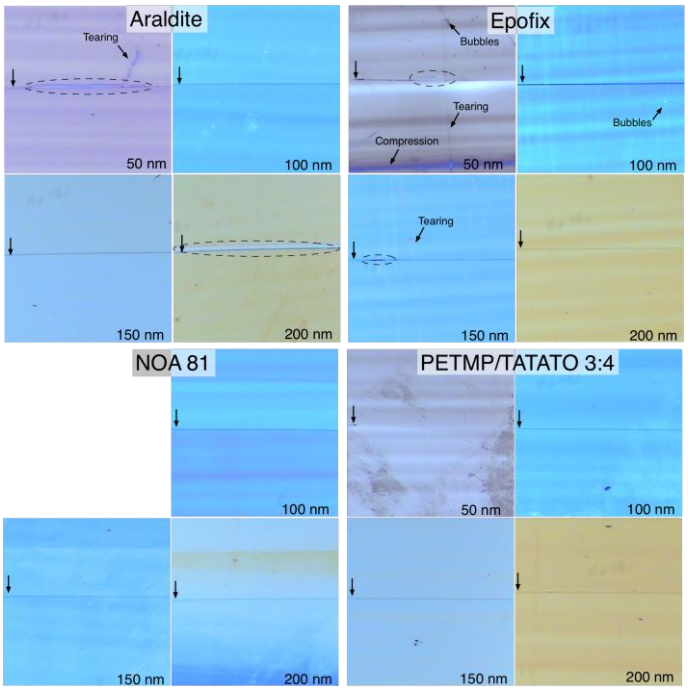

Figure 5.9: Optical micrographs (250X) of sections of the four embedding resins that could be nanoskived. The vertical arrows at the left of each image indicate the position of the gold nanowire and the dashed ovals indicate delamination of the resin from the gold. The thickness of each section is indicated in the lower left corner. The horizontal bands present in some images are the result of chattering, the severity of which depends on the mechanical properties of each resin. Sections of NOA 81 < 50 nm disintegrated upon formation and chattering was severe enough to preclude accurate section-thicknesses, which is evident from the predominantly blue color in the 200 nm section. Tearing, bubbles, and compression artifacts were predominant in the Epofix sections, while Araldite exhibited the most severe delamination.

This deviation is the result of the mechanical properties of the NOA 81 which is likely too ductile and produces too much friction against the advancing edge of the diamond knife. The result is uneven sections, which is the case in Figure 5.9 (lower-left) where only a band of orange-brown (i.e., 200 nm-thick resin) is apparent in the 200 nm section. The average thickness of these sections also alternates as the block advances by the set-thickness before

each stroke, but differing thicknesses of epoxy are skived (not pictured). The result is that NOA 81 is unsuitable for forming gold nanowires by nanoskiving at any thickness.

The most obvious feature of the Araldite (Figure 5.9; top-left) sections is delamination, which is indicated with dashed ovals and appears as almost complete adhesive failure in the 50 and 200 nm sections. While the degree of delamination varies between sections, the images shown in Figure 5.9 are representative. Aside from delamination, Araldite produces–unsurprisingly–very high quality sections with minimal chattering, which appears as horizontal bands of color. These bands of color are the result of the knife skipping (chattering) as it passes through the polymer and are the result of the compressibility of the polymer and the amount of friction generated at the trailing edge of the knife. Chattering should not be confused with transient vibrations, which can be controlled externally (e.g., with a dampening table). From these results we conclude that Araldite, while functional, is not an ideal embedding resin for gold structures.

Epofix, which is designed for ultramicrotomy on hard materials, performs very poorly at thicknesses below 100 nm. The 50 nm-thick section pictured in Figure 5.9 (top-right) is rife with artifacts, the most severe of which is the compression visible in the lower part of the section. Also present are bubbles, which form when the two parts of the pre-polymer are mixed and which cannot be removed completely before the resin cures. There is also significant tearing, which is usually the result of a knick in the diamond knife, but can also be caused by dust particles. In this case, we ascribe the tearing to a minor defect in the knife (which is very common) that is only apparent in the 50 nm-thick sections of Epofix because of the brittle nature of that resin. In addition to being difficult to trim, this brittleness also

leads to sections that craze and are predisposed to separating into pieces in the boat (not shown) as a result of tearing and compression artifacts. The most prominent artifact in the Epofix sections, surprisingly, is not delamination–which is visible to some extent in 50 and 150 nm-thick sections–but chattering, which is evident as prominent bands of color in all of the sections. While chattering is not necessarily detrimental to the formation of nanowires of gold, which are cut parallel to the edge of the knife, more complex metallic structures will not have a uniform height/thickness when sectioned using Epofix.

The only embedding resin that produced sections (nearly) free of artifacts and with no delamination at all thicknesses was 3:4 PETMP/TATATO. The only visible artifacts are smudges, which are the most pronounced in the 50 nm-thick sections shown in Figure 5.9 (bottom-right). It is not clear what causes these smudges, but they are not tears, bubbles, compression artifacts or the result of chattering nor do they appear to negatively affect the nanoskiving process. The 3:4 PETMP/TATATO sections were the easiest to trim and section, show almost no chattering, and form very stable sections even at thicknesses below 50 nm (not shown). Interestingly, the dark line indicating the position of the gold is barely discernable in the 50 nm-thick sections, which we ascribe to the small dimension of the gold wire (50 x 50 nm) and the excellent adhesion of the polymer to gold. It is clearly visible and free of any signs of delamination in the 100, 150, and 200 nm-thick sections. To verify that the embedding resins do not interfere with the electrical properties of the gold nanowires, we measured *I/V* curves for 100 nm-thick sections of Araldite, Epofix, NOA 81, and 3:4 PETMP/TATATO. We measured 50 nm-thick gold nanowires (~1 mm x 50 nm x 100 nm)

by painting small (~1 mm^2) pads of silver paste at either end of each nanowire and contacting them in a home-built probe station.

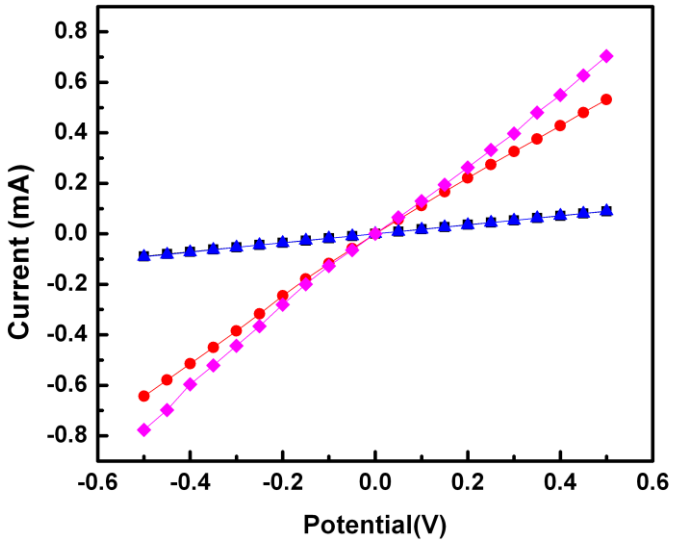

Figure 5.10: Plots of current (mA) versus potential (V) for 50 nm-thick gold nanowires fabricated using 100 nm-thick sections of Araldite (black squares), NOA 81 (blue triangles), Epofix (red squares), and 3:4 PETMP/TATATO (pink diamonds). Each trace is an average of four sections. All four wires exhibit ohmic *I/V* characteristics indicating that the wires are electrically continuous. The slightly lower conductivities of the wires in NOA 81 and Araldite are the result of differences in the lengths of the wires.

The resulting data are plotted in Figure 5.10 and show ohmic conduction for all four nanowires, indicating that none of the embedding resins affected the electrical properties of the gold nanowires. The magnitude of the current (~ 10^{-4} A) is consistent with previous measurements on gold nanowires of similar dimensions fabricated using nanoskiving.[29] The

slightly lower conductivities of NOA 81 and Araldite are the result of differences in the lengths of the nanowires.

From these measurements and the optical micrographs in Figure 5.9, we can conclude that all four resins are capable of producing electrically continuous gold nanowires; however, 3:4 PETMP/TATATO yields the least delamination and, qualitatively, the highest quality sectioning and general ease of handling the sections. Moreover, 3:4 PETMP/TATATO is photo-curable in a fraction of the time of the thermally-curable Araldite and Epofix epoxies. While delamination is, in this case, not a critical parameter–it leads to some deformation of the wires, but not catastrophic failure–it is of critical importance for delicate and/or complex metallic features and for applications that leverage the insulation that the polymer slab provides. For instance, nanowires fabricated using 3:4 PETMP/TATATO can be contacted using silver paste with no leakage (hence electrical shorts) to the supporting substrate, and the top face of the wire can be selectively functionalized with, for example, a SAM or addressed by a fluid for sensing applications.

For applications in which it is desirable to remove the polymer slab, leaving only the metallic nanostructure–in our case nanowires–on the substrate, we compared the time required to ash 100 nm-thick slabs of each of the four resins completely using oxygen plasma. We exposed each to 1 mbar of pure oxygen plasma until there were no traces of polymer remaining by optical microscopy. These results are summarized in Table III and show that the thiol-containing polymers (3:4 PETMP/TATATO and NOA 81) take considerably longer (30 min) to ash than do the epoxies, and that Araldite ashes in about one

third the time (5 min) of Epofix (15 min). We expect these times to scale according to the power output of the plasma oxidizer; we used a relatively low power plasma cleaner.

Table 5.3 Time required to ash 100 nm-thick sections with oxygen plasma (1 mbar).

Material	Oxygen Plasma Exposure (min)
Epofix	15
Araldite 502	5
NOA 81	30
PETMP/TATATO (3:4)	30

5.4. Conclusion

We identified new embedding resins for nanoskiving that have similar properties to conventional epoxy-based embedding resins, but are photocurable and have improved adhesion to gold because of the inclusion of thiol functional groups. We compared these thiol-containing resins to two conventional, benchmark epoxy-based resins (Araldite and Epofix). Of the thiol-containing materials in our study, the 3:4 PETMP/TATATO appears to have the most promising properties for nanoskiving. It cures quickly, possesses mechanical properties similar to commercial resins, adheres well to gold, and produces high-quality microtome sections. NOA 81 also produced samples that could be sectioned using an ultramicrotome, but the resulting sections had irregular thicknesses.

A draw-back of the 3:4 PETMP/TATATO system is that it shrinks slightly more than conventional epoxies, which may result in some deformation or stress in delicate samples.

We observed no evidence of this being an issue in our samples as determined by measuring the electrical properties of the gold nanowires, but it may be an issue for more sensitive geometries (e.g., fragile gold structures that might deform under stress). For particularly sensitive samples, users may consider exploring techniques from the literature to reduce thiol-ene shrinkage such as allyl sulfide addition-fragmentation chain transfer.[30,31] The ability to partially cure thiol-enes to produce oligomers prior to embedding provides an additional route to lower the shrinkage.

Physical and mechanical measurements suggest that the thiol-epoxy formulation – which can be formed by simply adding thiol to a commercial epoxy—could be a suitable resin. We found, however, that the rapid polymerization associated with this approach resulted in sample-to-sample variability, presumably due to poor mixing. Future work could focus on optimizing this formulation to control the rate of polymerization, although there appear to be few benefits of this resin relative to the 3:4 thiol-ene.

The improved adhesion of the thiol-containing embedding polymers to metals reduces the occurrence of delamination during sample preparation and microtome sectioning. We anticipate that the enhanced properties offered by thiol-containing systems, such as reduced cure time, excellent adhesion to gold, and sufficient hardness, will be useful for nanoskiving. The use of light to initiate the reaction allows for rapid prototyping but may also enable better spatial-temporal control of the resin during sample preparation. Nanoskiving of gold nanowires has already proven useful to numerous applications,[11,29] and with this new embedding resin there is increased potential for further use of this unconventional nanofabrication technique in a wider range of areas with more reliable sectioning.

5.5. References

[1] Xu, Q., Rioux, R. M., Dickey, M. D. & Whitesides, G. M. Nanoskiving: A New Method To Produce Arrays of Nanostructures. Acc Chem Res 41, 1566–1577 (2008).

[2] Gates, B. D., Xu, Q., Love, J. C., Wolfe, D. B. & Whitesides, G. M. Unconventional Nanofabrication. Annu. Rev. Mater. Res. 34, 339–372 (2004).

[3] Gates, B. D. et al. New Approaches to Nanofabrication: Molding, Printing, and Other Techniques. Chem Rev 105, 1171–1196 (2005).

[4] Xu, Q. et al. Fabrication of Large-Area Patterned Nanostructures for Optical Applications by Nanoskiving. Nano Lett 7, 2800–2805 (2007).

[5] Lipomi, D. J. et al. Integrated Fabrication and Magnetic Positioning of Metallic and Polymeric Nanowires Embedded in Thin Epoxy Slabs. ACS Nano 3, 3315–3325 (2009).

[6] Glauert, A. M. Practical Methods in Electron Microscopy. (Elsevier Science, 1974).

[7] Plummer, H. k. Reflections on the Use of Microtomy for Materials Science Specimen Preparation. Microsc. Microanal. 239–260 (1997). doi:10.1017/S1431927697970197

[8] Lipomi, D. J. et al. Survey of Materials for Nanoskiving and Influence of the Cutting Process on the Nanostructures Produced. ACS Appl. Mater. Interfaces 2, 2503–2514 (2010).

[9] Acetarin, J., Carlemalm, E., Kellenberger, E. & Villiger, W. Correlation of some mechanical properties of embedding resins with their behaviour in microtomy. J. Electron Microsc. Tech. 6, 63–79 (1987).

[10] Petrie, E. Epoxy Adhesive Formulations. (McGraw-Hill Professional, 2005).

[11] Lipomi, D. J., Martinez, R. V. & Whitesides, G. M. Use of Thin Sectioning (Nanoskiving) to Fabricate Nanostructures for Electronic and Optical Applications. Angew. Chem. Int. Ed. 50, 8566–8583 (2011).

[12] Pourhossein, P. & Chiechi, R. C. Directly Addressable Sub-3 nm Gold Nanogaps Fabricated by Nanoskiving Using Self-Assembled Monolayers as Templates. ACS Nano 6, 5566–5573 (2012).

[13] Love, J. C., Estroff, L. A., Kriebel, J. K., Nuzzo, R. G. & Whitesides, G. M. Self-Assembled Monolayers of Thiolates on Metals as a Form of Nanotechnology. Chem Rev 105, 1103–1170 (2005).

[14] Hoyle, C. E., Lee, T. Y. & Roper, T. Thiol-enes: Chemistry of the past with promise for the future. J. Polym. Sci. Part Polym. Chem. 42, 5301–5338 (2004).

[15] Lu, H., Carioscia, J. A., Stansbury, J. W. & Bowman, C. N. Investigations of step-growth thiol-ene polymerizations for novel dental restoratives. Dent. Mater. 21, 1129–1136 (2005).

[16] Hoyle, C. E., Lowe, A. B. & Bowman, C. N. Thiol-click chemistry: a multifaceted toolbox for small molecule and polymer synthesis. Chem. Soc. Rev. 39, 1355 (2010).

[17] Carioscia, J. A., Stansbury, J. W. & Bowman, C. N. Evaluation and control of thiol–ene/thiol–epoxy hybrid networks. Polymer 48, 1526–1532 (2007).

[18] Technical Data Sheets. Accessed 1/30/2015.
Epofix: www.emsdiasum.com/microscopy/technical/datasheet/1232.aspx ;
NOA 63: www.norlandprod.com/adhesives/noa%2063.html ;
NOA 81: www.norlandproducts.com/adhesives/noa%2081.html ;
Araldite 502: www.emsdiasum.com/microscopy/technical/datasheet/13900.aspx.

[19] Uhl, A., Mills, R. W., Rzanny, A. E. & Jandt, K. D. Time dependence of composite shrinkage using halogen and LED light curing. Dent. Mater. 21, 278–286 (2005).

[20] Mohan, A., Gurarslan, A., Joyner, X., Child, R. & Tonelli, A. E. Melt-crystallized nylon-6 nucleated by the constrained chains of its non-stoichiometric cyclodextrin inclusion compounds and the nylon-6 coalesced from them. Polymer 52, 1055–1062 (2011).

[21] Song, R. et al. Combinatorial peel tests for the characterization of adhesion behavior of polymeric films. Polymer 46, 1643–1652 (2005).

[22] Carioscia, J. A., Lu, H., Stanbury, J. W. & Bowman, C. N. Thiol-ene oligomers as dental restorative materials. Dent. Mater. 21, 1137–1143 (2005).

[23] Glauert, A. M. & Glauert, R. H. Araldite as an embedding medium for electron microscopy. J. Biophys. Biochem. Cytol. 4, 191–194 (1958).

[24] Gnaegi, H. Microsc. Microanal. 6 (Supplement 2: Proceedings), 314–316 (2000).

[25] Hagberg, E. C., Malkoch, M., Ling, Y., Hawker, C. J. & Carter, K. R. Effects of Modulus and Surface Chemistry of Thiol-Ene Photopolymers in Nanoimprinting. Nano Lett 7, 233–237 (2007).

[26] Frei, M., Aradhya, S. V., Koentopp, M., Hybertsen, M. S. & Venkataraman, L. Mechanics and Chemistry: Single Molecule Bond Rupture Forces Correlate with Molecular Backbone Structure. Nano Lett. 11, 1518–1523 (2011).

[27] Grandbois, M., Beyer, M., Rief, M., Clausen-Schaumann, H. & Gaub, H. E. How Strong Is a Covalent Bond? Science 283, 1727–1730 (1999).

[28] Rubio-Bollinger, G., Bahn, S. R., Agraït, N., Jacobsen, K. W. & Vieira, S. Mechanical Properties and Formation Mechanisms of a Wire of Single Gold Atoms. Phys. Rev. Lett. 87, 026101 (2001).

[29] Dawson, K. et al. Single Nanoskived Nanowires for Electrochemical Applications. Anal. Chem. 83, 5535–5540 (2011).

[30] Scott, T. F. Photoinduced Plasticity in Cross-Linked Polymers. Science 308, 1615–1617 (2005).

[31] Kloxin, C. J., Scott, T. F. & Bowman, C. N. Stress Relaxation via Addition−Fragmentation Chain Transfer in a Thiol-ene Photopolymerization. Macromolecules 42, 2551–2556 (2009).

CHAPTER 6. Summary and Outlook

6.1. Summary

Throughout this dissertation, we have demonstrated the tuning of mechanical properties and surface chemistry of polymeric materials for applications in micro- and nanofabrication. In particular, we used photochemistry to modify mechanical properties of PVMS networks, to graft ELPs to silicon wafers, and to cure thiol-ene based embedding resins for nanoskiving. We also demonstrated the strengthening of PVMS networks with the incorporation of silica nanoparticles. The importance of tunability of materials used in micro- and nanofabrication was highlighted for applications in soft lithography, microfluidics, biological systems, and nanowire preparation.

We postulated that PVMS would be an attractive alternative material for microchannel fabrication that offers several benefits in comparison with PDMS. PVMS, like other silicone elastomer networks, is optically transparent, easy to process, and flexible. The vinyl side groups in PVMS enable additional chemical reactions for property manipulation in microfluidics, as explored in this dissertation, as well as other applications. We successfully increased the modulus of PVMS using UV treatment by two orders of magnitude. Additionally, we demonstrated the use of a local modification of PVMS microchannels by selective delivery of photoinitiator, resulting in a small area of modification for use in solvent resistance. Furthermore, we evaluated the strengthening of PVMS with nanoparticles, which increased the elongation and toughness of the networks without creating rigid, brittle materials. These tough networks were less likely to tear when removed from the surface of a mold during replica molding. We also demonstrated thiol-ene cured PVMS networks with a modulus orders of magnitude higher than traditional siloxane elastomeric networks. While

thiol-ene cured polysiloxanes have been reported in the literature,[1,2] our PVMS has both silanol end groups as well as vinyl side groups, giving our system dual functionality. Feasibly, a PVMS network could be both end-group cured and then additionally hardened with thiol groups, similar to the method used for the UV-hardened microchannels in Chapter 2 of this dissertation.

Next, we explored the modification of vinyl-functional silicon surfaces with stimuli-responsive polypeptides as an analogue for the modification of PVMS microchannel surfaces in biological systems. We were motivated to create and study a densely grafted ELP surface, expecting that a densely packed surface would possess desirable reversible physicochemical behavior as a result of application of thermal stimuli. We found, however, that by attempting to pack high densities of polypeptides onto a surface, we lost the beneficial responsive properties. Because the LCST of an ELP is dependent on concentration, our highly concentrated ELP grafted surfaces have reached a packing density that prevents even cold water from resolubilizing the peptides. This work informs us of the delicate interplay of full surface coverage versus optimal stimulus response when grafting stimuli-responsive polypeptides.

As an extension of our work using photochemistry to tune mechanical properties of networks, we identified new embedding resins for nanoskiving with improved adhesion to gold because of the inclusion of thiol functional groups. We compared these thiol-containing resins to conventional, benchmark epoxy-based resins. Of the thiol-containing materials in our study, the stoichiometric ratio of 3:4 PETMP/TATATO appeared to have the most promising properties for nanoskiving. We preferred this resin due to the short cure time,

mechanical properties similar to commercial resins, good adhesion to gold, and production of high-quality microtomed sections. Physical and mechanical measurements suggest that the thiol-epoxy formulation, the combination of adding thiol to a commercial epoxy, could also be suitable resin; however this formulation suffered from excessive sample-to-sample variability. The improved adhesion of the thiol-containing embedding resins to gold reduces the occurrence of delamination during microtomy. The use of light to initiate the reaction allows for rapid prototyping and enables spatial-temporal curing control during sample preparation.

6.2. Outlook

For any application, polymer properties can be tuned through modification or by synthesis of a new polymer or polymer network. The appeal of polymer modification is the use of a material with known properties, merely tailoring either the surface chemistry or the bulk mechanical behavior to suit new fabrication techniques. Siloxane polymers are perhaps unique in the flexibility and tunability they offer. The silicon-oxygen backbone is by nature flexible but chemically and thermally stable. Mechanical properties of siloxanes can be tuned either through reinforcing particles or by increasing crosslink density. The beauty of this technique is that it enables researchers to use one polymer chain to generate both networks with elasticity and high elongation and rigid, glassy networks.

The UV treatment used to modify the mechanical and diffusive properties of PVMS operated by reacting the vinyl side groups together. However, introduction of increased chemical functionality by grafting molecules to the vinyl functional groups on the surface

enables further tailoring of the properties of PVMS microchannels. For example, grafting of dynamic covalent groups such as acylhydrazone groups to the vinyl side groups of PVMS would provide an alternate route for mechanical modification of network properties. Additionally, grafting groups with hydrophilicity or biologically compatible stimuli-reponsive behavior to the vinyl side groups of a PVMS microchannel will expand the utility of this technology into biotechnology. Indeed, PVMS and vinyl methyl siloxanes are being investigated for cell growth[3] and anti-biofouling currently, and have been used in a variety of applications to date.[4–6]

One potential area of development would be the use of PVMS/PDMS copolymers, which would limit the available functional groups while retaining mechanical properties. Using a copolymer, less extensive modification would be possible, though a critical concentration of vinyl groups must be available for crosslinking as used in Chapter 2 of this dissertation. Additionally, because of the lack of availability of PVMS on a commercial scale, Sylgard 184® could be used as a support structure for a thin layer of PVMS. In our work, we discovered that PVMS networks will adhere strongly to PDMS networks after exposure to oxygen plasma, which could be used to modify an otherwise inert PDMS network by attaching a PVMS network layer to the PDMS surface.

Although we only demonstrated the use of PVMS for resisting swelling in organic solvents, the potential applications of PVMS in microfluidics are boundless. For example, spatially patterning the surface energy or surface chemistry of a microchannel with PVMS could be faster and more precise than with Sylgard 184®.[7] Additionally, any number of small molecules or polymer chains could be grafted to PVMS by thiol-ene chemistry through the

vinyl groups, enabling precise tuning of the PVMS wettability or biofunctionality. An important aspect of using PVMS in a wider range of applications is the incorporation of nanoparticles to increase the mechanical robustness of the network. By incorporating nanoparticles into PVMS networks prior to modification with thiols, the fillers may potentially prevent wrinkling and enable the grafting of ELPs successfully. Another conceivable avenue of research for incorporation of nanoparticles into PVMS would be the addition of functional particles, including magnetic, catalytic, optically active, or conductive particles, creating a more versatile elastomeric network.[8]

We were unable to graft and characterize elastin-like copolypeptides on our PVMS networks, but this route is still an attractive possibility. Collaborators through the Triangle MRSEC program at Duke University have successfully grafted stimuli-responsive synthetic polymer brushes such as PNIPAM to PVMS networks for use in anti-biofouling research; these results are being prepared for publication currently. ELPs show great promise in biomolecular detection as stimuli-responsive trap-and-release functional groups. Incorporation of ELP-functionalized PVMS networks in microfluidic channels would be a simple, effective application of this technology, assuming grafting difficulties can be overcome.

Many interesting experimental results with PVMS were discovered on the path to the writing of this dissertation. One example is the unexpected self-organized buckling on rectangular PVMS networks which were UV-treated for long times; these samples were prepared for the purpose of evaluation in dynamic mechanical analysis. Because of the ordering of the buckles and cracks on the PVMS network surface, the samples were found to

have angle-specific diffraction characteristics. In Figures 6.1 and 6.2, this effect is demonstrated: under microscopy, the buckling and cracking is clearly seen. The images in Figure 6.2 show two samples which were rotated with respect to the camera, showing an angle dependent diffraction effect.

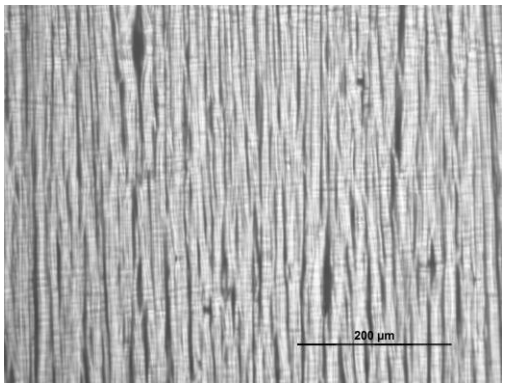

Figure 6.1: Optical microscopy of the surface of a PVMS network that has been infused with photoinitiator and UV treated for 7000 seconds.

In these samples, the alignment of buckles could be either parallel to the long axis or perpendicular, depending on the affinity of the network for the surface beneath it during UV treatment (PVMS adheres to glass well, but not as well to other substrates or to textiles). In Figure 6.2 a and b, the sample is rotated along the long axis of the sample, becoming transparent or diffracting light depending on rotation. In Figure 6.2 b and c, the other sample was rotated along the short axis of the sample. The PVMS network in the top of Figure 6.2 was UV-treated while resting on a glass slide, while the network in the bottom of the image was treated while resting on a Kimwipe.

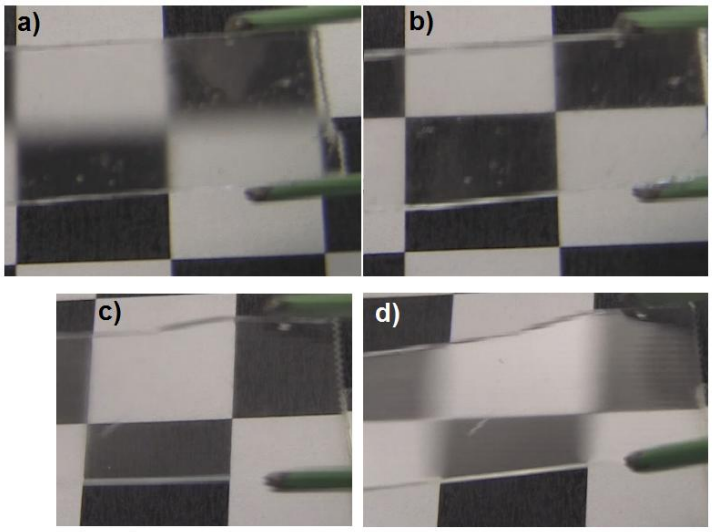

Figure 6.2: Video still images of UV-treated PVMS networks (treatment time 7000 seconds). A) and b) are the same sample which was UV-treated while on a glass slide, c) and d) was UV-treated while on a Kimwipe.

The potential for the application of photocurable PVMS networks in micro- and nanofabrication is vast, and hopefully will be explored by future researchers to its full potential.

6.3. References

[1] Cole, M. A. & Bowman, C. N. Evaluation of thiol-ene click chemistry in functionalized polysiloxanes. J. Polym. Sci. Part Polym. Chem. 51, 1749–1757 (2013).

[2] Müller, U., Kunze, A., Herzig, C. & Weis, J. Photocrosslinking of Silicones. Part 13. Photoinduced Thiol-Ene Crosslinking of Modified Silicones. J. Macromol. Sci. Part A 33, 439–457 (1996).

[3] Ahmed, S. et al. Poly(vinylmethylsiloxane) Elastomer Networks as Functional Materials for Cell Adhesion and Migration Studies. Biomacromolecules 12, 1265–1271 (2011).

[4] Yang, H.-K., Evren Özçam, A., Efimenko, K. & Genzer, J. Photochromic materials with tunable color and mechanical flexibility. Soft Matter 7, 3766 (2011).

[5] O'Shaughnessy, W. S., Gao, M. & Gleason, K. K. Initiated Chemical Vapor Deposition of Trivinyltrimethylcyclotrisiloxane for Biomaterial Coatings. Langmuir 22, 7021–7026 (2006).

[6] Trujillo, N. J., Wu, Q. & Gleason, K. K. Ultralow Dielectric Constant Tetravinyltetramethylcyclotetrasiloxane Films Deposited by Initiated Chemical Vapor Deposition (iCVD). Adv. Funct. Mater. 20, 607–616 (2010).

[7] Abate, A. R. et al. Photoreactive coating for high-contrast spatial patterning of microfluidic device wettability. Lab. Chip 8, 2157 (2008).

[8] Althues, H., Henle, J. & Kaskel, S. Functional inorganic nanofillers for transparent polymers. Chem. Soc. Rev. 36, 1454 (2007).

APPENDICES

Appendix A

A.1. Siloxane Synthesis

The history of siloxane synthesis dates back to 1872, when Ladenburg reported on the successful synthesis of a siloxane polymer.[1] Since that time, siloxanes have been synthesized, studied, and manufactured on a large commercial scale. The industrial precursors to siloxane polymers are usually dichlorosilanes.[1] A reaction of methylene chloride with silicon in the presence of a catalyst generates dimethyl dichlorosilane. The dichlorosilane molecules react with aqueous hydrochloric acid, forming short chain linear and cyclic siloxanes.[2] Although both linear and cyclic products are formed, tuning of the reaction conditions will favor one over the other as primary reaction products.[1] Hydroxyl-terminated linear short chains are used in condensation polymerization of siloxanes, while cyclic groups are used in ring-opening polymerization.[3]

A.1.1. Condensation Polymerization

Condensation reactions are step growth polymerizations in which a small molecule is liberated with each monomer addition. Industrial manufacturing of siloxanes has made use of polycondensation reactions of silanols for over 50 years.[4] Either an acid or a base can catalyze the condensation of silanols, with either system being a reversible reaction when water is present.[1] It is therefore important to remove water during condensation reactions in order to drive the reaction to the polymer chain as a primary product. The reaction rates of silanols vary with molecular size; for example, the single unit of dimethylsilanediol is twice as reactive as the dimer.[1]

The starting material we used in our work is called PJ Fluid, which is an intermediate product from Dow Corning containing short chain PVMS molecules with hydroxyl end groups. The polycondensation reaction, shown in Figure A.1, is a lithium hydroxide catalyzed condensation reaction with water as a by-product. An aqueous solution of lithium hydroxide is added to a pre-heated reaction vessel of linear silanol short chains. The reaction flask is kept above 100°C to vaporize the by-product, and a nitrogen purge is swept across the surface of the reaction mixture to transport the water out of the system. This mixture is continuously stirred and heated for several hours or until it becomes viscous. An addition of carbon dioxide in the form of dry ice terminates the reaction. Once cooled, the mixture is filtered through diatomaceous earth (Celite®).

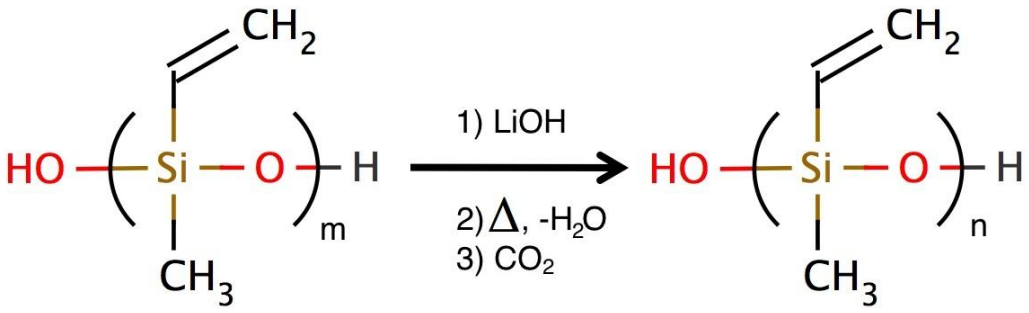

Figure A.1: Polycondensation reaction of short silanol oligomers into siloxane polymers using lithium hydroxide as a catalyst (m=4-6, n=100+).

Two purification methods were investigated for samples made using the condensation reaction. The first method was to dissolve the reaction mixture in diethyl ether, followed by a dropwise addition of methanol until the mixture became cloudy, indicating that the polymer

molecules precipitated out of solution. Once agitation was removed, the solution separated into two layers, with the polymer product as the bottom layer. The small molecules remaining in the reaction mixture migrated into the methanol phase and were removed by decanting the top layer. Any residual solvent in the bottom polymer layer was removed with several hours of rotary evaporation. For the second purification method, the PVMS was put into a separatory funnel with an excess of methanol. The funnel was then vigorously shaken for roughly 5 minutes, and degassed periodically. The funnel was left to separate, and the bottom layer containing PVMS was drawn off. This layer was then subjected to rotary evaporation to remove any remaining methanol. Both of these procedures were repeated two or more times until a final clear liquid with no solvent smell was obtained. The final product was then analyzed by gel permeation chromatography to determine molecular weight and polydispersity index.

The first PVMS synthesized by condensation reaction used 30 ppm LiOH and 500 mL PJ fluid at 120°C for 180 min. A second batch of PVMS used 40 ppm LiOH and 400 mL pre-filtered PJ fluid at 110°C for 110 minutes. As shown in Figure A.2, using a higher amount of lithium hydroxide resulted in a higher molecular weight as well as a broad distribution of molecular weights. This result is unexpected, as using a lower amount of catalyst for a longer time should result in a smaller PDI but an equally high molecular weight as the batch with a high amount of initiator. The molecular weights of polymers made by condensation and ring-opening polymerization, discussed below, are summarized in Table A.1. The preferable method for purification of condensation reaction polymers was determined to be using methanol only, not methanol and diethyl ether, due to the improved

removal of lower molecular weight compounds using the methanol-only method. This method of polymerization was fairly simple to perform, although an inability to obtain more PJ Fluid from Dow Corning necessitated the exploration of other polymerization reactions.

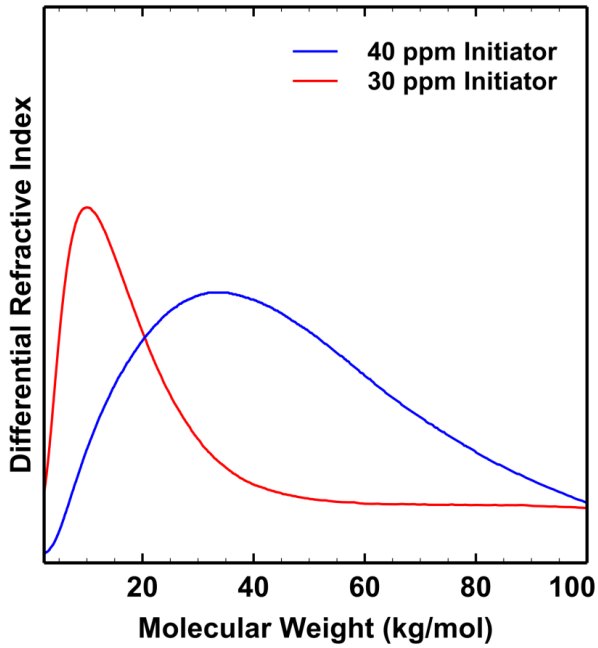

Figure A.2: Molecular weight distributions resulting from polycondensation reactions.

A.1.2. Ring Opening Polymerization

Ring opening polymerizations (ROP) occur through a number of mechanisms, including equilibrium ring-opening polymerization and ring-opening metathesis polymerization.[5] Generally, siloxane ROP consists of cationic or anionic processes that can be quenched at equilibrium or before equilibrium conditions are reached.[5] For anionic ring-

opening polymerization (AROP), the active propagation group is a silanolate anion paired with the initiator counterion.[5] The rate of polymerization decreases with an increasing counterion size; for example, sodium or potassium counterions result in a slower reaction rate than lithium counterions.[5] Siloxane AROP is significantly affected by the solvent and the presence of a promoter, such as DMSO, which can reduce aggregation of silanolate sites, therefore increasing yield.[5] The ring size is also an important factor for yield, as larger rings do not have the ring strain necessary for rapid conversion to polymer chains. By controlling the reaction kinetically, high yields of approximately 80-95% can be obtained.[6]

PVMS was synthesized by AROP as shown in the reaction scheme in Figure A.3.

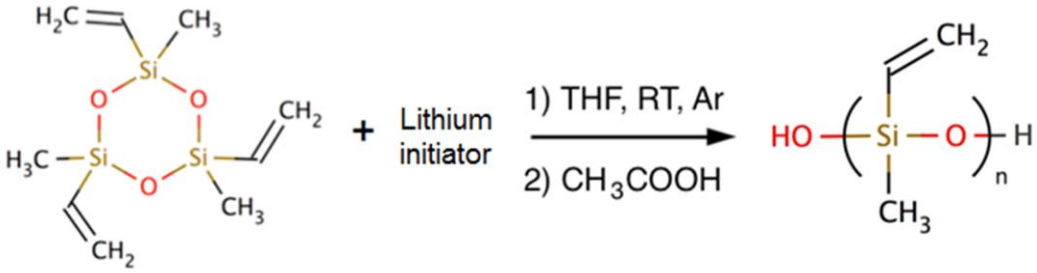

Figure A.3: Anionic ring-opening polymerization reaction of cyclic siloxanes into siloxane polymers using a lithium initiator (such as butyl lithium) as a catalyst (n=100+).

First, monomers were distilled from a mixture of siloxane groups (Dow Corning INT 4-2782 labeled “vinyl methyl cyclics") over activated molecular sieves to obtain only six-membered vinyl methyl siloxane cyclics (abbreviated VM3 or V3, abbreviated in the literature occasionally as VD3); the distilled monomers were then stored under argon. The distilled

material that was collected had a boiling point of 80-85°C under vacuum (at an absolute pressure of roughly 40 mmHg). The distilled and undistilled monomers were evaluated by gas chromatography/mass spectroscopy (GC-MS). The distillate did appear to be primarily six-membered cyclic groups, as demonstrated in Figure A.4. Prior to distillation, the cyclic mixture contained larger cyclics (Figure A.5).

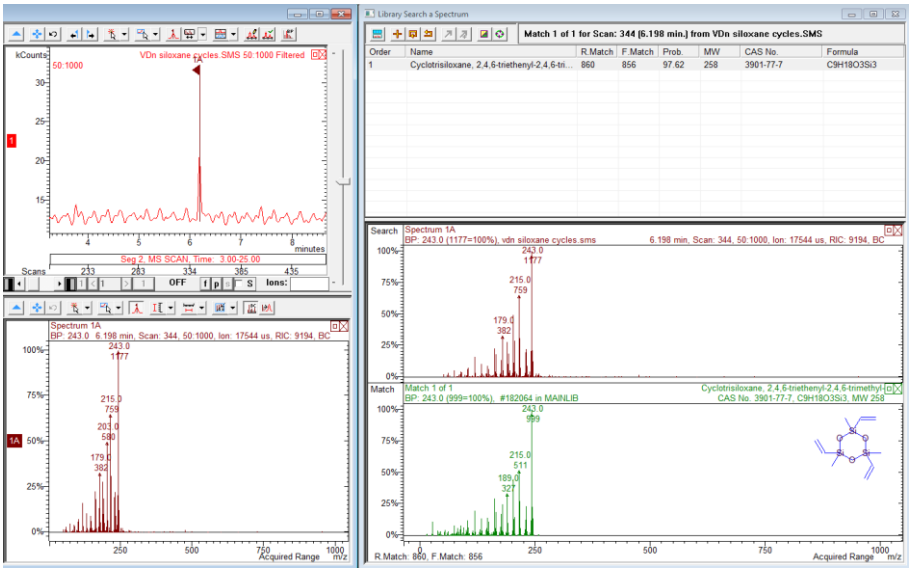

Figure A.4: Gas chromatography/mass spectrometry of vinyl methyl cyclic monomers after distillation.

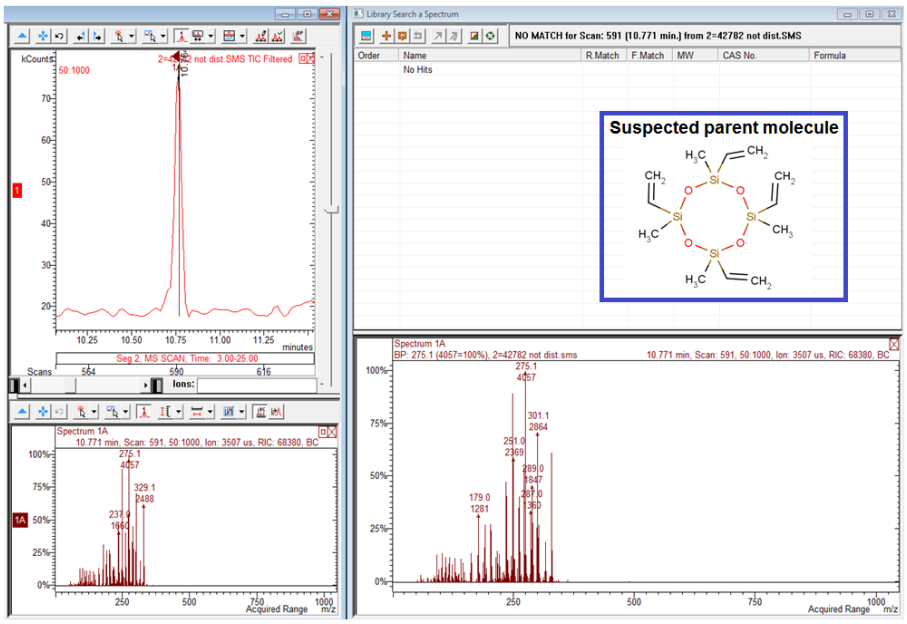

Figure A.5: Gas chromatography/mass spectrometry of vinyl methyl cyclic monomers before distillation.

The distilled vinyl methyl monomers were added to a flame-dried flask along with dry THF in an argon atmosphere. Lithium was introduced quickly and the reaction was stirred at room temperature until most monomers had reacted. Using commercially available butyl-lithium will create a polymer with only one functional end group. Although AROP is kinetically much faster than condensation, some reaction attempts were allowed to proceed several hours, after which the reaction was terminated with excess acetic acid, resulting in one hydroxyl end group. This mixture was then purified by first precipitating the polymer in methanol (twice) and then removing residual methanol with rotary evaporation. One small batch of PVMS homopolymer was made using this distillate and butyl lithium as the initiator. As an example, 0.12 mL BuLi (0.3 mmol), 7.75 mL VM3 (28.5 mmol), and 7.75 mL distilled THF were used. The ratio of moles of monomer to moles of lithium should theoretically determine the molecular weight of the final monomer; a ratio of 100 moles monomer (cycles, not 100 moles of each repeat unit) to 1 mole catalyst should result in a PVMS with MW of roughly 25,000 g/mol.

Using butyl lithium as a catalyst is convenient because it is commercially available, but in order to use the polymer as part of an alkoxy-cured network, both ends of the polymer should be functional. To make a polymer with two hydroxyl end groups, a bifunctional initiator was made. The method for making dilithium diphenylsilanolate (DLDPS) is well established.[7] First, diphenyl silane diol (DPSD) was dried using two approaches: either by several freeze-dry cycles, or by melting the DPSD under vacuum to evaporate any water present. Dry THF was distilled over sodium, and dry benzene was distilled over molecular sieves. Then, the dry benzene and dry THF (≈ 20 ppm water) were used in a 50/50 volume

ratio to make a solution with the dried silane diol. Butyl lithium was added dropwise until all the silane diol was converted into dilithium diphenylsilanolate.

Di- and triblock copolymers of PVMS and PDMS were made with butyl lithium or the DLDPS initiator (see Figure A.6 for reaction scheme, Figures A.8-11 for GPC results).

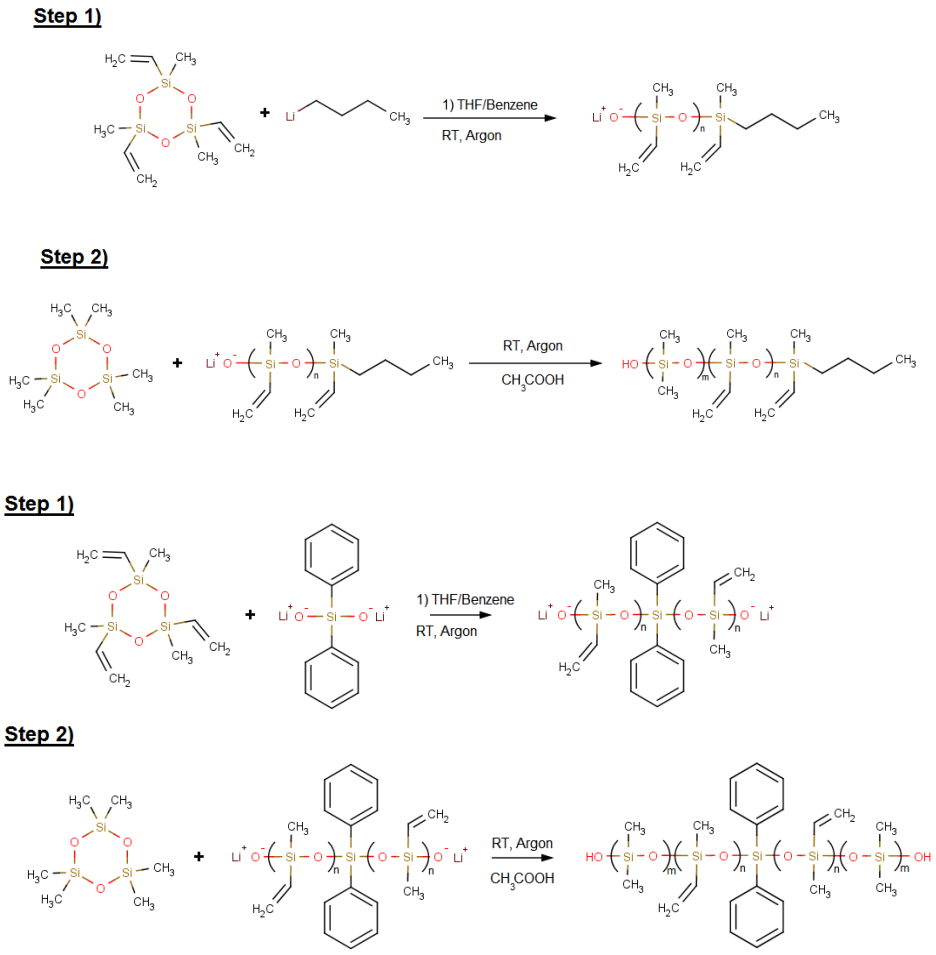

Figure A.6: Anionic ring-opening polymerization reaction of cyclic dimethyl and vinyl methyl siloxanes into diblock siloxane polymers using butyl lithium as a catalyst, and into triblock siloxane polymers using dilithium diphenylsilanolate as a catalyst (m and n=100+).

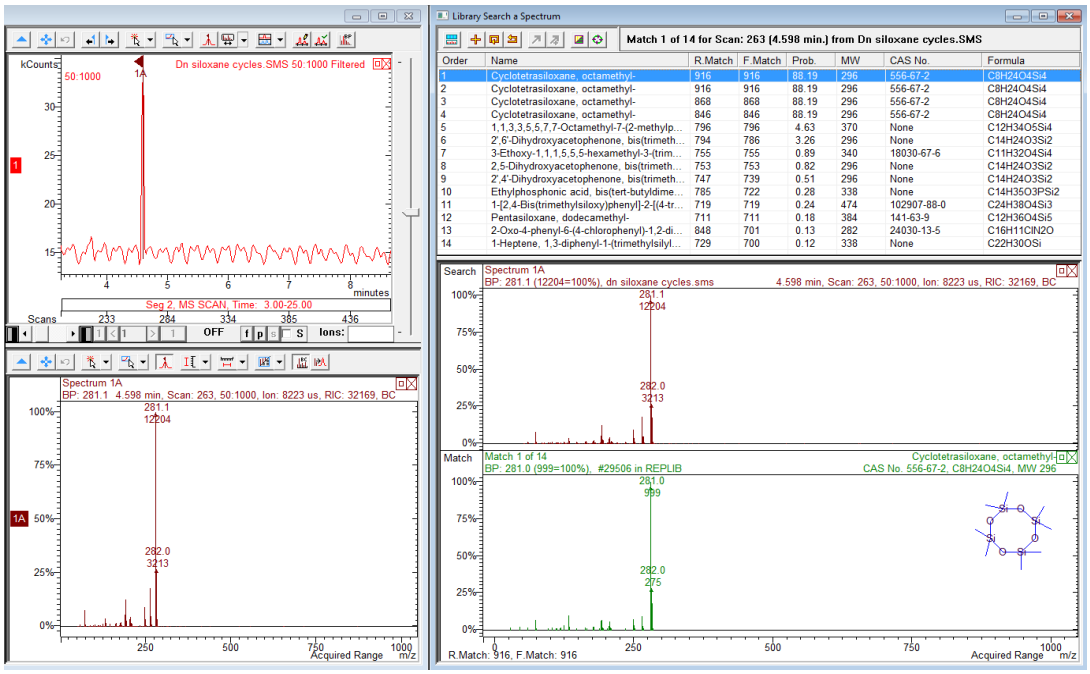

Figure A.7: Gas chromatography/mass spectrometry of dimethyl cyclic monomers after distillation.

Unfortunately, the yields for these reactions were low, as the distilled dimethyl siloxane cycles were primarily eight-membered rings (see Figure A.7), which are much less reactive than both six-membered rings of dimethyl cyclics and eight-membered rings of vinyl methyl cyclics.

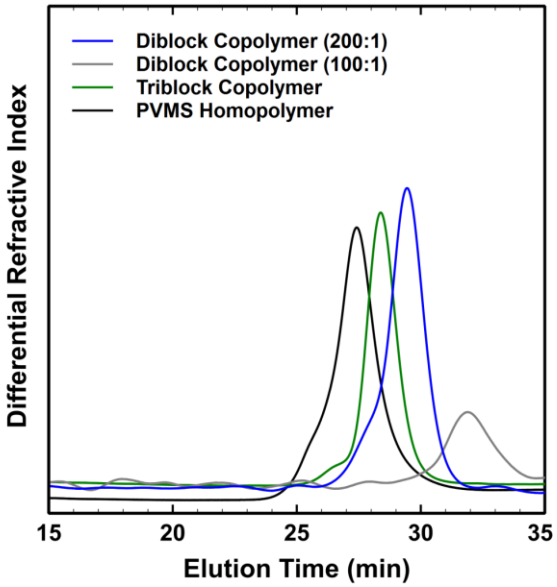

Figure A.8: Comparison of different AROP synthesis GPC results. Ratios are moles of monomer to initiator. Diblock and triblock copolymers are PDMS-PVMS copolymers.

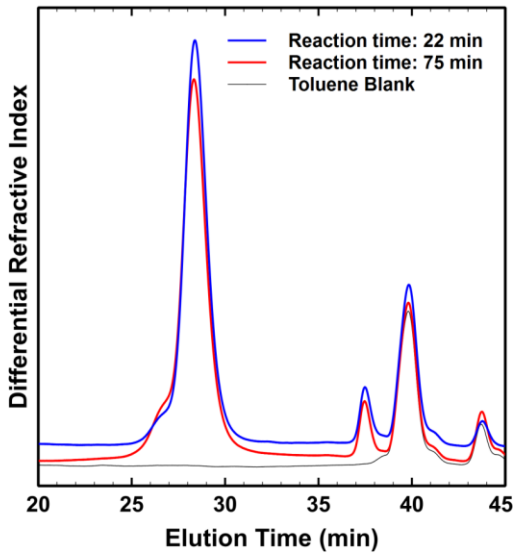

Figure A.9: Kinetic study of PVMS AROP using butyl lithium as a catalyst. Time indicated is the time of reaction after injecting lithium. The reaction goes to completion quickly.

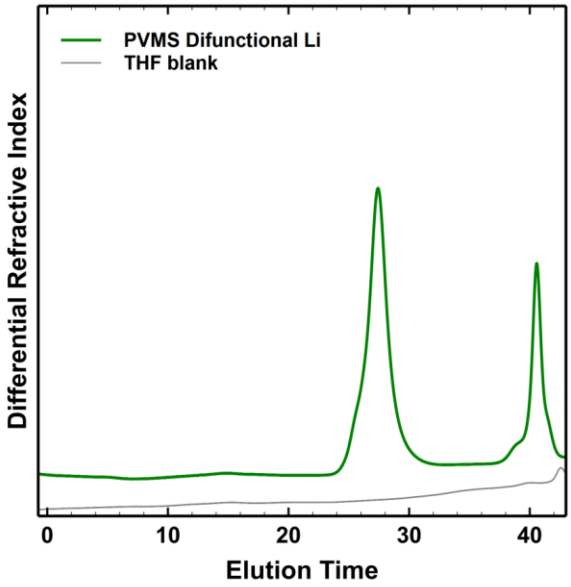

Figure A.10: PVMS homopolymer made with difunctional initiator, showing both polymer (at elution time ~28 min) and residual monomer (elution time ~41 min).

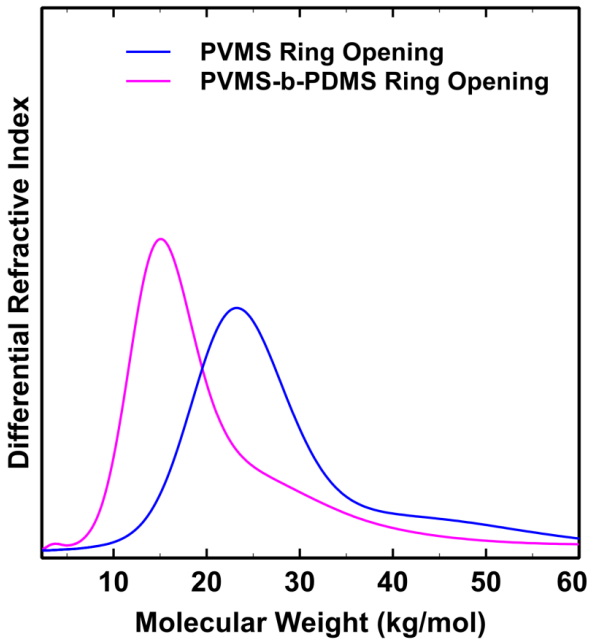

Figure A.11: Molecular weight comparison of PVMS and PVMS-co-PDMS made with butyl lithium catalyst using AROP. The copolymer is lower molecular weight due to the usage of eight-membered dimethyl siloxane cycles, which are less reactive than vinyl methyl siloxane cycles.

Many AROP reactions did not proceed properly due to the difficulty of preventing any air or water from entering the reaction vessel. First of all, the glassware and solvents must be thoroughly dried, and the THF in particular is difficult to keep sufficiently dry. Additionally, the difunctional initiator would deactivate over time due to exposure to water or air. Finally, when the reaction was allowed to proceed for long times, lower molecular weights may have resulted due to backbiting, which has been noted by other groups.[8] Reports from other researchers[9,10] indication that monomers are consumed by 90-95% within 3 hours (see Figure A.12). If the reaction proceeds with only 10% of the original amount of monomer remaining, it is possible that there will be more chain cleavage occurring, which will decrease the polymer molecular weight. Also, because the reactivity of monomers varies by the size of the ring as well as the constituents on the ring, the less reactive monomer should always be added first, followed by the more reactive monomer.[5]

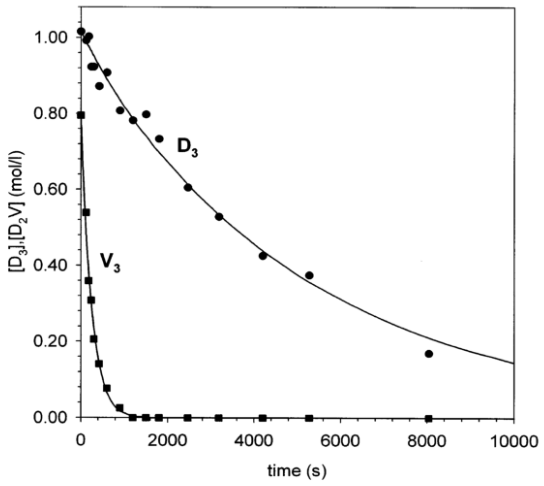

Figure A.12: Copolymerization of six-membered rings of both vinyl methyl siloxane (V3) and dimethyl siloxane (D3) in THF initiated with n-BuLi at 25°C.[11]

Although the starting material for the condensation reactions (PJ Fluid) is not currently available, it is also possible to make these short chain hydroxyl terminated PVMS and PDMS precursors in the lab. A dichlorosilane treated with an aqueous hydrochloric acid solution will give both short chain segments and rings.[2] These short chains can be used for condensation reactions for making PVMS, PDMS or random copolymers of PDMS/PVMS.

Table A.1 Summary of synthesized PVMS and PDMS-PVMS copolymers. Molecular weights are rounded to the nearest thousand g/mol. N/A indicates the molecular weight or PDI were not determined, usually due to insufficient yields.

Synthesis Date	Polymer Type	Synthesis Method	Molecular Weight (g/mol)	PDI	Initiator Type, Amount
5-17-2010	PVMS Homopolymer	Condensation	10,000	1.438	LiOH, 30 ppm
5-28-2010	PVMS Homopolymer	Condensation	33,000	2.443	LiOH, 40 ppm
6-28-2011	PVMS Homopolymer	AROP	*N/A*	*N/A*	BuLi, 1 mol Li:100 mol Monomer
6-30-2011	PVMS-co-PDMS Di	AROP	*N/A*	*N/A*	BuLi, 100 mol D3: 250 mol V3:1 mol Li
7-13-2011	PVMS-co-PDMS Di	AROP	*N/A*	*N/A*	BuLi, 100 mol D3: 100 mol V3:1 mol Li
7-21-2011	PVMS-co-PDMS Di	AROP	*N/A*	*N/A*	BuLi, 80 mol D3: 20 mol V3:1 mol Li
4-4-2012	PVMS Homopolymer (Kinetic Study)	AROP	25,000	1.077	BuLi, 100 mol V3: 1 mol Li
4-6-2012	PVMS-co-PDMS Di	AROP	8,000	1.066	100 mol monomer: Li
5-16-2012	P(DMS-co-PVMS) diblock	AROP	29,000	1.046	300 mol D3: 56 mol V3: 1 mol Li
8-28-2012	PVMS Homopolymer	AROP	39,000	*N/A*	DLDPS, 300 mol V3 : 1 mol DLDPS (2 mol Li)
8-9-2013	PVMS Homopolymer	AROP	78,000	1.584	400 mol V3: 1 mol Li
5-23-2013	PVMS Homopolymer	Condensation	15,000	*N/A*	LiOH, 10 ppm

A.2. References

[1] *Silicon-Containing Polymers - The Science and Technology of Their Synthesis and Applications*. (Kluwer Academic Publishers, 2000).

[2] Efimenko, K. *et al.* Rapid formation of soft hydrophilic silicone elastomer surfaces. *Polymer* **46,** 9329–9341 (2005).

[3] Clarson, S. J. *Siloxane polymers*. (Prentice Hall, 1993).

[4] Grzelka, A. *et al.* Polysiloxanol condensation and disproportionation in the presence of a superacid. *J. Organomet. Chem.* **689,** 705–713 (2004).

[5] Dubois, P., Coulembier, O. & Raquez, J.-M. *Handbook of ring-opening polymerization*. (Wiley-VCH, 2009).

[6] Chojnowski, J. & Rózga, K. Synthesis of linear polysiloxanes with electron-donating organophosphorus pendant groups by kinetically controlled ring-opening polymerization. *J. Inorg. Organomet. Polym.* **2,** 297–317 (1992).

[7] Battjes, K. P., Kuo, C.-M., Miller, R. L. & Saam, J. C. Strain-Induced Crystallization in Poly[methyl(3,3,3-trifluoropropyl)siloxane] Networks. *Macromolecules* **28,** 790–792 (1995).

[8] Herczynska, L. *et al.* Synthesis of microsequential methylvinylsiloxane–dimethylsiloxane copolymers by nonequilibrium copolymerization. *J. Polym. Sci. Part Polym. Chem.* **36,** 137–145 (1998).

[9] Cypryk, M. & Delczyk-Olejniczak, B. Copolymerization of functional cyclotrisiloxanes - a reactivity comparison. *Polimery* **55,** 503–511 (2010).

[10] Chojnowski, J., Cypryk, M., Fortuniak, W., Rózga-Wijas, K. & Ścibiorek, M. Controlled synthesis of vinylmethylsiloxane–dimethylsiloxane gradient, block and alternate copolymers by anionic ROP of cyclotrisiloxanes. *Polymer* **43,** 1993–2001 (2002).

[11] Chojnowski, J., Cypryk, M., Fortuniak, W., Ścibiorek, M. & Rózga-Wijas, K. Synthesis of Branched Polysiloxanes with Controlled Branching and Functionalization by Anionic Ring-Opening Polymerization. *Macromolecules* **36,** 3890–3897 (2003).

Appendix B

Materials Views
www.MaterialsViews.com

ADVANCED FUNCTIONAL MATERIALS
www.afm-journal.de

FULL PAPER

Ultrastretchable Fibers with Metallic Conductivity Using a Liquid Metal Alloy Core

*Shu Zhu, Ju-Hee So, Robin Mays, Sharvil Desai, William R. Barnes, Behnam Pourdeyhimi, and Michael D. Dickey**

The fabrication and characterization of fibers that are ultrastretchable and have metallic electrical conductivity are described. The fibers consist of a liquid metal alloy, eutectic gallium indium (EGaIn), injected into the core of stretchable hollow fibers composed of a triblock copolymer, poly[styrene-*b*-(ethylene-*co*-butylene)-*b*-styrene] (SEBS) resin. The hollow fibers are easy to mass-produce with controlled size using commercially available melt processing methods. The fibers are similar to conventional metallic wires, but can be stretched orders of magnitude further while retaining electrical conductivity. Mechanical measurements with and without the liquid metal inside the fibers show the liquid core has a negligible impact on the mechanical properties of the fibers, which is in contrast to most conductive composite fibers. The fibers also maintain the same tactile properties with and without the metal. Electrical measurements show that the fibers increase resistance as the fiber elongates and the cross sectional area narrows. Fibers with larger diameters change from a triangular to a more circular cross-section during stretching, which has the appeal of lowering the resistance below that predicted by theory. To demonstrate their utility, the ultrastretchable fibers are used as stretchable wires for earphones and for a battery charger and perform as well as their conventional parts.

1. Introduction

This paper describes the fabrication and characterization of ultra-stretchable fibers with metallic conductivity formed by injecting a moldable liquid metal into hollow elastomeric fibers. We fabricated the hollow fibers by melt processing commercial a thermoplastic elastomer (Kraton G1643). Injecting a liquid metal alloy, eutectic gallium indium (EGaIn, 75% Ga, 25% In by weight, melting point 15.7 °C[1,2]), into these fibers produces conductive wires encased in an insulating polymer shell. Because the metal is a liquid at room temperature, it flows and maintains metallic conductivity while stretching the fibers significantly (up to ≈700% strain). Stretchable and flexible conductive fibers may be useful for incorporating electronic function into non-rigid substrates (e.g., textiles, filters, clothing, paper, and sensors).[3–5]

A number of flexible electronic devices, including flexible circuits, waveguides, and epidermal electronics have been fabricated from rigid materials that are rendered flexible by using a thin form factor.[6–8] Coercing these thin films into wavy shapes on elastomeric substrates offers a route to make them stretchable and thus, more durable in mechanically demanding applications. An alternative approach for stretchable electronics is to use intrinsically stretchable conductors such as conductive pastes (e.g., pastes of carbon nanotubes or metal particles), composites, or liquids.[9–11] These stretchable conductors are useful for wires, interconnects, metamaterials, and antennas.

Conductive fibers are an attractive platform for flexible and stretchable electronics because fibers are inexpensive, inherently flexible, can be formed into 2D and 3D fabrics, and can be mass produced via melt processing with very high speeds (>1000 m/min). The most common methods to impart conductivity into melt processed fibers include coating the fibers with conductive films (e.g., metals or carbon)[12–14] or creating conductive composites by introducing electrically conductive additives (e.g., graphite or carbon,[15–18] metal nanoparticles,[19] conductive polymers[17,20–23] such as polyaniline and poly-3-hexylthiophene). To ensure conductivity through the fiber, a composite fiber requires the addition of a sufficient amount of an additive to reach percolation. Thus, the mechanical properties (modulus, toughness, tactility, yield point) of the fiber may change in unintended ways; coating methods have similar effects. Moreover, the composite fibers rarely result in metallic conductivity and conductive polymers tend to degrade due to oxidation.[12,24] Also, in some applications (e.g., commercial wires), it may be undesirable to have the current carrying components exposed to the exterior of the fiber. Commercial wires (e.g., copper wire insulated with polymer) are flexible due to

S. Zhu, J.-H. So, R. L. Mays, Dr. S. Desai, Prof. M. D. Dickey
Department of Chemical and Biomolecular Engineering
North Carolina State University
911 Partners Way, Raleigh, NC 27695, USA
E-mail: michael_dickey@ncsu.edu
W. R. Barnes, Prof. B. Pourdeyhimi,
The Nonwovens Institute,
North Carolina State University,
1000 Main Campus Dr., Raleigh, NC 27606, USA

DOI: 10.1002/adfm.201202405

their thin cross-section, but are not stretchable.[25,26] We sought to demonstrate a new approach to create conductive fibers that would be simple, highly conductive, and stretchable without modifying the mechanical or tactile properties of the fiber. The present work is distinguished by 1) the ability of the fibers to maintain metallic conductivity with ultralarge strains; 2) the geometry of the fiber (a conductive core surrounded by an insulating shell, which is similar to conventional wires); and 3) the mechanical and tactile properties of the fiber, which are altered minimally since the fiber shell is unadulterated polymer.

We fabricated the fibers by injecting a moldable liquid metal into hollow fibers. The metal, EGaIn, is liquid at room temperature with a low viscosity and a high conductivity ($\sigma = 3.4 \times 10^4$ S/cm[27]). The liquid metal forms spontaneously a thin oxide skin at room temperature that reforms rapidly when ruptured. The metal can be injected into capillaries, microchannels, and hollow fibers by exceeding the pressure required to rupture the skin.[2] Once it is in the capillary, a new skin forms rapidly and holds it into place. This ability to mold the metal into non-spherical shapes has been utilized to fabricate microelectrodes,[28] stretchable antennas,[11,29,30] stretchable interconnects and conductors,[31,32] soft diodes,[33] and flexible solar cells.[34] Here, we harness this property to demonstrate ultrastretchable, conductive wires inside hollow elastomeric fibers.

Poly[styrene-*b*-(ethylene-*co*-butylene)-*b*-styrene] (SEBS) resin is a thermoplastic elastomer with low modulus, high tensile strength (stress at break ≈10 MPa), high stretchability, and good resistance to most chemicals.[35] SEBS resins are used widely in the production of handles and grips, medical equipment, roofing and many other applications due to their rubber-like properties. We chose a particular type of SEBS resin, Kraton G1643 because it is commercially available, highly stretchable (strain at break >900%) and easy to melt process. This particular resin consists of 20% styrene endblocks and 80% ethylene-butylene midblock[35] and gel permeation chromatography shows it to have a number average molecular weight (M_n) of 116 000 and a weight average molecular weight (M_w) of 139 000 with a polydispersity index (PDI) of 1.19. Here, we describe the fabrication and characterization of stretchable conductive fibers and demonstrate their function as a stretchable charger and as a stretchable cable for earphones.

2. Results

We produced hollow fibers by melt extruding SEBS through a die consisting of a circular slit divided into three equal segments. As the polymer exits the slits and as it is drawn, it flows and forms a hollow fiber. The fibers exited the extruder in a downward motion (i.e., in the direction of gravity) and a collection roller dictated the speed with which the fibers were drawn through a water bath at room temperature. To control the dimensions of the hollow fibers, we varied the spinning rate of the collection roller. **Figure 1** shows the cross sectional dimensions of the fibers for spinning rates ranging from 25 to 1000 m/min (dimensions for free-fall fibers appear in Figure 1b at 0 m/min). In all cases, the fibers have a triangular cross section, which is most likely due to the geometry of the die. The inner diameter of the fabricated fiber varied from 360 to

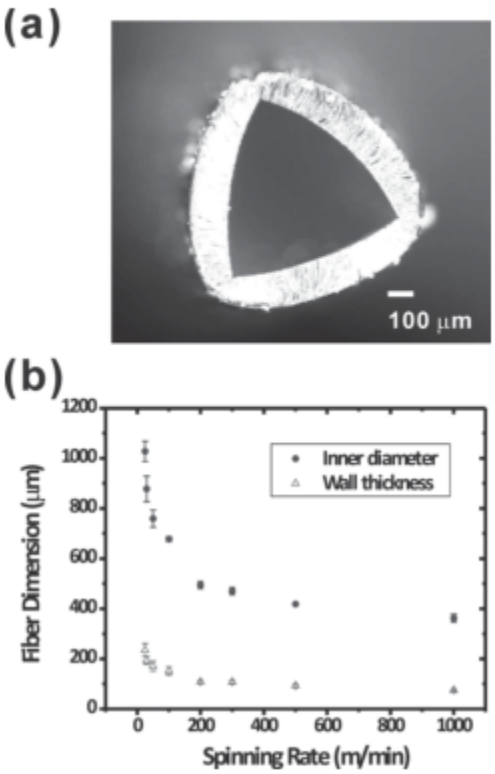

Figure 1. a) Optical image of the cross-section of a hollow fiber formed at 100 m/min. b) The inner diameter (ID) and wall thickness (WT) of the fibers decreased with increased spinning rate.

1030 μm (we define the inner diameter as the average of the lengths of the three lines that originate from the vertexes and bisect the triangular cross-section of the core of the fiber) and the thickness of the walls of the fiber ranges from 75 to 240 μm. As expected, faster spinning rates produced smaller fibers since the extruder kept the mass flow rate constant. The outer diameter of the fibers appears to level out at higher spinning rates. We varied the quench distance (i.e., the distance between the die and the water bath), but did not observe significant changes in fiber geometry (±25 μm over all distances allowed by the experimental setup).

It is straightforward to inject the metal into the hollow fibers. A long segment of hollow fiber can be filled with liquid metal using a syringe and then cut into several pieces with desired lengths. The longest segment we attempted to fill was ≈1 m long and it filled easily. Injecting the metal requires overcoming the interfacial forces, which scale inversely with the diameter of the fibers.[2] Pressures of ≈0.1 atm are sufficient to overcome these forces for the dimensions of fibers used in this study. The pressure required to overcome viscous drag is only

Adv. Funct. Mater. 2013,
DOI: 10.1002/adfm.201202405

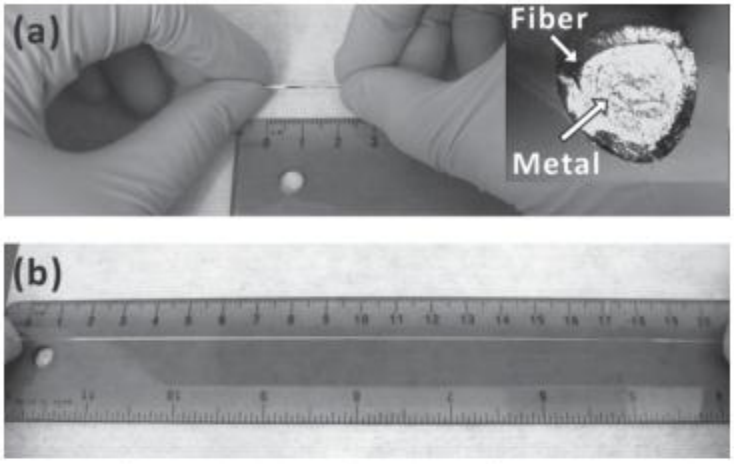

Figure 2. a) A relaxed, 2 cm section of an ultrastretchable conductive fiber. The shiny core of its cross-section (inset) is the liquid metal. b) The fiber is stretched to 20 cm and the metal appears to uniformly fill the stretched fiber.

significant at large injection velocities or long lengths of fiber due to the low viscosity of the metal. The oxidized skin of the metal prevents the metal from flowing out of the fiber when the fiber is not disturbed (e.g., squeezed significantly). The inset in **Figure 2**a shows that the metal remains flush with the cut end of the fiber.

We hypothesized that the incorporation of the metal impacts minimally the mechanical properties of the fibers since the metal is a low viscosity liquid and flows readily in response to applied strain. An extensometer measured the mechanical properties of both the hollow and filled fibers. **Figure 3** shows the stress–strain profiles of the fibers for two spinning rates

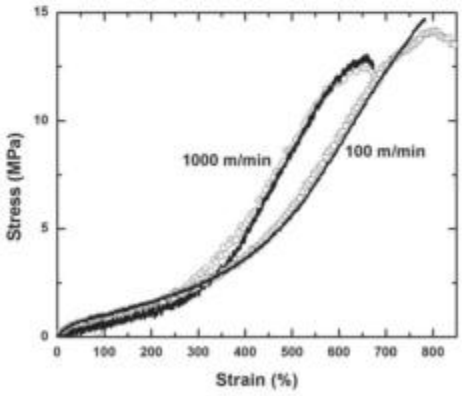

Figure 3. The stress–strain plots of elastomeric hollow (hollow symbols) and filled (solid lines) fibers with two different spinning rates. The fibers have the same mechanical properties with and without the metal.

spanning an order of magnitude in spin speed (100 m/min and 1000 m/min). The plots show the typical properties of thermoplastic elastomers: low modulus and high tensile strength. Although the fibers have very similar mechanical properties, as expected, fibers made with the lowest spinning rate can be strained the furthest before the point of failure. At the lowest spinning rate (100 m/min), we found that the fibers could be stretched to 800–1000% strain before reaching the point of failure. Figure 3 shows that the fibers with and without the metal have nearly identical mechanical properties, which illustrates the negligible effects of the liquid metal on the mechanical properties of the fibers.

For many applications, a practical consideration is the effect of multiple strain cycles on the performance of the fiber. We performed cyclic testing on the fibers produced at 1000 m/min to quantify the effects of repeated strain on the mechanical properties. **Figure 4**a shows that after the first cycle (0 to 800 to 0% strain), subsequent strain cycles overlap nearly perfectly with minimal signs of hysteresis. After the first cycle, there is ≈50% unrecoverable strain (i.e., the "set"), which does not change with subsequent cycles. This result suggests there is some plastic deformation during the first strain cycle, but negligible plastic deformation during subsequent cycles. Fibers fabricated with other spinning rates showed similar behavior. We also performed cyclic testing on the fibers at lower amounts of strain (0 to 50 to 0% strain), which may be more representative of strains encountered in actual applications (e.g., textiles). At these strain cycles, there is only ≈5% unrecoverable strain (Figure 4b). At extreme levels of strain (i.e., 800%), the fibers produced at 1000 m/min broke after 20–40 cycles. The durability improved for fibers produced at 100 m/min, which broke typically after 80–100 cycles at 800% strain. At intermediate strains (i.e., 50% and 400% strain), the fibers did not break after hundreds of cycles.

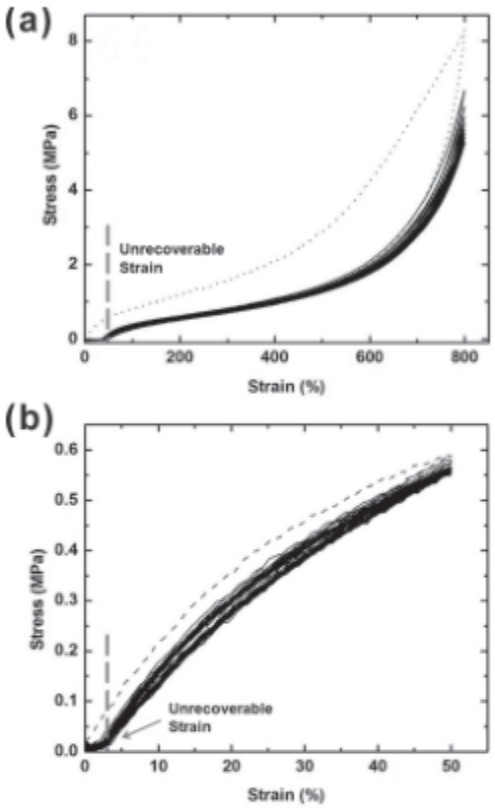

Figure 4. Cyclic tests of the mechanical properties of the hollow fibers fabricated with a spinning rate of 1000 m/min at a) 800% and b) 50% strain. The first cycle is indicated with a dashed line and subsequent cycles are solid lines. A vertical line marks the amount of unrecoverable strain resulting from plastic deformation.

The electrical resistance of the fiber should increase as a function of applied strain since the length of the fiber increases while the cross-sectional area decreases. We measured the resistance as a function of strain and normalized all measurements by the resistance at zero strain such that the initial normalized resistance is 1. The resistance R of a wire depends on its resistivity ρ, length L, and cross-sectional area A, as described in Pouillet's law. Assuming that the polymer sheath has a Poisson's ratio of 0.5 and the metal is incompressible, then the resistance of the fiber should be proportional to the change in the square of the length based solely on geometry. We developed two sets of theoretical resistance values: one is based on the assumption that the cross-sectional area remains triangular while stretching and the other one assumes it becomes circular (i.e., for a given circumference, the cross-sectional area for a circle is 65% larger than an equilateral triangle and thus, the resistance through a circular cross section should be lower). The experimental data, in principle, should be within these bounds for the given assumptions.

Figure 5 shows that the resistance increases as a function of strain. The fibers with a smaller cross sectional area (1000 m/min) have an electrical resistance that agrees nearly perfectly with that predicted by the model for a triangular cross-sectional area. The resistance of these fibers increases dramatically beyond the last plotted point (≈600% strain). The fibers with a larger cross sectional area (100 m/min) initially have an electrical resistance similar to the theoretical resistance for a triangular cross section but then deviate gradually to lower values and follow the resistance prediction for a circular cross-section until 700–800% strain, at which point the resistance rises rapidly. The fibers maintained electrical continuity to ≈1000% strain, albeit at significantly higher resistances. Figure 5a represents the best case

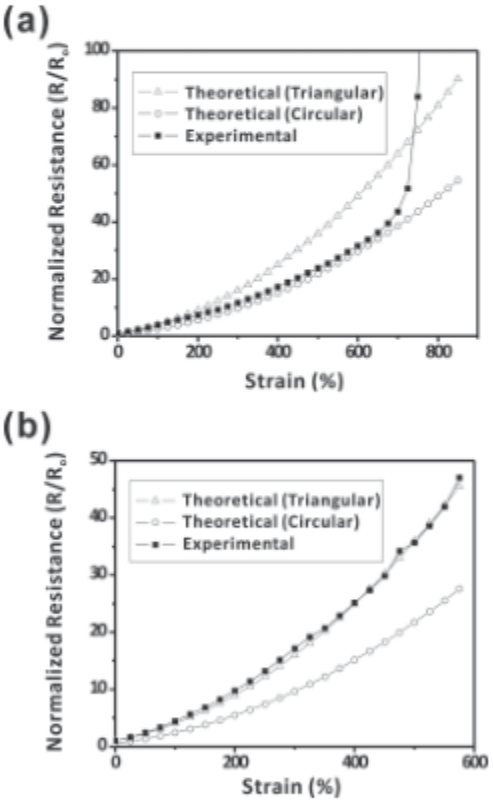

Figure 5. The experimental (filled squares) and theoretical resistance (empty triangles and circles) of conductive fibers with two different spinning rates of a) 100 and b) 1000 m/min. The triangles indicate the geometrical effects of elongation and the circles represent the effect of changes in cross-sectional geometry during elongation.

Adv. Funct. Mater. **2013**,
DOI: 10.1002/adfm.201202405

scenario; in some samples (100 m/min), the resistance would increase rapidly as low as 400% strain. The loss of conductivity coincides with the physical collapse of the fibers. The metallic conductivity recovers upon returning the fibers back to a non-stressed state (in some cases, massaging the fibers is required to regain continuity).

The geometric model captures the general trends in Figure 5 and suggests that the resistance is less than or equal to that expected from a triangular shaped fiber. We compared the cross-sectional geometry of the 100 and 1000 m/min fibers during elongation. The cross-section of the fiber with 100 m/min spinning rate appears to become circular while the fibers with 1000 m/min spinning rate maintain their triangular cross section (see Figure S1,S2 in the Supporting Information), which is consistent with the results of Figure 5. The ability of the fibers produced at 1000 m/min to maintain a triangular profile during elongation could be a result of the smaller size (i.e., increasing the circumference of the fiber should make the side walls easier to deform). Regardless of these subtle effects, the key advance of this work is the remarkable conductivity at large strains.

The fibers have a resistivity of $\sim 3 \times 10^{-5}$ Ω cm until the strain at which the resistance increases rapidly. This value is expected based on the conductivity of the metal (some papers in the literature utilize units of resistance normalized by the length of the fiber, in which case the 100 m/min and 1000 m/min fibers at 500% strain have values of 0.08 and 0.24 Ω/cm). This metallic conductivity exceeds the most conductive composite fibers in the literature (by approximately a factor of 30)[36] and the resistivity is within an order of magnitude of conventional rigid copper wires. The elongation also nearly matches some of the most stretchable conductive fibers in the literature while exceeding the conductivity by four orders of magnitude.[22]

A potential drawback of a liquid core encased in an elastomeric shell is that the metal can flow and increase its resistance when pinched. We performed some qualitative experiments to emulate conditions the fiber may encounter during handling. We intentionally pinched the 100 m/min fiber using pressure from our fingers and found the resistance to increase by an order of magnitude, but not lose electrical continuity. The resistance returned to its initial value when we stopped pinching the fiber. The resistance increased two orders of magnitude, but did not lose its electrical continuity when we concentrated the pressure using our finger nails. The resistance recovered to its pre-pinched value after releasing the force and massaging the fiber. These qualitative experiments underscore a limitation of using soft materials, yet suggest that it is challenging to completely eliminate electrical continuity by hand.

To demonstrate the utility of stretchable fibers in electronic applications, we utilized the fibers as wires of a charger and earphones for a portable music player (iPod). We cut a portion of an iPod charger line and inserted four stretchable fibers (two power wires and two data transmission wires) as shown in **Figure 6**a. We used adhesive to bond the stretchable fibers to the rigid wires of the iPod. The iPod began charging when connected to a computer through the stretchable charger, and continued charging while we repeatedly stretched and relaxed the fibers (see Video S1 in the Supporting information). We found that the stretchable charger replenished the battery at approximately the same rate as the commercial charger (see

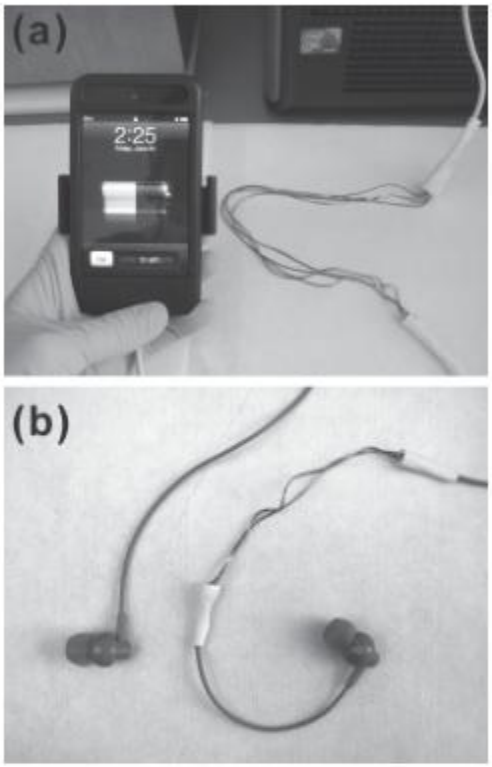

Figure 6. a) Stretchable charger for an iPod and b) stretchable cable for earphones.

Supporting Information). We also inserted the fibers to replace a portion of the wires for earphones (Figure 6b) and the earphones continued to play music without noticeable degredation to volume or sound quality when elongated (see Video S2 in the Supporting information). We repeated several tens of cycles of stretching (~300% strain) and relaxing the wires of the iPod charger and the earphones and their performance did not change in any apparent way. In both examples, the stretchable fibers have a lower resistance per unit length than the commercial wires and thus it is expected that there should be no degradation in performance.

3. Conclusion

This study provides an alternative approach to generate ultra-stretchable conductive fibers by simply injecting liquid alloy (EGaIn) into hollow polymeric (Kraton SEBS) fibers. The dimensions of the conductive fibers can be manipulated by varying the spinning rate of collecting rollers during the melt spinning process. The fibers have the same mechanical and tactile

properties with and without the metal. Metallic electrical continuity can be maintained to greater than 700% strain depending on the dimensions of the fiber, which we believe represents one of the best combinations of conductivity and stretchability for conductive fibers reported to date. The conductive fibers can be incorporated into numerous applications including flexible electronics, smart garments, stretchable wires, inductors, interconnects, and antennas. A limitation of this approach is the liquid core of the fibers can collapse under concentrated pressure or at large strains, although conductivity can be restored. For applications that do not require ultra-stretchability, other polymers may be more appropriate for achieving the desired mechanical stability while retaining metallic conductivity. Likewise, the mechanical properties of the fibers here are limited only by the properties of the polymer, which in principle could be rendered even more stretchable (with less hysteresis and improved durability) by the incorporation of block-selective oils.[37]

4. Experimental Section

Fabrication of Hollow Fibers: Hollow fibers were fabricated using a melt drawing process used widely in the non-wovens industry. A pilot scale Fuji Filter Melt Spinning Tester (MST-CII Special Type) was used. The instrument melt extruded the polymer resin at 230 °C and 400 psi through a hollow configured die. It was customary to use three or four slits to form hollow fibers. The die consisted of a circular slit divided into three equal sections. The circle had an outer diameter of 2 mm and inner diameter of 1.5 mm. The slits were 3 mm deep and the sections were separated by 0.2 mm. A series of rollers mechanically drew the extruded hollow fibers through a water bath at room temperature to cool the fibers and the final roller collected them and dictated the "spinning rate". The quench distance (i.e., the distance from the die to the water bath) was varied between 51 and 97 cm, and the speed of the gear pump that meters the polymer (between 20 and 47 rpm) was also varied. These changes had minimal effects on the fiber dimensions (e.g., for a draw rate of 1000 m/min, a range of diameters from 320 μm to 350 μm was observed, depending on the conditions). Taken in sum, these results suggest that other methods may be necessary to make even smaller fibers (e.g., different die dimensions).

Injection of Liquid Metal: The liquid metal was injected into the hollow fibers to fabricate stretchable conductive fibers. A needle on a syringe filled with the liquid metal and threaded into the fiber provided the source of the conductive core of conductive fibers. For cases in which the inner diameter of the needle was larger than the diameter of the fiber, the fiber was inserted into the needle and sealed with glue so that the syringe would force the metal into the fiber.

Mechanical Characterization: The mechanical properties of both hollow and filled fibers with different dimensions were measured using an Instron 5943 with a 1kN load cell. Two hydraulic grips held 1 inch sections of fiber and stretched it at a constant rate of 10 cm/min. During elongation, a computer recorded the gauge length between the two grips and converted the measured force into pressure based on the cross-sectional area of the fiber. For the cyclic testing a 10 N load cell was used, and linear velocities of 10 cm/min for the fibers drawn at 100 m/min and 3 cm/min for the fibers drawn at 1000 m/min were used to decrease the experimental noise.

Electrical Characterization: A customized digitally controlled stretcher extended the conductive fibers at 1 mm/s while measuring the resistance using a four point probe measurement. Copper wire inserted into both open ends of the fibers provided electrical connections between the liquid metal and the probe clamps from the source meter. The resistance of these wires was measured to be 13.4 mΩ, which agreed with the theoretical value based on the resistivity of copper and the physical dimensions of the wires. To prevent any slippage that might occur during fiber stretching, loose loops of the fiber were assembled at each end of the conductive fibers. The loops had a diameter of about 0.25 inch while leaving a 1 inch straight section in between the loops as the effective original sample length. A drop of glue encased the loops and the copper wire connections, and their resistance was subtracted from the overall resistance measurement to isolate the contributions from the stretchable portion of the fiber. A four point probe technique using a Keithley 2400 measured the overall resistance (through the copper wires, loops, and stretchable portion of the fiber).

Supporting Information

Supporting Information is available from the Wiley Online Library or from the author.

Acknowledgements

This work was supported by the National Science Foundation (CAREER Award CMMI-0954321) and the NSF's Research Triangle MRSEC (DMR-1121107). The authors thank Dr. Steve Smith and Prof. Rich Spontak for the GPC measurements and helpful discussions.

Received: August 22, 2012
Revised: October 29, 2012

[1] S. J. French, D. J. Saunders, G. W. Ingle, *J. Phys. Chem.* **1938**, *42*, 265.
[2] M. D. Dickey, R. C. Chiechi, R. J. Larsen, E. A. Weiss, D. A. Weitz, G. M. Whitesides, *Adv. Funct. Mater.* **2008**, *18*, 1097.
[3] R. F. Service, *Science* **2003**, *301*, 909.
[4] P. Gibbs, H. H. Asada, *J. Neuroeng. Rehabil.* **2005**, *2*, 7.
[5] D.-H. Kim, J. A. Rogers, *Adv. Mater.* **2008**, *20*, 4887.
[6] J. A. Rogers, T. Someya, Y. Huang, *Science* **2010**, *327*, 1603.
[7] D.-H. Kim, J. Xiao, J. Song, Y. Huang, J. A. Rogers, *Adv. Mater.* **2010**, *22*, 2108.
[8] R.-H. Kim, D.-H. Kim, J. Xiao, B. H. Kim, S.-I. Park, B. Panilaitis, R. Ghaffari, J. Yao, Li Ming, Z. Liu, V. Malyarchuk, D. G. Kim, A.-P. Le, R. G. Nuzzo, D. L. Kaplan, F. G. Omenetto, Y. Huang, Z. Kang, J. A. Rogers, *Nat. Mater.* **2010**, *9*, 929.
[9] K.-Y. Chun, Y. Oh, J. Rho, J.-H. Ahn, Y.-J. Kim, H. R. Choi, S. Baik, *Nat. Nanotechnol.* **2010**, *5*, 853.
[10] T. Sekitani, Y. Noguchi, K. Hata, T. Fukushima, T. Aida, T. Someya, *Science* **2008**, *321*, 1468.
[11] J.-H. So, J. Thelen, A. Qusba, G. J. Hayes, G. Lazzi, M. D. Dickey, *Adv. Funct. Mater.* **2009**, *19*, 3632.
[12] X. Jin, C. Xiao, S. An, G. Jia, *J. Mater. Sci.* **2007**, *42*, 4384.
[13] N. J. Pinto, P. Carrion, J. X. Quinones, *Mater. Sci. Eng., A* **2004**, *366*, 1.
[14] D. Zabetakis, M. Dinderman, P. Schoen, *Adv. Mater.* **2005**, *17*, 734.
[15] G. Che, B. B. Lakshmi, C. R. Martin, E. R. Fisher, R. S. Ruoff, *Chem. Mater.* **1998**, *10*, 260.
[16] Z. Li, G. Luo, F. Wei, Y. Huang, *Compos. Sci. Technol.* **2006**, *66*, 1022.
[17] A. Soroudi, M. Skrifvars, *Synth. Met.* **2010**, *160*, 1143.
[18] W. Thongruang, R. J. Spontak, C. M. Balik, *Polymer* **2002**, *43*, 3717.
[19] G. Mattana, P. Cosseddu, B. Fraboni, G. G. Malliaras, J. P. Hinestroza, A. Bonfiglio, *Org. Electron.* **2011**, *12*, 2033.
[20] B. Kim, V. Koncar, E. Devaux, C. Dufour, P. Viallier, *Synth. Met.* **2004**, *146*, 167.

[21] C. R. Rios-Soberanis, R. A. Ley-Bonilla, R. H. Cruz-Estrada, C. V. Cupul-Manzano, L. M. Rangel-Rodríguez, A. Caballero-Can, *Polym. Int.* **2009**, *58*, 817.
[22] A. J. Granero, P. Wagner, K. Wagner, J. M. Razal, G. G. Wallace, M. in het Panhuis, *Adv. Funct. Mater.* **2011**, *21*, 955.
[23] P. Sukitpaneenit, T. Thanpitcha, A. Sirivat, C. Weder, R. Rujiravanit, *J. Appl. Polym. Sci.* **2007**, *106*, 4038.
[24] J. Stejskal, I. Sapurina, J. Proke, J. Zemek, *Synth. Met.* **1999**, *105*, 195.
[25] S. P. Lacour, D. Chan, S. Wagner, T. Li, Z. Suo, *Appl. Phys. Lett.* **2006**, *88*, 204103.
[26] T. Li, Z. Huang, Z. Suo, S. P. Lacour, S. Wagner, *Appl. Phys. Lett.* **2004**, *85*, 3435.
[27] D. Zrnic, D. S. Swatik, *J. Less-Common Met.* **1969**, *18*, 67.
[28] J.-H. So, M. D. Dickey, *Lab Chip* **2011**, *11*, 905.
[29] M. R. Khan, G. J. Hayes, J.-H. So, G. Lazzi, M. D. Dickey, *Appl. Phys. Lett.* **2011**, *99*, 013501.
[30] M. Kubo, X. Li, C. Kim, M. Hashimoto, B. J. Wiley, D. Ham, G. M. Whitesides, *Adv. Mater.* **2010**, *22*, 2749.
[31] J. Park, S. Wang, M. Li, C. Ahn, J. K. Hyun, D. S. Kim, D. K. Kim, J. A. Rogers, Y. Huang, S. Jeon, *Nat. Commun.* **2012**, *3*, 916.
[32] H.-J. Kim, C. Son, B. Ziaie, *Appl. Phys. Lett.* **2008**, *92*, 011904/1.
[33] J.-H. So, H.-J. Koo, M. D. Dickey, O. D. Velev, *Adv. Funct. Mater.* **2011**, *22*, 625.
[34] D. J. Lipomi, B. C. K. Tee, M. Vosgueritchian, Z. Bao, *Adv. Mater.* **2011**, *23*, 1771.
[35] KRATON, G1643 M Polymer, http://docs.kraton.com/tl_warehouse/pdf_data_docs/WG_4140_WG29E4.tmp.pdf (accessed December 2012).
[36] D. Wakuda, K. Suganuma, *Appl. Phys. Lett.* **2011**, *98*, 073304.
[37] J. H. Laurer, R. Bukovnik, R. J. Spontak, *Macromolecules* **1996**, *29*, 5760.